DOMAIN ORGANIZATION OF MUTANT HUNTINGTIN FIBRILS

Thesis by

Charles W. Bugg

In Partial Fulfillment of the Requirements

for the Degree of

Doctor of Philosophy

California Institute of Technology

Pasadena, California

2011

(Defended July 28, 2010)

Acknowledgements

This work was funded by grants from the NINDS, the Hereditary Disease Foundation, and CHDI.

I thank Pamela Bjorkman for the pET32a-HD46Q construct used in the fibril EPR work. For the intracellular antibody work, I thank Eric Schweitzer for providing the PC12 cells carrying inducible huntingtin, David Baltimore for providing lentiviral production plasmids, the MRC Center for Protein Engineering for providing the Griffin.1 library, Elena Cattaneo for providing ST14A cells, David Colby and Dane Wittrup for providing V_L12.3, and Amber Southwell for providing AAV expressing V_L12.3.

I would like to especially thank my advisor Paul Patterson for his support during a tough slog through graduate school. He allowed me the freedom to explore my own ideas and when they failed, helped to pick me up again when I wanted to quit. His guidance was indispensible. Special thanks also go to my coadvisor Ralf Langen for his continued optimism and enthusiasm when we were down to the wire and nothing seemed to work. I might have thrown in the towel, but for his support.

I would like to thank the other members of my thesis committee, Steve Mayo and Doug Rees, for their support and probing questions that spurred me to delve even deeper into the material.

My thanks go to current and former Patterson lab members Ali Khoshnan, Amber Southwell, Jan Ko, Susan Ou, Limin Shi, Natalia Malkova, Ben Deverman, Erin Watkin, Sylvian Bauer, Catherine Bregere, Elaine Hsiao, Stephen Smith, Puja Saluja,

Kelly Lin, Moises Gallegos, and James Li, as well as current and former Langen lab members Mario Isas, Balachandran Hegde, Prabha Hegde, Jobin Varkey, Sahar Bedrood, Christine Jao, Yujin Kim, Mark Ambroso, Natalie Kegulian for guidance, help, and discussions. I would like to especially acknowledge Konstantin Piatkov of the Varshavsky lab at Caltech for his help with protein purification and Torsten Fischer for his patience with an EPR novice.

I would like to thank Kathleen Hamilton and Laura Rodriguez for their help in getting things done. My great appreciation also goes to the BMB option secretary, Alison Ross, for all her help and pleasant conversations. I would like to thank Jose Gonzalez and Bill Lease for help in purchasing and with equipment.

A special thank you goes to my undergraduate research mentor Faqing Huang for taking a chance on me.

I would like to express my heartfelt thanks to my parents for their love and support, as well as for pushing me and not letting me quit. My gratitude also goes out to my sister Gwen for listening to me and loving me.

Above all, I would like to thank my family, for making my life better than it has ever been. My three beautiful daughters, Hailey, Alina, and Aurora always made me smile when times were tough. Finally, thank you Julia for doing most of it alone these last few months while I pushed to finish.

Abstract

Huntington's disease is a progressive, fatal neurodegenerative disorder caused by a polyglutamine (polyQ) expansion in exon 1 of the huntingtin gene (HDx1). A hallmark of the disease is the formation of fibrillar aggregates within cells. *In vitro*, HDx1 with a polyQ expansion forms fibrils that have a cross beta structure common to amyloid fibrils, but little else is definitively known about HDx1 fibril structure. We used electron paramagnetic resonance spectroscopy to study the organization of the major domains (N-terminus, polyQ, C-terminus) of HDx1 with 46Q within the fibril. Our data show that HDx1 fibrils do not have a parallel, in-register structure like most other disease-associated amyloid fibrils. The C-terminus is highly dynamic and is attached like a tail to the polyQ domain, which is mostly immobilized and forms the core of the fibril. However, the C-terminal portion of the polyQ lies outside the core and has a mobility similar to the C-terminus. The N-terminus produced heterogeneous spectra, indicating that it is able to sample multiple conformations. In sum, our study excluded the parallel, in-register arrangement of beta strands within HDx1 fibrils and represents a first step toward a high-resolution structure of HDx1 fibrils.

Contents

List of Figures

Chapter 1

Introduction

Clinical features of Huntington's disease

Huntington's disease (HD) is a progressive and ultimately fatal neurodegenerative disorder affecting about 1 in 10,000 people in North America and Europe (Harper, 1992). Although HD can manifest any time between the ages of one and eighty, most patients are in middle age when they are diagnosed. Typical patients are diagnosed when presenting with chorea (Walker, 2007). However, in the prodromal phase, symptoms occur that are not unique to HD, such as depression (Julien et al., 2007), anxiety, apathy, irritability (Kingma et al., 2008; Kloppel et al., 2010), extroverted hostility (Vassos et al., 2007), memory problems (Berrios et al., 2002; Wolf et al., 2009), as well as a host of other neuropsychiatric and subtle motor symptoms that increase in severity as the onset of overt disease grows closer (Biglan et al., 2009). There is no cure, and treatments are only available for a subset of symptoms, i.e., psychiatric drugs for cognitive problems and tetrabenazine for chorea (Mestre et al., 2009). Symptoms grow progressively worse and most patients die 15 to 20 years after diagnosis, usually from aspiration pneumonia, inanition, dysphagia, or falls (Walker, 2007).

Classification and genetics

HD is one of nine known diseases (HD, spinobulbar muscular atrophy, dentatorubral pallidoluysian atrophy, and spinal cerebellar ataxias (SCAs) 1, 2, 3, 6,

7, and 17) that arise from a CAG expansion in the region of a gene coding for a glutamine tract (Zoghbi and Orr, 2000). The mutated proteins in these polyglutamine (polyQ) diseases are unrelated, being dissimilar in sequence outside of the polyQ expansion, and diverse in cellular functions (Gatchel and Zoghbi, 2005). HD is a monogenic, autosomal dominant disease, resulting from a CAG expansion in the IT15 gene on chromosome 4p16.3 (The Huntington's Disease Collaborative Research Group, 1993). The gene product of IT15, huntingtin (Htt), is a 348 kDa protein with 57 exons. The polyQ tract occurs in the first exon (HDx1) and varies in length in normal Htt. The vast majority of people have between 10 and 29 CAG repeats, while fewer than one percent of the population has 30-35 repeats (Kremer et al., 1994). Expansion of the polyQ beyond a threshold of about 39 causes HD. The intermediate repeat lengths 35-39 are incompletely penetrant (McNeil et al., 1997; Wexler et al., 2004; Quarrell et al., 2007), and there are several case reports of HD with expansions normally considered nontoxic (Kenney et al., 2007; Groen et al., 2010). The age of onset is negatively correlated with the repeat length (Andrew et al., 1993; Brinkman et al., 1997). Most patients have repeats of 40-58Q and the disease manifests at middle age. Longer repeat lengths are associated with a more severe disease progression (Ravina et al., 2008). While there is no significant difference in the age of onset for homozygotes versus heterozygotes (Wexler et al., 1987; Alonso et al., 2002; Wexler et al., 2004), the course of the disease may be more severe in homozygotes (Squitieri et al., 2003). Repeats above 60Q are associated with juvenile HD, defined as an onset before age 20. In contrast to adult-

onset HD patients, juvenile HD patients present with dystonia, parkinsonism, and seizures, and typically have little chorea (Geevasinga et al., 2006; Walker, 2007).

Neurodegeneration/gross structural changes

Although HD neuropathology is classically described as degeneration of the striatum, especially the caudate (Vonsattel et al., 1985), with concomitant ventricular enlargement (Vardi et al., 1979; Aylward et al., 1991), most brain structures are affected in HD (Rosas et al., 2003; Fennema-Notestine et al., 2004; Tabrizi et al., 2009). Striatal medium spiny neurons, especially those that express enkephalin and project to the external globus pallidus, are particularly vulnerable (Walker, 2007). The extent of striatal volume loss is correlated with the repeat length (Rosas et al., 2001). The degeneration of the affected areas begins decades before the onset of overt symptoms (Jurgens et al., 2008; Biglan et al., 2009). There is regional thinning of the cortex in manifest (Rosas et al., 2002) and premanifest HD (Rosas et al., 2005). This is predominantly due to the degeneration of projection neurons in cortical layers V and VI (Hedreen et al., 1991). While not greatly affected in adult-onset HD, cerebellar Purkinje cells degenerate markedly in juvenile HD (Vonsattel and DiFiglia, 1998).

Aggregates

Another prominent neuropathological feature that is common to most polyQ diseases—with the exception of SCA 2, 6, and 17—is that the mutant protein aggregates intracellularly (Zoghbi and Orr, 2000). Amino-terminal fragments of Htt

form ubiquitinated inclusions in nuclei and dystrophic neurites in the cortex and striatum of HD patients (DiFiglia et al., 1997; Sieradzan et al., 1999). However, the extent of aggregation does not correlate simply with cell death. Aggregates are found to primarily form in cortical neurons, in comparison with the more severely degenerated striatum, where only 1-4% of neurons are found to have Htt aggregates (Gutekunst et al., 1999). There are also differences in the distribution of aggregates among cortical regions. Neurons in the more severely affected motor cortex, which makes major connections to the striatum, contain relatively few intranuclear inclusions, compared with neurons in the superior frontal gyrus, which makes few connections with the striatum (van Roon-Mom et al., 2006). Within the striatum, aggregates are mainly found in the spared NADPH-diaphorase interneurons and only rarely in the vulnerable calbindin-positive medium spiny neuron population (Kuemmerle et al., 1999). In these studies, aggregates are found mainly in the neuropil or perikarya; nuclear inclusions are only found in the most severe cases of HD. However, in primary neuronal culture, cerebellar neurons readily develop intranuclear inclusions, but do not die as quickly as cortical neurons (Tagawa et al., 2004).

Huntingtin fibrils

Aggregates contain fibrillar, amyloid-like Htt (Huang et al., 1998), and HDx1 with expanded polyQ spontaneously forms similar fibrils *in vitro* (Scherzinger et al., 1997). Fibril formation by HDx1 depends on polyQ repeat length, concentration, and time (Scherzinger et al., 1999). Aggregation proceeds through beta-sheet rich

globular intermediates, which then assemble into protofibrils, and finally fibrils (Poirier et al., 2002). Oligomeric precursors are 6-7 nm in diameter, while fibrils are 10-12 nm in diameter and 100 nm to several micrometers in length (Scherzinger et al., 1997; Poirier et al., 2002). Individual fibrils bundle together and form aggregates that can appear ribbon-like (Scherzinger et al., 1997; Poirier et al., 2002). Another atomic force microscopy (AFM) study of HDx1 fibrils described them as only about 5 nm in diameter and branched (Dahlgren et al., 2005). These would correspond roughly to the size of protofibrils (4-5 nm) seen by Poirier when Congo red was added to inhibit fibril maturation (Poirier et al., 2002). It is unclear whether the small fibrils seen by Dahlgren et al. were immature, or whether there was another factor that altered the morphology. One possible candidate might be the ionic strength; Dahlgren only used one quarter of the amount of salt used by the other groups. Another possibility is temperature. HDx1 fibrils have different toxicities and other properties, depending on the temperature at which they are produced (Nekooki-Machida et al., 2009).

With Aβ, a key protein in Alzheimer's disease, fibril morphology is known to be sensitive to subtle variations in pH, buffer composition, temperature, and protein concentration (Petkova et al., 2005). It is also sensitive to agitation; fibrils formed from agitated samples are morphologically different from those formed in quiescent samples (Petkova et al., 2005; Tycko, 2006) and they differ in properties such as toxicity (Petkova et al., 2005). Indeed, morphologically distinct Aβ fibrils can form in the same sample (Meinhardt et al., 2009).

Some of the difficulties with fibril heterogeneity can be avoided by taking advantage of a prion-like property of amyloid fibrils, i.e., premade fibrils will faithfully propagate their own structure. Thus, fibril seeds can be made and added to each reaction, and will produce daughter fibrils that have identical properties and structures of the parent fibrils (Petkova et al., 2005). Recently, it was shown that Htt fibrils share this property (Nekooki-Machida et al., 2009).

Fibril toxicity

HDx1 contains three domains, the N-terminus, polyQ, and proline-rich C-terminus. At some distance from the flanking regions, the polyQ region in soluble Htt is disordered, with no appreciable, stable secondary structure (Crick et al., 2006; Kim et al., 2009). However, some antibodies directed at the glutamine region appear to distinguish between different epitopes (Legleiter et al., 2009), implying that there are a number of transient polyQ structures that can be stabilized or induced by antibody binding. At least some polyQ conformations are likely to be toxic, since intracellular antibodies directed against polyQ increase aggregation and toxicity (Khoshnan et al., 2002).

There is some evidence that a soluble monomer or oligomer of Htt is the toxic species. Fibrillar precursors of aggregates are generic toxins (Baglioni et al., 2006). Blocking Htt inclusion formation increases the apoptosis of striatal neurons in culture (Saudou et al., 1998). Htt aggregates themselves do not sensitize cells to apoptotic stress, indicating that they may not be toxic (Chun et al., 2002), although nuclear polyglutamine aggregates can kill cells (Yang et al., 2002). The hypothesis

that inclusion formation is protective gains further support from automated microscopy experiments, in which neurons that form aggregates early survive longer than those that form aggregates later (Arrasate et al., 2004). In fact, in this work, the levels of soluble mutant huntingtin correlate negatively with survival in several cellular models of HD.

However, the controversy regarding the relevance of aggregates to toxicity has not been resolved. Intracellular antibodies that reduce aggregation also reduce toxicity (Khoshnan et al., 2002; Colby et al., 2004; Southwell et al., 2008), and vice versa (Khoshnan et al., 2002; Kvam et al., 2009). This may mean that the antibodies stabilize a toxic species that is also prone to aggregation. Thus, some fibril structures could be very closely related to the structure of the toxic soluble species. One recent study shows that some oligomers are readily incorporated into fibrils, indicating that only minor structural rearrangements must be made (Legleiter et al., 2010). One potential implication is that the structure of the fibril could be closely related to the structure of fibrillar oligomers, which are not stable and therefore difficult to study. Another possibility is that some fibrils are themselves toxic, while others are benign. Indeed, HDx1 fibrils made *in vitro* at low temperature are toxic to cells, whereas fibrils made at physiological temperature are not (Nekooki-Machida et al., 2009). Thus, even if they are not directly toxic, fibrils may still represent a stable sink or reservoir of the toxic species. Understanding their structure may give further insight into the structure of more ephemeral fibrillar species, which may be toxic.

Amyloid structure

Fibrils of Htt appear to have an amyloid structure, i.e., they bind Congo red with green birefringence (Huang et al., 1998) and are rich in beta sheets (Heiser et al., 2000; Poirier et al., 2002). Amyloid is a structural motif that is common to protein deposits found in more than twenty diseases, including Alzheimer's and Parkinson's disease, type 2 diabetes, and the prionoses. Amyloid was classically defined by its the ability to bind certain dyes. More recently, amyloid fibril specific antibodies have been generated that bind to many amyloids that differ in their primary sequence, indicating a common backbone structure (Kayed et al., 2007). Amyloid fibrils have a common Fourier transform infrared spectroscopy (FTIR) signature (Zandomeneghi et al., 2004), which is also found in Htt fibrils (Poirier et al., 2002). In x-ray diffraction studies, amyloid fibrils, including Htt (Perutz et al., 2002b), display a meridional reflection at 4.8 Å and an equatorial reflection around 10 Å, although the exact location and intensity of the latter is variable and depends on side chain composition (Sunde et al., 1997). This is known as a cross-beta pattern. Beta strands are oriented perpendicular to the fibril axis, with main chain hydrogen bonds running parallel to the fibril axis. The distance separating the main chains gives rise to the meridional 4.8 Å reflection. This results in beta sheets running parallel to the fibril axis, made up of strands from different polypeptides (Fig. 1). The approximately 10 Å equatorial reflection arises due to lateral stacking of sheets and can vary slightly with the side chain composition of the strands.

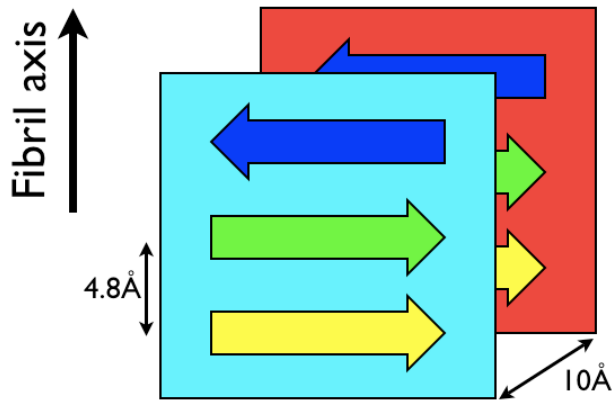

Figure 1. Structure of a generic amyloid fibril. Beta strands separated by 4.8 Å are perpendicular to the fibril axis and can be parallel or antiparallel. Main chain hydrogen bonds run parallel to the fibril axis and connect the strands, forming a beta sheet. Adjacent beta sheets are separated by about 10 Å.

Although amyloid protofibrils classically share the two features of beta strands running perpendicular to the fibril axis and intersheet stacking, these requirements can be satisfied in a variety of ways. Thus, there is no unique amyloid structure; they can differ substantially in their fine structure (Jahn et al., 2010). The exact structure will be determined by the length of the strands, their arrangement relative to one another, i.e., parallel versus antiparallel, and their connectivity, i.e., are the strands connected within the same sheet, between sheets, or not at all. The fine structures of several amyloid protofibrils have been investigated using solid-state nuclear magnetic resonance (NMR) or electron paramagnetic resonance (EPR). Aβ amyloid structures can differ in the length of their amyloidogenic core regions as well as the arrangement of beta strands. The smallest Aβ amyloid, octanoyl Aβ (16-22) has a core of seven amino acids with beta strands arranged parallel and in

register, i.e., identical residues from adjacent proteins stack (Gordon et al., 2004). Octanoyl Aβ is unusual, since nearly all amyloids containing cores of less than 20 amino acids have beta strands that are antiparallel, including Aβ (11-25) (Petkova et al., 2004), Aβ (16-22) (Balbach et al., 2000), Aβ (14-23) (Bu et al., 2007), and Aβ (34-42) (Lansbury et al., 1995). Amyloid cores longer than 20 amino acids almost exclusively form parallel, in-register beta sheets in which identical residues in adjacent proteins stack in close proximity (Margittai and Langen, 2008). This includes Aβ (1-40) (Balbach et al., 2002) and Aβ (1-42) (Antzutkin et al., 2002), as well as other disease-associated amyloids, such as islet amyloid polypeptide (IAPP) in type 2 diabetes (Jayasinghe and Langen, 2004; Luca et al., 2007), α-synuclein in Parkinson's disease (Der-Sarkissian et al., 2003; Chen et al., 2007), tau in tauopathies (Margittai and Langen, 2004, 2006), human prion protein in transmissible spongiform encephalopathies (Cobb et al., 2007) and beta 2 microglobulin in dialysis related amyloidosis (Iwata et al., 2006).

Polyglutamine structure

Molecular mechanics calculations indicate that poly-L-amino acid chains can spontaneously form a μ-helix, which contains a central pore (Monoi, 1995). Polyglutamine is especially stable and can permeabilize membranes when more than 37Q are in the chain (Monoi et al., 2000). However, this structure does not explain the observed reflections of polyQ aggregates (Sharma et al., 2005). Based on an x-ray diffraction study of poly-L-glutamine ($D_2Q_{15}K_2$), Perutz originally proposed that polyglutamine formed beta sheets held together by main chain and side chain

hydrogen bonds (Perutz et al., 1994). However, based on the same data, but ignoring a major reflection at 8.3Å, Perutz later proposed a different model for amyloid fibrils consisting of a beta helix with each turn of the helix consisting of 20 glutamines (Perutz et al., 2002a). Main chain hydrogen bonds along the fibril axis provide stability, when more than one turn is present, forming a hollow, water-filled nanotube. The side chain amides also form hydrogen bonds running roughly parallel to the axis of the fibril, stabilizing the structure. Perutz speculated that this structure could explain why fewer than 40 CAG repeats are not toxic in polyQ diseases, since two turns (40Q) would be required to form a stable hydrogen-bonded structure. Many amyloid proteins share an ability to permeabilize membranes (Kayed et al., 2004; Glabe and Kayed, 2006). Similarly to the μ-helix, the Perutz structure suggested a means of toxicity, in which the nanotube inserts itself into a cell membrane, increasing its permeability to ions (Singer and Dewji, 2006). This initially made the beta helix nanotube an attractive generic amyloid structure.

Molecular dynamics studies have confirmed that Perutz's structure is at least theoretically possible. Its stability increases greatly when the number of glutamines exceeds 30, if one begins with a fully hydrogen bonded structure (Ogawa et al., 2008). One study predicted a compact ellipsoid structure with 41Q and hollow nanotubes with higher numbers of Gln residues (Merlino et al., 2006). Another study concluded that circular geometries are unfavorable but that a triangular arrangement with 18 residues per coil is stable (Stork et al., 2005), more in line with the toxicity threshold of Htt of 36Q. Although direct experimental evidence for the structure is lacking, annular intermediates have been observed for Htt (Wacker et

al., 2004; Legleiter et al., 2010), which form spontaneously in computational studies modeling polyQ (Marchut and Hall, 2006).

However, hydrogen/deuterium exchange experiments have cast doubt on the Perutz model as a general model for amyloid fibrils (Dzwolak et al., 2006). Also, x-ray diffraction experiments using polyQ peptides of various lengths show no structural changes in peptides larger than 40Q (Sharma et al., 2005). In this study, the polyQ peptides form slabs of beta sheets and do not form nanotubes. Furthermore, the calculated diffraction pattern for a hollow nanotube does not match the experimentally observed pattern (Jahn et al., 2010).

An alternative interpretation of Perutz's x-ray data was offered by Sikorski and Atkins (Sikorski and Atkins, 2005), who argue that the data support an antiparallel beta-sheet structure formed by hairpins of the $D_2Q_{15}K_2$ peptide, in which the intersheet distance is shifted to 8.3 Å (not 10 Å) due to interdigitation of the glutamine side chains. In this model, the mainchain hydrogen bonds along the fibril axis alternate between intra- and intermolecular bonds. The calculated diffraction pattern from this model matches very well with the experimental data (Jahn et al., 2010).

Another group obtained crystal structures of assemblies formed by polyglutamine peptides of different lengths (Q8, Q15, Q45)(Sharma et al., 2005). Although it is not clear what relation these assemblies bear to fibrils, all form similar beta crystallites, in which extended antiparallel beta strands stack to form sheets. The model for Q45 indicates that it has multiple reverse turns and four strands that each has seven Gln residues (Fig. 2). These four strands form a beta sheet, which can

then assemble head to tail with other beta sheets along the fibril axis. This model is supported by kinetic experiments, in which Q45 appears to form an antiparallel beta sheet structure consisting of strands of five to eight glutamines connected by four-residue reverse turns induced by interspersed proline/glycine pairs or D-proline (Thakur and Wetzel, 2002). In an extension of this work, Poirier introduced proline/glycine pairs into the polyQ region of HDx1 to induce reverse turns. In this case, HDx1 maintains its aggregation potential, as well as its toxicity (Poirier et al., 2005), indicating that antiparallel beta sheets may be important in the formation of Htt fibrils. While these experiments may support a beta sheet that has reverse turns, the interspersed residues may also accommodate other types of turns, as there are few conformational constraints in mixed chiral (D-L) amino acid sequences (Venkatraman et al., 2001).

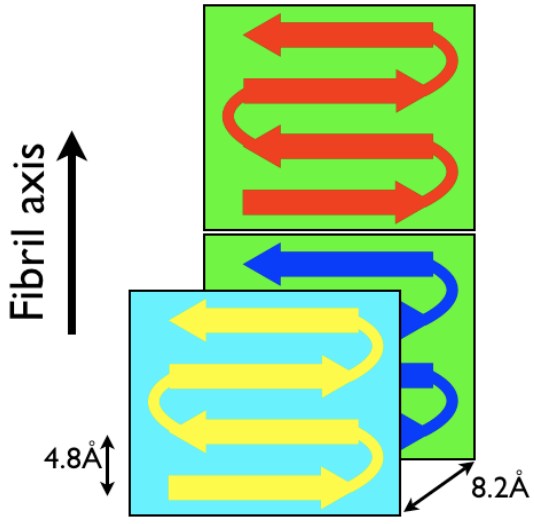

Figure 2. A beta reverse turn model for polyglutamine and HDx1. Reverse turns connect beta strands, forming a beta sheet that is parallel. Each molecule contributes multiple beta strands to each sheet.

In a possible contradiction to the antiparallel beta sheet model, fluorescence energy transfer occurs in mutant Htt when the donor and acceptor molecules are on the same end of the polyglutamine strand, indicating that a parallel beta strand may be dominant (Takahashi et al., 2008). However, although other glutamine containing proteins did not give FRET signals when the fluorophores were on opposite sides of the molecules, this was not specifically tested for Htt. Furthermore, since the distances measured by FRET are relatively large, this may merely indicate that the C-termini are within FRET distance (<100Å) of each other, rather than speak to the arrangement of strands within the glutamine region.

Flanking regions

Recent work on Htt has focused on the role of flanking regions in modulating fibril formation. Removal of the polyproline sequences C-terminal to the glutamine caused aggregation of a GST-HDx1 fusion protein without cleavage of the GST moiety (Hollenbach et al., 1999). In a crystal structure of monomeric, nonfibrillar Htt, the polyproline region C-terminal to the polyQ stretch adopts a polyproline helix conformation (Kim et al., 2009), which can propagate into the polyQ region. In synthetic peptides, polyproline stretches reduce the tendency of polyglutamine to adopt a beta sheet structure (Darnell et al., 2007; Darnell et al., 2009), as well as reduce the kinetics of aggregation (Bhattacharyya et al., 2006; Thakur et al., 2009).

The 17 amino acid N-terminus may transiently adopt an alpha helical structure (Atwal et al., 2007; Kim et al., 2009; Thakur et al., 2009), which can

similarly extend into the polyQ region (Kim et al., 2009). As the polyQ length increases, the N-terminal sequence greatly accelerates aggregation, whether it is N-terminal or C-terminal to the polyQ region (Thakur et al., 2009). As the polyQ length increases, the N-terminus becomes elongated (Thakur et al., 2009) and either disordered (Williamson et al., 2009) or possibly adopts beta sheet conformation (Lakhani et al., 2010). Finally, the N-terminus interacts with other unfolded N-termini, which may initiate a complex aggregation mechanism (Thakur et al., 2009). Indeed, the nonpolar face of the alpha helical region (amino acids 4-12) may normally interact homotypically with other N-termini (Tam et al., 2009) and heterotypically with membranes (Atwal et al., 2007).

Electron Paramagnetic Resonance

Electron paramagnetic resonance (EPR) is a spectroscopic method that takes advantage of the splitting of electron spin energy levels of unpaired electrons in an applied magnetic field. When an external magnetic field is applied, the electron spin of an unpaired electron will tend to align with the field or against it. This separation of the energy levels is known as the Zeeman effect, and the amount of the energy required to flip the spin of the electron depends on the magnitude of the applied magnetic field. It is this energy that is measured in EPR. In order to measure the EPR spectrum, either the microwave-frequency energy used to excite the electron or the magnetic field is held constant, while the other is swept. In a typical experiment, the energy is held constant, while the magnetic field is swept.

This gives an EPR spectrum, which is reported as the first derivative of the absorbance plotted against magnetic field.

Furthermore, the electron is influenced by magnetic fields stemming from the nucleus of its atom, leading to hyperfine coupling. It is well known that this interaction is orientation dependent and leads to anisotropic broadening of the EPR spectrum. However, if the motion of the nucleus relative to the electron is fast on the EPR timescale (<1 nanosecond), the field experienced by the electron averages out and the broadening disappears. This makes EPR-sensitive electrons useful reporters of molecular motion.

Site-directed spin labeling

In site-directed spin labeling (SDSL), a cysteine is introduced into a protein using site-directed mutagenesis. This cysteine is then labeled with an EPR-sensitive spin label, usually a disulfide-coupled nitroxide radical (Figure 3A). An EPR spectrum is then collected, which gives information on the backbone mobility (Columbus and Hubbell, 2002). Mobile residues will have three sharp lines (Figure 3B), while broadening occurs at immobile residues (Figure 3B). If labels approach to within 20Å, as is expected for amyloid fibrils, the labels can interact, leading to broadening of the spectrum and a decrease in amplitude of the central line (Figure 3C). This broadening can be exploited to get distance information by comparing fully labeled protein spectra with those of sparsely labeled protein and calculating a broadening function (Altenbach et al., 2001). If multiple labels are very close, such that their electron orbitals overlap, spin exchange occurs (Figure 3D). This is

common in disease-associated amyloid fibrils and indicates a parallel in-register structure (Margittai and Langen, 2008). Finally, paramagnetic reagents can be used to probe whether a site lies buried or at the surface and at what distance it is from the hydrophobic interface (Altenbach et al., 2005). Taken together, these methods can give atomistic resolution structures (Jao et al., 2008) comparable with nuclear magnetic resonance or X-ray crystallography structures.

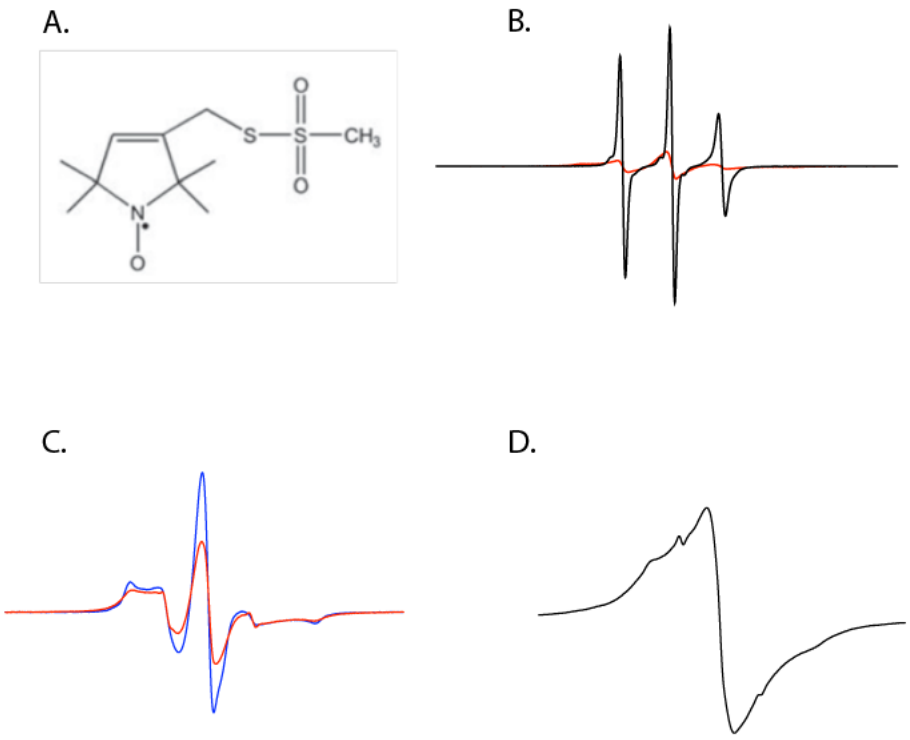

Figure 3. Principles of SDSL EPR. A. [1-oxy-2, 2, 5, 5-tetramethyl-pyrroline-3-methyl]-methanethiosulfonate (MTSL) is commonly used to label cysteines for EPR. B. Changes in a site as it goes from mobile to immobilized (red spectrum). C. Spectral changes in a weakly interacting site. D. Spin exchange in an amyloid fibril that is parallel and in-register.

Application to HDx1 fibrils

A very brief summary of what is definitively known about the structure of HDx1 fibrils is that they have a cross-beta structure. Beyond that, much is inferred from circumstantial evidence derived from naked glutamine homopolymers and the soluble HDx1 protein. There is little direct evidence from structural experiments to support or exclude any specific model. It is not clear which residues form the amyloid core, what the arrangement of the strands is, or how the flanking regions are accommodated in the fibril. EPR can be used to obtain structural information at several levels of resolution and has been successfully used to derive structures for disease-associated amyloid fibrils (Margittai and Langen, 2008). It is an ideal technique to begin to more closely define the structure of HDx1 fibrils.

REFERENCES

Alonso ME, Yescas P, Rasmussen A, Ochoa A, Macias R, Ruiz I, Suastegui R (2002) Homozygosity in Huntington's disease: new ethical dilemma caused by molecular diagnosis. Clin Genet 61:437-442.

Altenbach C, Oh KJ, Trabanino RJ, Hideg K, Hubbell WL (2001) Estimation of inter-residue distances in spin labeled proteins at physiological temperatures: experimental strategies and practical limitations. Biochemistry 40:15471-15482.

Altenbach C, Froncisz W, Hemker R, McHaourab H, Hubbell WL (2005) Accessibility of nitroxide side chains: absolute Heisenberg exchange rates from power saturation EPR. Biophys J 89:2103-2112.

Andrew SE, Goldberg YP, Kremer B, Telenius H, Theilmann J, Adam S, Starr E, Squitieri F, Lin B, Kalchman MA, et al. (1993) The relationship between trinucleotide (CAG) repeat length and clinical features of Huntington's disease. Nat Genet 4:398-403.

Antzutkin ON, Leapman RD, Balbach JJ, Tycko R (2002) Supramolecular structural constraints on Alzheimer's beta-amyloid fibrils from electron microscopy and solid-state nuclear magnetic resonance. Biochemistry 41:15436-15450.

Arrasate M, Mitra S, Schweitzer ES, Segal MR, Finkbeiner S (2004) Inclusion body formation reduces levels of mutant huntingtin and the risk of neuronal death. Nature 431:805-810.

Atwal RS, Xia J, Pinchev D, Taylor J, Epand RM, Truant R (2007) Huntingtin has a membrane association signal that can modulate huntingtin aggregation, nuclear entry and toxicity. Hum Mol Genet 16:2600-2615.

Aylward EH, Schwartz J, Machlin S, Pearlson G (1991) Bicaudate ratio as a measure of caudate volume on MR images. AJNR Am J Neuroradiol 12:1217-1222.

Baglioni S, Casamenti F, Bucciantini M, Luheshi LM, Taddei N, Chiti F, Dobson CM, Stefani M (2006) Prefibrillar amyloid aggregates could be generic toxins in higher organisms. J Neurosci 26:8160-8167.

Balbach JJ, Petkova AT, Oyler NA, Antzutkin ON, Gordon DJ, Meredith SC, Tycko R (2002) Supramolecular structure in full-length Alzheimer's beta-amyloid fibrils: evidence for a parallel beta-sheet organization from solid-state nuclear magnetic resonance. Biophys J 83:1205-1216.

Balbach JJ, Ishii Y, Antzutkin ON, Leapman RD, Rizzo NW, Dyda F, Reed J, Tycko R (2000) Amyloid fibril formation by A beta 16-22, a seven-residue fragment of the Alzheimer's beta-amyloid peptide, and structural characterization by solid state NMR. Biochemistry 39:13748-13759.

Berrios GE, Wagle AC, Markova IS, Wagle SA, Rosser A, Hodges JR (2002) Psychiatric symptoms in neurologically asymptomatic Huntington's disease gene carriers: a comparison with gene negative at risk subjects. Acta Psychiatr Scand 105:224-230.

Bhattacharyya A, Thakur AK, Chellgren VM, Thiagarajan G, Williams AD, Chellgren BW, Creamer TP, Wetzel R (2006) Oligoproline effects on polyglutamine conformation and aggregation. J Mol Biol 355:524-535.

Biglan KM, Ross CA, Langbehn DR, Aylward EH, Stout JC, Queller S, Carlozzi NE, Duff K, Beglinger LJ, Paulsen JS (2009) Motor abnormalities in premanifest persons with Huntington's disease: the PREDICT-HD study. Mov Disord 24:1763-1772.

Brinkman RR, Mezei MM, Theilmann J, Almqvist E, Hayden MR (1997) The likelihood of being affected with Huntington disease by a particular age, for a specific CAG size. Am J Hum Genet 60:1202-1210.

Bu Z, Shi Y, Callaway DJ, Tycko R (2007) Molecular alignment within beta-sheets in Abeta(14-23) fibrils: solid-state NMR experiments and theoretical predictions. Biophys J 92:594-602.

Chen M, Margittai M, Chen J, Langen R (2007) Investigation of alpha-synuclein fibril structure by site-directed spin labeling. J Biol Chem 282:24970-24979.

Chun W, Lesort M, Lee M, Johnson GV (2002) Mutant huntingtin aggregates do not sensitize cells to apoptotic stressors. FEBS Lett 515:61-65.

Cobb NJ, Sonnichsen FD, McHaourab H, Surewicz WK (2007) Molecular architecture of human prion protein amyloid: a parallel, in-register beta-structure. Proc Natl Acad Sci U S A 104:18946-18951.

Colby DW, Chu Y, Cassady JP, Duennwald M, Zazulak H, Webster JM, Messer A, Lindquist S, Ingram VM, Wittrup KD (2004) Potent inhibition of huntingtin aggregation and cytotoxicity by a disulfide bond-free single-domain intracellular antibody. Proc Natl Acad Sci U S A 101:17616-17621.

Columbus L, Hubbell WL (2002) A new spin on protein dynamics. Trends Biochem Sci 27:288-295.

Crick SL, Jayaraman M, Frieden C, Wetzel R, Pappu RV (2006) Fluorescence correlation spectroscopy shows that monomeric polyglutamine molecules form collapsed structures in aqueous solutions. Proc Natl Acad Sci U S A 103:16764-16769.

Dahlgren PR, Karymov MA, Bankston J, Holden T, Thumfort P, Ingram VM, Lyubchenko YL (2005) Atomic force microscopy analysis of the Huntington protein nanofibril formation. Nanomedicine 1:52-57.

Darnell G, Orgel JP, Pahl R, Meredith SC (2007) Flanking polyproline sequences inhibit beta-sheet structure in polyglutamine segments by inducing PPII-like helix structure. J Mol Biol 374:688-704.

Darnell GD, Derryberry J, Kurutz JW, Meredith SC (2009) Mechanism of cis-inhibition of polyQ fibrillation by polyP: PPII oligomers and the hydrophobic effect. Biophys J 97:2295-2305.

Der-Sarkissian A, Jao CC, Chen J, Langen R (2003) Structural organization of alpha-synuclein fibrils studied by site-directed spin labeling. J Biol Chem 278:37530-37535.

DiFiglia M, Sapp E, Chase KO, Davies SW, Bates GP, Vonsattel JP, Aronin N (1997) Aggregation of huntingtin in neuronal intranuclear inclusions and dystrophic neurites in brain. Science 277:1990-1993.

Dzwolak W, Loksztejn A, Smirnovas V (2006) New insights into the self-assembly of insulin amyloid fibrils: an H-D exchange FT-IR study. Biochemistry 45:8143-8151.

Fennema-Notestine C, Archibald SL, Jacobson MW, Corey-Bloom J, Paulsen JS, Peavy GM, Gamst AC, Hamilton JM, Salmon DP, Jernigan TL (2004) In vivo evidence of cerebellar atrophy and cerebral white matter loss in Huntington disease. Neurology 63:989-995.

Gatchel JR, Zoghbi HY (2005) Diseases of unstable repeat expansion: mechanisms and common principles. Nat Rev Genet 6:743-755.

Geevasinga N, Richards FH, Jones KJ, Ryan MM (2006) Juvenile Huntington disease. J Paediatr Child Health 42:552-554.

Glabe CG, Kayed R (2006) Common structure and toxic function of amyloid oligomers implies a common mechanism of pathogenesis. Neurology 66:S74-78.

Gordon DJ, Balbach JJ, Tycko R, Meredith SC (2004) Increasing the amphiphilicity of an amyloidogenic peptide changes the beta-sheet structure in the fibrils from antiparallel to parallel. Biophys J 86:428-434.

Groen JL, de Bie RM, Foncke EM, Roos RA, Leenders KL, Tijssen MA (2010) Late-onset Huntington disease with intermediate CAG repeats: true or false? J Neurol Neurosurg Psychiatry 81:228-230.

Gutekunst CA, Li SH, Yi H, Mulroy JS, Kuemmerle S, Jones R, Rye D, Ferrante RJ, Hersch SM, Li XJ (1999) Nuclear and neuropil aggregates in Huntington's disease: relationship to neuropathology. J Neurosci 19:2522-2534.

Harper PS (1992) The epidemiology of Huntington's disease. Hum Genet 89:365-376.

Hedreen JC, Peyser CE, Folstein SE, Ross CA (1991) Neuronal loss in layers V and VI of cerebral cortex in Huntington's disease. Neurosci Lett 133:257-261.

Heiser V, Scherzinger E, Boeddrich A, Nordhoff E, Lurz R, Schugardt N, Lehrach H, Wanker EE (2000) Inhibition of huntingtin fibrillogenesis by specific antibodies and small molecules: implications for Huntington's disease therapy. Proc Natl Acad Sci U S A 97:6739-6744.

Hollenbach B, Scherzinger E, Schweiger K, Lurz R, Lehrach H, Wanker EE (1999) Aggregation of truncated GST-HD exon 1 fusion proteins containing normal range and expanded glutamine repeats. Philos Trans R Soc Lond B Biol Sci 354:991-994.

Huang CC, Faber PW, Persichetti F, Mittal V, Vonsattel JP, MacDonald ME, Gusella JF (1998) Amyloid formation by mutant huntingtin: threshold, progressivity and recruitment of normal polyglutamine proteins. Somat Cell Mol Genet 24:217-233.

Huntington's Disease Collaborative Research Group (1993) A novel gene containing a trinucleotide repeat that is expanded and unstable on Huntington's disease chromosomes. Cell 72:971-983.

Iwata K, Fujiwara T, Matsuki Y, Akutsu H, Takahashi S, Naiki H, Goto Y (2006) 3D structure of amyloid protofilaments of beta2-microglobulin fragment probed by solid-state NMR. Proc Natl Acad Sci U S A 103:18119-18124.

Jahn TR, Makin OS, Morris KL, Marshall KE, Tian P, Sikorski P, Serpell LC (2010) The common architecture of cross-beta amyloid. J Mol Biol 395:717-727.

Jao CC, Hegde BG, Chen J, Haworth IS, Langen R (2008) Structure of membrane-bound alpha-synuclein from site-directed spin labeling and computational refinement. Proc Natl Acad Sci U S A 105:19666-19671.

Jayasinghe SA, Langen R (2004) Identifying structural features of fibrillar islet amyloid polypeptide using site-directed spin labeling. J Biol Chem 279:48420-48425.

Julien CL, Thompson JC, Wild S, Yardumian P, Snowden JS, Turner G, Craufurd D (2007) Psychiatric disorders in preclinical Huntington's disease. J Neurol Neurosurg Psychiatry 78:939-943.

Jurgens CK, van de Wiel L, van Es AC, Grimbergen YM, Witjes-Ane MN, van der Grond J, Middelkoop HA, Roos RA (2008) Basal ganglia volume and clinical correlates in 'preclinical' Huntington's disease. J Neurol 255:1785-1791.

Kayed R, Sokolov Y, Edmonds B, McIntire TM, Milton SC, Hall JE, Glabe CG (2004) Permeabilization of lipid bilayers is a common conformation-dependent activity of soluble amyloid oligomers in protein misfolding diseases. J Biol Chem 279:46363-46366.

Kayed R, Head E, Sarsoza F, Saing T, Cotman CW, Necula M, Margol L, Wu J, Breydo L, Thompson JL, Rasool S, Gurlo T, Butler P, Glabe CG (2007) Fibril specific, conformation dependent antibodies recognize a generic epitope common to amyloid fibrils and fibrillar oligomers that is absent in prefibrillar oligomers. Mol Neurodegener 2:18.

Kenney C, Powell S, Jankovic J (2007) Autopsy-proven Huntington's disease with 29 trinucleotide repeats. Mov Disord 22:127-130.

Khoshnan A, Ko J, Patterson PH (2002) Effects of intracellular expression of anti-huntingtin antibodies of various specificities on mutant huntingtin aggregation and toxicity. Proc Natl Acad Sci U S A 99:1002-1007.

Kim MW, Chelliah Y, Kim SW, Otwinowski Z, Bezprozvanny I (2009) Secondary structure of Huntingtin amino-terminal region. Structure 17:1205-1212.

Kingma EM, van Duijn E, Timman R, van der Mast RC, Roos RA (2008) Behavioural problems in Huntington's disease using the Problem Behaviours Assessment. Gen Hosp Psychiatry 30:155-161.

Kloppel S, Stonnington CM, Petrovic P, Mobbs D, Tuscher O, Craufurd D, Tabrizi SJ, Frackowiak RS (2010) Irritability in pre-clinical Huntington's disease. Neuropsychologia 48:549-557.

Kremer B, Goldberg P, Andrew SE, Theilmann J, Telenius H, Zeisler J, Squitieri F, Lin B, Bassett A, Almqvist E, et al. (1994) A worldwide study of the Huntington's disease mutation. The sensitivity and specificity of measuring CAG repeats. N Engl J Med 330:1401-1406.

Kuemmerle S, Gutekunst CA, Klein AM, Li XJ, Li SH, Beal MF, Hersch SM, Ferrante RJ (1999) Huntington aggregates may not predict neuronal death in Huntington's disease. Ann Neurol 46:842-849.

Kvam E, Nannenga BL, Wang MS, Jia Z, Sierks MR, Messer A (2009) Conformational targeting of fibrillar polyglutamine proteins in live cells escalates aggregation and cytotoxicity. PLoS One 4:e5727.

Lakhani VV, Ding F, Dokholyan NV (2010) Polyglutamine induced misfolding of huntingtin exon1 is modulated by the flanking sequences. PLoS Comput Biol 6:e1000772.

Lansbury PT, Jr., Costa PR, Griffiths JM, Simon EJ, Auger M, Halverson KJ, Kocisko DA, Hendsch ZS, Ashburn TT, Spencer RG, et al. (1995) Structural model for the beta-amyloid fibril based on interstrand alignment of an antiparallel-sheet comprising a C-terminal peptide. Nat Struct Biol 2:990-998.

Legleiter J, Mitchell E, Lotz GP, Sapp E, Ng C, DiFiglia M, Thompson LM, Muchowski PJ (2010) Mutant huntingtin fragments form oligomers in a polyglutamine length-dependent manner in vitro and in vivo. J Biol Chem 285:14777-14790.

Legleiter J, Lotz GP, Miller J, Ko J, Ng C, Williams GL, Finkbeiner S, Patterson PH, Muchowski PJ (2009) Monoclonal antibodies recognize distinct conformational epitopes formed by polyglutamine in a mutant huntingtin fragment. J Biol Chem 284:21647-21658.

Luca S, Yau WM, Leapman R, Tycko R (2007) Peptide conformation and supramolecular organization in amylin fibrils: constraints from solid-state NMR. Biochemistry 46:13505-13522.

Marchut AJ, Hall CK (2006) Spontaneous formation of annular structures observed in molecular dynamics simulations of polyglutamine peptides. Comput Biol Chem 30:215-218.

Margittai M, Langen R (2004) Template-assisted filament growth by parallel stacking of tau. Proc Natl Acad Sci U S A 101:10278-10283.

Margittai M, Langen R (2006) Side chain-dependent stacking modulates tau filament structure. J Biol Chem 281:37820-37827.

Margittai M, Langen R (2008) Fibrils with parallel in-register structure constitute a major class of amyloid fibrils: molecular insights from electron paramagnetic resonance spectroscopy. Q Rev Biophys 41:265-297.

McNeil SM, Novelletto A, Srinidhi J, Barnes G, Kornbluth I, Altherr MR, Wasmuth JJ, Gusella JF, MacDonald ME, Myers RH (1997) Reduced penetrance of the Huntington's disease mutation. Hum Mol Genet 6:775-779.

Meinhardt J, Sachse C, Hortschansky P, Grigorieff N, Fandrich M (2009) Abeta(1-40) fibril polymorphism implies diverse interaction patterns in amyloid fibrils. J Mol Biol 386:869-877.

Merlino A, Esposito L, Vitagliano L (2006) Polyglutamine repeats and beta-helix structure: molecular dynamics study. Proteins 63:918-927.

Mestre T, Ferreira J, Coelho MM, Rosa M, Sampaio C (2009) Therapeutic interventions for symptomatic treatment in Huntington's disease. Cochrane Database Syst Rev:CD006456.

Monoi H (1995) New tubular single-stranded helix of poly-L-amino acids suggested by molecular mechanics calculations: I. Homopolypeptides in isolated environments. Biophys J 69:1130-1141.

Monoi H, Futaki S, Kugimiya S, Minakata H, Yoshihara K (2000) Poly-L-glutamine forms cation channels: relevance to the pathogenesis of the polyglutamine diseases. Biophys J 78:2892-2899.

Nekooki-Machida Y, Kurosawa M, Nukina N, Ito K, Oda T, Tanaka M (2009) Distinct conformations of in vitro and in vivo amyloids of huntingtin-exon1 show different cytotoxicity. Proc Natl Acad Sci U S A 106:9679-9684.

Ogawa H, Nakano M, Watanabe H, Starikov EB, Rothstein SM, Tanaka S (2008) Molecular dynamics simulation study on the structural stabilities of polyglutamine peptides. Comput Biol Chem 32:102-110.

Perutz MF, Johnson T, Suzuki M, Finch JT (1994) Glutamine repeats as polar zippers: their possible role in inherited neurodegenerative diseases. Proc Natl Acad Sci U S A 91:5355-5358.

Perutz MF, Finch JT, Berriman J, Lesk A (2002a) Amyloid fibers are water-filled nanotubes. Proc Natl Acad Sci U S A 99:5591-5595.

Perutz MF, Pope BJ, Owen D, Wanker EE, Scherzinger E (2002b) Aggregation of proteins with expanded glutamine and alanine repeats of the glutamine-rich and asparagine-rich domains of Sup35 and of the amyloid beta-peptide of amyloid plaques. Proc Natl Acad Sci U S A 99:5596-5600.

Petkova AT, Buntkowsky G, Dyda F, Leapman RD, Yau WM, Tycko R (2004) Solid state NMR reveals a pH-dependent antiparallel beta-sheet registry in fibrils formed by a beta-amyloid peptide. J Mol Biol 335:247-260.

Petkova AT, Leapman RD, Guo Z, Yau WM, Mattson MP, Tycko R (2005) Self-propagating, molecular-level polymorphism in Alzheimer's beta-amyloid fibrils. Science 307:262-265.

Poirier MA, Jiang H, Ross CA (2005) A structure-based analysis of huntingtin mutant polyglutamine aggregation and toxicity: evidence for a compact beta-sheet structure. Hum Mol Genet 14:765-774.

Poirier MA, Li H, Macosko J, Cai S, Amzel M, Ross CA (2002) Huntingtin spheroids and protofibrils as precursors in polyglutamine fibrilization. J Biol Chem 277:41032-41037.

Quarrell OW, Rigby AS, Barron L, Crow Y, Dalton A, Dennis N, Fryer AE, Heydon F, Kinning E, Lashwood A, Losekoot M, Margerison L, McDonnell S, Morrison PJ, Norman A, Peterson M, Raymond FL, Simpson S, Thompson E, Warner J (2007) Reduced penetrance alleles for Huntington's disease: a multi-centre direct observational study. J Med Genet 44:e68.

Ravina B, Romer M, Constantinescu R, Biglan K, Brocht A, Kieburtz K, Shoulson I, McDermott MP (2008) The relationship between CAG repeat length and clinical progression in Huntington's disease. Mov Disord 23:1223-1227.

Rosas HD, Hevelone ND, Zaleta AK, Greve DN, Salat DH, Fischl B (2005) Regional cortical thinning in preclinical Huntington disease and its relationship to cognition. Neurology 65:745-747.

Rosas HD, Goodman J, Chen YI, Jenkins BG, Kennedy DN, Makris N, Patti M, Seidman LJ, Beal MF, Koroshetz WJ (2001) Striatal volume loss in HD as measured by MRI and the influence of CAG repeat. Neurology 57:1025-1028.

Rosas HD, Liu AK, Hersch S, Glessner M, Ferrante RJ, Salat DH, van der Kouwe A, Jenkins BG, Dale AM, Fischl B (2002) Regional and progressive thinning of the cortical ribbon in Huntington's disease. Neurology 58:695-701.

Rosas HD, Koroshetz WJ, Chen YI, Skeuse C, Vangel M, Cudkowicz ME, Caplan K, Marek K, Seidman LJ, Makris N, Jenkins BG, Goldstein JM (2003) Evidence for more widespread cerebral pathology in early HD: an MRI-based morphometric analysis. Neurology 60:1615-1620.

Saudou F, Finkbeiner S, Devys D, Greenberg ME (1998) Huntingtin acts in the nucleus to induce apoptosis but death does not correlate with the formation of intranuclear inclusions. Cell 95:55-66.

Scherzinger E, Sittler A, Schweiger K, Heiser V, Lurz R, Hasenbank R, Bates GP, Lehrach H, Wanker EE (1999) Self-assembly of polyglutamine-containing huntingtin fragments into amyloid-like fibrils: implications for Huntington's disease pathology. Proc Natl Acad Sci U S A 96:4604-4609.

Scherzinger E, Lurz R, Turmaine M, Mangiarini L, Hollenbach B, Hasenbank R, Bates GP, Davies SW, Lehrach H, Wanker EE (1997) Huntingtin-encoded polyglutamine expansions form amyloid-like protein aggregates in vitro and in vivo. Cell 90:549-558.

Sharma D, Shinchuk LM, Inouye H, Wetzel R, Kirschner DA (2005) Polyglutamine homopolymers having 8-45 residues form slablike beta-crystallite assemblies. Proteins 61:398-411.

Sieradzan KA, Mechan AO, Jones L, Wanker EE, Nukina N, Mann DM (1999) Huntington's disease intranuclear inclusions contain truncated, ubiquitinated huntingtin protein. Exp Neurol 156:92-99.

Sikorski P, Atkins E (2005) New model for crystalline polyglutamine assemblies and their connection with amyloid fibrils. Biomacromolecules 6:425-432.

Singer SJ, Dewji NN (2006) Evidence that Perutz's double-beta-stranded subunit structure for beta-amyloids also applies to their channel-forming structures in membranes. Proc Natl Acad Sci U S A 103:1546-1550.

Southwell AL, Khoshnan A, Dunn DE, Bugg CW, Lo DC, Patterson PH (2008) Intrabodies binding the proline-rich domains of mutant huntingtin increase its turnover and reduce neurotoxicity. J Neurosci 28:9013-9020.

Squitieri F, Gellera C, Cannella M, Mariotti C, Cislaghi G, Rubinsztein DC, Almqvist EW, Turner D, Bachoud-Levi AC, Simpson SA, Delatycki M, Maglione V, Hayden MR, Donato SD (2003) Homozygosity for CAG mutation in Huntington disease is associated with a more severe clinical course. Brain 126:946-955.

Stork M, Giese A, Kretzschmar HA, Tavan P (2005) Molecular dynamics simulations indicate a possible role of parallel beta-helices in seeded aggregation of poly-Gln. Biophys J 88:2442-2451.

Sunde M, Serpell LC, Bartlam M, Fraser PE, Pepys MB, Blake CC (1997) Common core structure of amyloid fibrils by synchrotron X-ray diffraction. J Mol Biol 273:729-739.

Tabrizi SJ, Langbehn DR, Leavitt BR, Roos RA, Durr A, Craufurd D, Kennard C, Hicks SL, Fox NC, Scahill RI, Borowsky B, Tobin AJ, Rosas HD, Johnson H, Reilmann R, Landwehrmeyer B, Stout JC (2009) Biological and clinical manifestations of Huntington's disease in the longitudinal TRACK-HD study: cross-sectional analysis of baseline data. Lancet Neurol 8:791-801.

Tagawa K, Hoshino M, Okuda T, Ueda H, Hayashi H, Engemann S, Okado H, Ichikawa M, Wanker EE, Okazawa H (2004) Distinct aggregation and cell death patterns among different types of primary neurons induced by mutant huntingtin protein. J Neurochem 89:974-987.

Takahashi T, Kikuchi S, Katada S, Nagai Y, Nishizawa M, Onodera O (2008) Soluble polyglutamine oligomers formed prior to inclusion body formation are cytotoxic. Hum Mol Genet 17:345-356.

Tam S, Spiess C, Auyeung W, Joachimiak L, Chen B, Poirier MA, Frydman J (2009) The chaperonin TRiC blocks a huntingtin sequence element that promotes the conformational switch to aggregation. Nat Struct Mol Biol 16:1279-1285.

Thakur AK, Wetzel R (2002) Mutational analysis of the structural organization of polyglutamine aggregates. Proc Natl Acad Sci U S A 99:17014-17019.

Thakur AK, Jayaraman M, Mishra R, Thakur M, Chellgren VM, Byeon IJ, Anjum DH, Kodali R, Creamer TP, Conway JF, Gronenborn AM, Wetzel R (2009) Polyglutamine disruption of the huntingtin exon 1 N terminus triggers a complex aggregation mechanism. Nat Struct Mol Biol 16:380-389.

Tycko R (2006) Molecular structure of amyloid fibrils: insights from solid-state NMR. Q Rev Biophys 39:1-55.

van Roon-Mom WM, Hogg VM, Tippett LJ, Faull RL (2006) Aggregate distribution in frontal and motor cortex in Huntington's disease brain. Neuroreport 17:667-670.

Vardi J, Flechter S, Rabi JM, Streifler M (1979) R.H.I.S.A. -- cysternography study in sporadic choreo-athetotic syndrome accompanied with dementia (sporadic Huntington disease). Riv Patol Nerv Ment 100:245-254.

Vassos E, Panas M, Kladi A, Vassilopoulos D (2007) Higher levels of extroverted hostility detected in gene carriers at risk for Huntington's disease. Biol Psychiatry 62:1347-1352.

Venkatraman J, Shankaramma SC, Balaram P (2001) Design of folded peptides. Chem Rev 101:3131-3152.

Vonsattel JP, DiFiglia M (1998) Huntington disease. J Neuropathol Exp Neurol 57:369-384.

Vonsattel JP, Myers RH, Stevens TJ, Ferrante RJ, Bird ED, Richardson EP, Jr. (1985) Neuropathological classification of Huntington's disease. J Neuropathol Exp Neurol 44:559-577.

Wacker JL, Zareie MH, Fong H, Sarikaya M, Muchowski PJ (2004) Hsp70 and Hsp40 attenuate formation of spherical and annular polyglutamine oligomers by partitioning monomer. Nat Struct Mol Biol 11:1215-1222.

Walker FO (2007) Huntington's Disease. Semin Neurol 27:143-150.

Wexler NS, Young AB, Tanzi RE, Travers H, Starosta-Rubinstein S, Penney JB, Snodgrass SR, Shoulson I, Gomez F, Ramos Arroyo MA, et al. (1987) Homozygotes for Huntington's disease. Nature 326:194-197.

Wexler NS et al. (2004) Venezuelan kindreds reveal that genetic and environmental factors modulate Huntington's disease age of onset. Proc Natl Acad Sci U S A 101:3498-3503.

Williamson TE, Vitalis A, Crick SL, Pappu RV (2009) Modulation of Polyglutamine Conformations and Dimer Formation by the N-Terminus of Huntingtin. J Mol Biol.

Wolf RC, Vasic N, Schonfeldt-Lecuona C, Ecker D, Landwehrmeyer GB (2009) Cortical dysfunction in patients with Huntington's disease during working memory performance. Hum Brain Mapp 30:327-339.

Yang W, Dunlap JR, Andrews RB, Wetzel R (2002) Aggregated polyglutamine peptides delivered to nuclei are toxic to mammalian cells. Hum Mol Genet 11:2905-2917.

Zandomeneghi G, Krebs MR, McCammon MG, Fandrich M (2004) FTIR reveals structural differences between native beta-sheet proteins and amyloid fibrils. Protein Sci 13:3314-3321.

Zoghbi HY, Orr HT (2000) Glutamine repeats and neurodegeneration. Annu Rev Neurosci 23:217-247.

Chapter 2

Domain Organization of Mutant Huntingtin Fibrils

Charles W. Bugg, Torsten Fischer, Paul H. Patterson, and Ralf Langen

INTRODUCTION

Huntington's disease (HD) is a progressive, fatal neurodegenerative disorder caused by a polyglutamine (polyQ) expansion mutation in the first exon of huntingtin gene (Htt), a large protein with 57 exons (The Huntington's Disease Collaborative Research Group, 1993). Like other polyQ diseases (Zoghbi and Orr, 2000), there is a threshold of about 40Q beyond which the patient gets the disease, and the age of onset of the disease (Brinkman et al., 1997) and the severity (Ravina et al., 2008) are inversely correlated with the length of the expansion. Adult patients typically have 40-58Q and are diagnosed in middle age after presenting with dancelike motor symptoms known as chorea (Walker, 2007). Expansions beyond 60Q cause juvenile HD (age of onset <20) and are associated with symptoms of dystonia, parkinsonism, and seizures with relatively little chorea (Geevasinga et al., 2006). HD is associated with neurodegeneration, especially of the caudate nucleus of the striatum (Vonsattel et al., 1985), and the severity of neurodegeneration correlates with polyQ length (Rosas et al., 2001).

Expressing mutant Htt in mice as a transgene causes motor deficits that resemble the human disease. Expression of Htt exon 1 (HDx1) with a polyQ expansion is sufficient to cause disease in mice (Mangiarini et al., 1996). These mice have several symptoms of HD, including choreiform movements. Mouse models that

express HDx1 have a more severe and shorter disease course than those that express full-length mutant Htt (Hodgson et al., 1999; Reddy et al., 1999).

A hallmark of HD in mice and humans is the formation of intracellular and intranuclear inclusions. In patients, these inclusions consist largely of N-terminal fragments of mutant Htt that are often ubiquitinated (DiFiglia et al., 1997; Sieradzan et al., 1999). Aggregates purified from HD patients' brains bind Congo red with green birefringence, indicating that they have an amyloid structure (Huang et al., 1998). *In vitro*, mutant HDx1 spontaneously forms fibrils that similarly bind Congo red (Huang et al., 1998). Fourier transform infrared spectrometry was used to show that these fibrils have a beta sheet signature similar to amyloid fibrils (Poirier et al., 2002). Furthermore, HDx1 fibrils have an x-ray diffraction pattern consistent with the cross-beta structure characteristic of amyloid fibrils (Perutz et al., 2002b). In the cross-beta structure, beta strands separated by 4.8 Å run normal to the fibril axis and form a sheet that is parallel to the fibril axis. Sheets associate laterally at an intersheet distance of 8-10 Å.

Building on the basic skeleton provided by the cross-beta model, amyloid fibrils mainly differ in the length of the strands, the arrangement of their strands (parallel vs. antiparallel), as well as their connectivity (within the same sheet or between adjacent sheets), which determines the number of strands a single molecule contributes to a sheet. Altering these parameters gives rise to amyloid models consisting of single unconnected beta strands (Gordon et al., 2004), beta sandwiches (Petkova et al., 2002; Luca et al., 2007) and superpleated sheets (Kajava et al., 2004), in which the connection runs between adjacent sheets, and antiparallel

beta sheets in which strands within a sheet are connected by hairpin turns (Thakur and Wetzel, 2002; Poirier et al., 2005; Sharma et al., 2005). Notable exceptions to this architecture are beta solenoids (Wasmer et al., 2008) and beta helices (Perutz et al., 2002a). Computational modeling of the beta helix suggests that it may flatten to resemble a compact ellipsoid (Merlino et al., 2006), in which case it could closely resemble the cross-beta architecture with each molecule contributing two or more strands to each of two adjacent sheets. Most disease-causing amyloids, including Aβ (Alzheimer's disease), α-synuclein (Parkinson's disease), tau (tauopathies), islet amyloid polypeptide (type 2 diabetes), and prion protein (transmissible spongiform encephalopathies), have a parallel, in-register arrangement of beta strands, in which identical residues in adjacent strands stack (Margittai and Langen, 2008). However, it is unknown what the structure of the HDx1 fibril core is.

HDx1 consists of three domains, the N-terminal 17 amino acids, the glutamine region that is thought to form the cross-beta structure, and a C-terminus that is rich in prolines. The flanking regions in HDx1 modulate its aggregation. Aggregation may be promoted by the N-terminus, which may be alpha helical in nonfibrillar Htt, but becomes unfolded when a polyQ expansion is present (Thakur et al., 2009). The proline-rich C-terminus is thought to retard fibril formation by preventing the structural transition of the polyQ region. Its removal causes aggregation of an otherwise soluble GST-HDx1 fusion protein (Hollenbach et al., 1999). A crystal structure for soluble wildtype Htt supports this hypothesis (Kim et al., 2009). In this structure, a polyproline helix extends from the C-terminus into the polyQ domain. Similarly, an N-terminal alpha helix extends into the glutamine

domain while the interior of the polyQ remains disordered. Thus, there is a considerable literature describing the role of flanking regions in soluble, nonfibrillar HDx1, but the arrangement of the flanking regions in the fibril has not been investigated.

We have used electron paramagnetic resonance to characterize the domain organization of HDx1 aggregates. We show that much of the polyQ region is immobilized in the fibril, but does not have the parallel, in-register signature characteristic of many other disease-causing amyloid structures. The C-terminus remains mobile and acts to increase the mobility of the C-terminal portion of the polyQ region. Finally, the N-terminus has complex EPR spectra, indicating that it can assume different conformations, either within the same fibril or in different fibrils.

RESULTS

HDx1 forms fibrils and becomes less mobile

HDx1 with 46Q and an N-terminal thioredoxin fusion protein was labeled at specific sites (Figure 1A) using the EPR-sensitive spin label, MTSL. Upon cleavage of the fusion partner, HDx1 forms fibrils (100-500 nm length, 10-12 nm diameter) that are predominantly found in bundles of laterally associated fibrils (Figure 1B). Our findings are consistent with fibril dimensions and morphology found in previous studies (Scherzinger et al., 1997; Scherzinger et al., 1999; Poirier et al., 2002).

As shown for a representative site, the fusion protein has three sharp lines characteristic of a mobile site in a non-globular protein (Figure 1C, black spectrum). Upon fibril formation, the EPR spectrum broadens and decreases in amplitude as

the site becomes immobilized in the fibril (Figures 1C and 1D, red spectra). The shapes of EPR spectra depend on both mobility and spin-spin interaction. To distinguish between the two one can do sparse labeling, i.e., only 1-10% of fibrils are labeled. This was done as indicated with the representative sites (Figures 1D and 1E, blue spectra). While some effect of spin-spin interaction is present, overall the spectral features are very similar indicating that the spin-spin interaction does not cause significant spectral distortions. This is different from the case of tau (and other proteins with parallel, in-register structure) where the stacking of multiple residues causes spin exchange (Figure 1F). Thus, neither of the sites shown is located in a region of parallel, in-register structure.

TRX-HDx1 fusion protein is an extended, random-coil protein

EPR spectra were collected from the uncleaved fusion protein mutants (Figure 2). All spectra consist of three sharp lines typical of highly mobile sites. Some broadening is evident at the N-terminal and the glutamine sites that is not present in the C-terminus. The fusion protein is large enough (28 kDa calculated MW) that the mobility is not due to rapid tumbling of the protein. We were unable to measure the mobility of soluble HDx1 without its fusion partner, since it aggregates rapidly upon cleavage. The mobility indicates that no sites are buried, consistent with an extended, non-globular structure.

HDx1 fibrils do not have a parallel, in-register EPR signature

HDx1 fibrils do not exhibit any evidence of spin exchange. There are no broad single resonance lines in any domain (Figure 3, red spectra) that would be an indication of multiple labels stacking in close proximity. Thus, the HDx1 aggregates formed in this study do not have the parallel, in-register EPR signature common to other disease-causing amyloid fibrils.

Across the entire molecule, there is little evidence of spin-spin interaction, as shown by the modest changes in the spectra upon dilution of labeled HDx1 with unlabeled HDx1 (Figure 3, blue spectra). The changes upon dilution were most notable in the N-terminus and polyQ region, showing that labels in this region interact with each other more strongly than in the C-terminus.

HDx1 C-terminus lies outside the fibril core

All the C-terminal sites examined have three easily discernible, relatively sharp resonance lines upon fibril formation (Figure 3). Hence, these sites remain very mobile and there is a notable increase in mobility the more distal the site is from the glutamine region. These data indicate that the C-terminus represent a highly dynamic and poorly ordered tail that is anchored at the glutamine region and has an ever-larger range of motion the farther away from the dock one gets. Thus, the C-terminus is not part of a highly ordered core of the fibril, where one would expect strong immobilization.

Glutamine domain is mostly immobilized in fibrils

In marked contrast to the behavior observed for C-terminal sites, fibril formation causes significant line broadening for sites in the glutamine region (Figure 3). All of the spectra are characteristic of the strong immobilization typically seen at the core of amyloid fibrils. Only position 63, which is adjacent to the proline region in the C-terminus exhibits an additional, more mobile component (Figure 3, see arrow), indicating that this residue is not as ordered and likely resides in a transition region between the highly ordered glutamine region and the C-terminus. The existence of such a gradual transition region is further supported by the spectrum for position 64. This residue is the first position in the proline region and exhibits spectral features similar to those at position 63.

N-terminus exhibits complex spectra, indicative of multiple conformations

While the spectra from most sites in the glutamine region or C-terminus can either be classified as highly buried or highly dynamic, the N-terminal spectra are more complex, indicating multiple structural states. All sites clearly have a sharp, mobile component in addition to various broader, more immobile components. These results indicate that N-terminal site can exist in different states, some of which can be highly dynamic and some of which are much more immobilized. These sharp lines, although similar to those of the fusion protein, are not due to uncleaved fusion protein, as the fusion protein spectra could not be used to fully subtract out the sharp lines, and no evidence of fusion protein is found in the spectra for sites outside the N-terminal region. Similarly, we also tested whether potentially

unpolymerized or soluble material could account for the sharp lines. Subtraction of the supernatant containing the soluble material remaining after fibril formation does not account for the sharp lines, however. In sum, we infer that the N-terminus takes on multiple conformations under the present conditions.

Distances between labels are broadly distributed

Distances between labels can be obtained by deriving a broadening function from the difference in spectra obtained from fully labeled and sparsely labeled fibrils. In the present study, deconvolution of the fully labeled and underlabeled spectra reveals that the distances are broadly distributed across the entire protein. Several representative distributions (Figure 4) show that there is a peak between 9 and 10 Å, which is within the expected intersheet distance in the cross-beta structure. Besides the intersheet distance, there are no other distinct peaks, only broad distributions that are probably due to labels that are at many different distances within the same sheet as well as on neighboring sheets. The distance distributions are generally centered around 12-15 Å for the N-terminus and polyQ, and beyond 15 Å for the C-terminus. Continuous wave EPR can only resolve distances less than 20 Å, so the distances in the C-terminus are near the limit of what can be measured in our experiment. The intersheet peak is also noticeably smaller in the C-terminus, indicating that the C-terminus is largely outside of the cross-beta structure.

DISCUSSION

The goal of this study was to characterize the domain organization of mutant HDx1 fibrils. To this end, we generated 19 spin labeled derivatives of mutant HDx1 and used EPR to characterize the mobility of the three major domains of HDx1 in solution and within fibrils. Importantly, our study reveals that, unlike other disease-associated amyloid fibrils, HDx1 fibrils in our experiment do not have a parallel, in-register structure under our conditions. This indicates that HDx1, or possibly polyQ proteins as a class, may be unique among disease-associated amyloids.

Mobilities of residues can be compared by drawing a line width plot, which is actually calculated from the inverse of the width of the central resonance line for each site. As revealed by the line width plot (Figure 5), prior to aggregation, HDx1 is an extended, non-globular protein with high mobility at all the sites examined. These results are in agreement with a previous circular dichroism and nuclear magnetic resonance study of this same thioredoxin-HDx1 fusion protein without cysteine mutations, which indicated that HDx1 is a random coil without significant, stable alpha helix or beta sheet secondary structure (Bennett et al., 2002). In our study, there is some broadening that remains relatively constant throughout the N-terminus, persists until residue 30 in the glutamine region, and then decreases steadily until the C-terminus. This is unlikely to be an effect of the fusion partner, since one would expect a steady decrease throughout the N-terminus in that case. Moreover, there is a flexible linker between the thioredoxin and HDx1 domains. Immobilization of a site, such as by binding with an antibody, can be detected by a decrease in mobility up to about ten residues away. Thus, this linker is long enough

(22 amino acids) that there should be no immobilization due to the thioredoxin apparent in the N-terminus. Consequently, it is more likely that the decreased mobility in the N-terminus and beginning of the glutamine is due to the formation of either a transient inter- or intramolecular interaction or a transient secondary structure. Recent data indicate that N-termini can interact homotypically (Tam et al., 2009) and that this interaction initiates aggregation (Thakur et al., 2009). However, if only the N-terminus interacted, one would expect broadening to steadily decrease in the polyQ region and disappear within ten residues of the last immobilized N-terminal residue, i.e., by residue 27. Since the broadening only diminishes beyond residue 30, there are likely to be additional weak intramolecular interactions between glutamines, or the glutamine region and other domains. In support of this, a recent computational study indicated that in polyQ peptides attached to the N-terminus of Htt, intramolecular interactions between glutamines increased with polyQ length (Williamson et al., 2010). Another study found a weak ability of the glutamine to cross-link to the N-terminus (Tam et al., 2009). Another possibility is that there is a structure to the N-terminus that persists into the glutamine region. A recent crystal structure of soluble wildtype HDx1 supports this interpretation. In that study, the N-terminus adopted an alpha helical structure that extended from 1 to 14 residues into the glutamine region (Kim et al., 2009). More extensive EPR studies will be needed to clarify what causes the broadening.

Upon fibril formation, most of the polyQ domain becomes immobilized. The immobilization extends from the N-terminus to at least residue 48 in the glutamine region, as seen in the line width plot (Figure 5). This is consistent

with the burial of this region within the amyloid core, which is further supported by the presence of a peak at the expected intersheet distance. The distance analysis indicates that at least some N-termini lie within the amyloid core, judging from the presence of a peak corresponding to the expected intersheet distance (Figure 4). Taking the N-terminus and the glutamine region together, the amyloidogenic core is at least 31 to 48 residues in length (≥31Q and possibly 17 N-terminal amino acids).

No part of the amyloid core shows any evidence of spin exchange, which indicates that there is no stacking of multiple residues in a parallel, in-register arrangement of beta strands. While unusual, since nearly all reported fibrils with amyloid cores over 20 amino acids in length have a parallel, in-register beta strand arrangement, this is not necessarily surprising. The parallel, in-register arrangement may be preferred by many proteins because it maximizes hydrophobic contacts, since like residues stack with each other. However, since polyQ is a homopolymer and one glutamine is as hydrophobic as the next, there is no intrinsic reason for residues at identical sites in the primary sequence to stack. Indeed, the broad distance distributions indicate that there may be no true fixed positions within the fibril; i.e., in two different molecules, the same residue in the primary structure may be at different positions in the secondary structure. This could increase the number of distances exponentially.

The immobilization of the glutamine region diminishes beyond residue 48 to such an extent that glutamine 63, the final glutamine of the polyQ domain, is as mobile as the adjacent proline residue 64. Within the C-terminus, the mobility increases steadily, reaching a value nearly identical to the fusion protein by residue

111 (Figure 5). Thus, the end of the glutamine region and the entire C-terminus lie outside of the core of the amyloid fibril. It is interesting that instead of becoming immobilized by the glutamines, the C-terminus seems to impose its mobility upon the adjacent polyQ region. It has been shown that C-terminal proline stretches inhibit aggregation of polyQ (Bhattacharyya et al., 2006) and HDx1 (Hollenbach et al., 1999; Thakur et al., 2009), possibly by inducing a polyproline helix within the glutamine stretch (Darnell et al., 2007). It is unclear how far into the glutamine region this effect on mobility extends. In a recent crystallography study of soluble wildtype HDx1, the four glutamines adjacent to the C-terminus were in an extended conformation, instead of random coil (Kim et al., 2009). While the extension of the proline results from the soluble HDx1 to the fibril is attractive, we cannot rule out that there is simply some overhang of glutamines at the end of the amyloid core that is insufficiently long to form a stable beta strand. Experiments using different polyQ lengths may shed some light on this. Further study will be necessary to define the structure of the C-terminus, as well as the C-terminal portion of the glutamine region, although we have already obtained some promising data using another EPR technique, known as double electron-electron resonance.

For the fibrils, the line width plot (Figure 5) for the N-terminus obscures its heterogeneity, since nearly every residue has two components. It is not clear whether the heterogeneity of the N-terminus is due to different morphology of fibrils or whether different conformations occur within the same fibril. Additionally, many of our fibril reactions still contain some large amorphous oligomers, so we cannot exclude that these contribute to the heterogeneity N-terminal spectra. One

can imagine that with a homopolymer, which lacks an intrinsic anchoring point, some N-termini could be sandwiched between two polyglutamine beta strands, while others may extend out from the amyloid core and have varying degrees of mobility, like a frayed rope. A recently published computational study found that in HDx1 with 47Q, the N-terminus could indeed adopt a beta strand conformation and become sandwiched between two glutamine strands (Lakhani et al., 2010). Alternatively, HDx1 fibrils may contain mixed parallel/antiparallel beta sheets. In this case, some N-termini in adjacent proteins would be on the same side of the sheet and could interact and become immobilized. Other N-termini would be on opposite sides of the fibril core and could not interact and would be quite heterogeneous in structure.

Since the broad distance distributions (Figure 4) likely represent residues in the same sheet and in nearby sheets, we are unable to exclude any specific structure except the parallel, in-register structure. A parallel structure is still possible, provided that there is no close stacking of multiple labels. One study found that FRET in mutant HDx1 fibrils only occurred when donor and acceptor fluorophores were on the same end of the protein, indicating that there may be a parallel beta strand structure in the fibril (Takahashi et al., 2008). Other evidence indicates that polyQ polymers (Thakur and Wetzel, 2002; Sharma et al., 2005) and HDx1 (Poirier et al., 2005) may form antiparallel beta sheets consisting of strands seven or eight glutamines in length, connected by beta hairpin turns. In that case, small beta sheets formed from individual HDx1 molecules would stack head to tail, forming a larger beta sheet parallel to the fibril axis. Such an arrangement would also preclude the

stacking of multiple labels in close proximity, since multiple intervening beta strands would separate them. In this case, the number of beta strands would determine the exact distance between the labels within a sheet. Other possible models include a beta solenoid (Wasmer et al., 2008) or a beta helix (Perutz et al., 2002a).

We have elucidated the domain organization of HDx1 in fibrils. Our study represents a first step toward a high-resolution structure of HDx1 fibrils. Future studies using a more exhaustive set of distance constraints from single- and double-labeled mutants will allow us to obtain a more precise idea of the arrangement of glutamine strands, as well as the various conformations of the N-terminus. Recent spin labeling work, which has combined continous wave EPR, pulsed EPR and computational refinement has shown that detailed 3-dimensional structures can be obtained using this approach (Jao et al., 2004).

MATERIALS AND METHODS

Protein expression, labeling, and purification

Using site-directed mutagenesis, both thioredoxin cysteines were mutated to serines in pET32a-HD46Q to create a parent construct for making cysteine mutants of Htt. Cysteine mutations were introduced by site-directed mutagenesis into the parent construct, which expresses a thioredoxin fused to the N-terminus of Htt that has 46 glutamines and a C-terminal His tag. Overnight cultures of BL21(DE3) were diluted fiftyfold into LB medium and grown at 37°C to 0.6 OD_{600}. IPTG was added to 1 mM and the temperature was reduced to 30°C for 4 hours. Pellets were collected

by centrifugation at 3500 g, resuspended in 20 mM Tris-HCl pH 8.0, 300 mM NaCl, and 10 mM imidazole containing 1X CelLytic B Cell Lysis reagent (Sigma, St. Louis, MO) and incubated for 20 minutes at room temperature on a rocker. Lysates were clarified by centrifugation at 21,000 g for 10 minutes and incubated with Ni-NTA agarose beads (Qiagen, Valencia, CA) for 1 hour at 4°C on a rocker. Beads were decanted into an Econo-Pac chromatography column (Biorad, Hercules, CA) and washed with several column volumes of 20 mM Tris-HCl pH 8.0, 300 mM NaCl, 20 mM imidazole. Purified proteins were eluted with 20mM Tris-HCl, pH 8.0, 300mM NaCl, 250 mM imidazole. Volumes were reduced to approximately 250 μl using an Amicon Ultra-4 or Ultra-15 3000 MWCO centrifugal filter (Millipore, Billerica, MA), after which the protein was incubated with an equal volume of immobilized TCEP disulfide reducing gel (Pierce, Rockford, IL) for 1 hour at room temperature. Following reduction, the disulfides were spin-labeled by incubation with a 5 to 15-fold excess of MTSL spin label (Toronto Research Chemicals, Inc., North York, Ontario, Canada) for one hour at room temperature. Labeled protein was FPLC purified on a Superdex-75 gel-filtration column (Pharmacia, Uppsala, Sweden) using phosphate buffered saline (137 mM NaCl, 2.7 mM KCl, 10 mM Na_2HPO_4, 1.76 mM NaH_2PO_4), adjusted to pH 6.8 with phosphoric acid, containing 1mM EDTA. For dilution spectra, unlabeled fusion protein without cysteines was purified in the same manner, except no MTSL was added. Unlabeled fusion protein without cysteines used to make seeds was purified similarly, except during FPLC, 50 mM Tris-HCl pH 8.0, 150 mM NaCl, 1 mM EDTA was used.

Seeds

Unlabeled fusion protein without cysteines in 50 mM Tris-HCl pH 8.0, 150 mM NaCl, 1 mM EDTA was diluted to 5 μM (225 μg/ml). To cleave the thioredoxin tag and initiate fibril formation, EKMax (Invitrogen, Carlsbad, CA) was added to 1 unit per 10 μg NTRX-Q46. The reaction was incubated without agitation at 4°C for three days, until fibril formation appeared complete by electron microscopy. Fibrils were collected by ultracentrifugation at 150,000 g for 20 minutes and resuspended in one tenth of the original volume. To fragment the fibrils, this suspension was then sonicated on maximum power for 10 minutes at 30 second intervals. Sonicated seeds were stored at –80°C.

Fibril Formation

All Htt protein concentrations were measured by BCA assay and adjusted to 225 μg/ml (5 μM) for fibril formation. For mobility measurements, reactions were set up using 10% labeled mutant protein and 90% unlabeled protein without cysteines. To measure spin-spin interactions, reactions containing 100% labeled protein were used. To ensure that all mutants formed fibrils with the same morphology, all reactions were seeded with 10% preaggregated seed fibrils and fibril formation was initiated by the addition of 1 unit EKMax per 10 μg protein. Reactions were incubated overnight at 4°C without agitation. Fibrils were collected by ultracentrifugation at 150,000 g for 20 minutes and resuspended in 7μl PBS, pH 6.8, with 1 mM EDTA.

Electron microscopy

Prior to ultracentrifugation, 6 µl of fibrils were removed and adsorbed onto copper mesh electron microscopy grids (Electron Microscopy Sciences, Hatfield, PA) for two minutes. These grids were negatively stained with 2% uranyl acetate for two minutes. Subsequently, the grids were examined with a JEOL JEM-1400 electron microscope at 100 kV and photographed using a Gatan digital camera.

Continuous wave EPR spectra

After ultracentrifugation, the resuspended fibrils were loaded into quartz capillaries (0.6 mm inner diameter x 0.84 mm outer diameter) and EPR spectra were recorded on an X-band Bruker EMX spectrometer at room temperature. The scan width was 150 gauss at an incident microwave power of 12.60 mW. EPR spectra of fusion proteins were also collected. All spectra were normalized to the same number of spin labels using double integration. Dipolar broadening simulations to obtain distance information (Altenbach et al., 2001) were performed using the program ShortDistances100, developed by Christian Altenbach and available for download at his website http://sites.google.com/site/altenbach/Home.

REFERENCES

Altenbach C, Oh KJ, Trabanino RJ, Hideg K, Hubbell WL (2001) Estimation of inter-residue distances in spin labeled proteins at physiological temperatures: experimental strategies and practical limitations. Biochemistry 40:15471-15482.

Bennett MJ, Huey-Tubman KE, Herr AB, West AP, Jr., Ross SA, Bjorkman PJ (2002) Inaugural Article: A linear lattice model for polyglutamine in CAG-expansion diseases. Proc Natl Acad Sci U S A 99:11634-11639.

Bhattacharyya A, Thakur AK, Chellgren VM, Thiagarajan G, Williams AD, Chellgren BW, Creamer TP, Wetzel R (2006) Oligoproline effects on polyglutamine conformation and aggregation. J Mol Biol 355:524-535.

Brinkman RR, Mezei MM, Theilmann J, Almqvist E, Hayden MR (1997) The likelihood of being affected with Huntington disease by a particular age, for a specific CAG size. Am J Hum Genet 60:1202-1210.

Darnell G, Orgel JP, Pahl R, Meredith SC (2007) Flanking polyproline sequences inhibit beta-sheet structure in polyglutamine segments by inducing PPII-like helix structure. J Mol Biol 374:688-704.

DiFiglia M, Sapp E, Chase KO, Davies SW, Bates GP, Vonsattel JP, Aronin N (1997) Aggregation of huntingtin in neuronal intranuclear inclusions and dystrophic neurites in brain. Science 277:1990-1993.

Geevasinga N, Richards FH, Jones KJ, Ryan MM (2006) Juvenile Huntington disease. J Paediatr Child Health 42:552-554.

Gordon DJ, Balbach JJ, Tycko R, Meredith SC (2004) Increasing the amphiphilicity of an amyloidogenic peptide changes the beta-sheet structure in the fibrils from antiparallel to parallel. Biophys J 86:428-434.

Hodgson JG, Agopyan N, Gutekunst CA, Leavitt BR, LePiane F, Singaraja R, Smith DJ, Bissada N, McCutcheon K, Nasir J, Jamot L, Li XJ, Stevens ME, Rosemond E, Roder JC, Phillips AG, Rubin EM, Hersch SM, Hayden MR (1999) A YAC mouse model for Huntington's disease with full-length mutant huntingtin, cytoplasmic toxicity, and selective striatal neurodegeneration. Neuron 23:181-192.

Hollenbach B, Scherzinger E, Schweiger K, Lurz R, Lehrach H, Wanker EE (1999) Aggregation of truncated GST-HD exon 1 fusion proteins containing normal range and expanded glutamine repeats. Philos Trans R Soc Lond B Biol Sci 354:991-994.

Huang CC, Faber PW, Persichetti F, Mittal V, Vonsattel JP, MacDonald ME, Gusella JF (1998) Amyloid formation by mutant huntingtin: threshold, progressivity and recruitment of normal polyglutamine proteins. Somat Cell Mol Genet 24:217-233.

Huntington's Disease Collaborative Research Group (1993) A novel gene containing a trinucleotide repeat that is expanded and unstable on Huntington's disease chromosomes. Cell 72:971-983.

Jao CC, Der-Sarkissian A, Chen J, Langen R (2004) Structure of membrane-bound alpha-synuclein studied by site-directed spin labeling. Proc Natl Acad Sci U S A 101:8331-8336.

Kajava AV, Baxa U, Wickner RB, Steven AC (2004) A model for Ure2p prion filaments and other amyloids: the parallel superpleated beta-structure. Proc Natl Acad Sci U S A 101:7885-7890.

Kim MW, Chelliah Y, Kim SW, Otwinowski Z, Bezprozvanny I (2009) Secondary structure of Huntingtin amino-terminal region. Structure 17:1205-1212.

Lakhani VV, Ding F, Dokholyan NV (2010) Polyglutamine induced misfolding of huntingtin exon1 is modulated by the flanking sequences. PLoS Comput Biol 6:e1000772.

Luca S, Yau WM, Leapman R, Tycko R (2007) Peptide conformation and supramolecular organization in amylin fibrils: constraints from solid-state NMR. Biochemistry 46:13505-13522.

Mangiarini L, Sathasivam K, Seller M, Cozens B, Harper A, Hetherington C, Lawton M, Trottier Y, Lehrach H, Davies SW, Bates GP (1996) Exon 1 of the HD gene with an expanded CAG repeat is sufficient to cause a progressive neurological phenotype in transgenic mice. Cell 87:493-506.

Margittai M, Langen R (2008) Fibrils with parallel in-register structure constitute a major class of amyloid fibrils: molecular insights from electron paramagnetic resonance spectroscopy. Q Rev Biophys 41:265-297.

Merlino A, Esposito L, Vitagliano L (2006) Polyglutamine repeats and beta-helix structure: molecular dynamics study. Proteins 63:918-927.

Perutz MF, Finch JT, Berriman J, Lesk A (2002a) Amyloid fibers are water-filled nanotubes. Proc Natl Acad Sci U S A 99:5591-5595.

Perutz MF, Pope BJ, Owen D, Wanker EE, Scherzinger E (2002b) Aggregation of proteins with expanded glutamine and alanine repeats of the glutamine-rich and asparagine-rich domains of Sup35 and of the amyloid beta-peptide of amyloid plaques. Proc Natl Acad Sci U S A 99:5596-5600.

Petkova AT, Ishii Y, Balbach JJ, Antzutkin ON, Leapman RD, Delaglio F, Tycko R (2002) A structural model for Alzheimer's beta -amyloid fibrils based on experimental constraints from solid state NMR. Proc Natl Acad Sci U S A 99:16742-16747.

Poirier MA, Jiang H, Ross CA (2005) A structure-based analysis of huntingtin mutant polyglutamine aggregation and toxicity: evidence for a compact beta-sheet structure. Hum Mol Genet 14:765-774.

Poirier MA, Li H, Macosko J, Cai S, Amzel M, Ross CA (2002) Huntingtin spheroids and protofibrils as precursors in polyglutamine fibrilization. J Biol Chem 277:41032-41037.

Ravina B, Romer M, Constantinescu R, Biglan K, Brocht A, Kieburtz K, Shoulson I, McDermott MP (2008) The relationship between CAG repeat length and clinical progression in Huntington's disease. Mov Disord 23:1223-1227.

Reddy PH, Charles V, Williams M, Miller G, Whetsell WO, Jr., Tagle DA (1999) Transgenic mice expressing mutated full-length HD cDNA: a paradigm for locomotor changes and selective neuronal loss in Huntington's disease. Philos Trans R Soc Lond B Biol Sci 354:1035-1045.

Rosas HD, Goodman J, Chen YI, Jenkins BG, Kennedy DN, Makris N, Patti M, Seidman LJ, Beal MF, Koroshetz WJ (2001) Striatal volume loss in HD as measured by MRI and the influence of CAG repeat. Neurology 57:1025-1028.

Scherzinger E, Sittler A, Schweiger K, Heiser V, Lurz R, Hasenbank R, Bates GP, Lehrach H, Wanker EE (1999) Self-assembly of polyglutamine-containing huntingtin fragments into amyloid-like fibrils: implications for Huntington's disease pathology. Proc Natl Acad Sci U S A 96:4604-4609.

Scherzinger E, Lurz R, Turmaine M, Mangiarini L, Hollenbach B, Hasenbank R, Bates GP, Davies SW, Lehrach H, Wanker EE (1997) Huntingtin-encoded polyglutamine expansions form amyloid-like protein aggregates in vitro and in vivo. Cell 90:549-558.

Sharma D, Shinchuk LM, Inouye H, Wetzel R, Kirschner DA (2005) Polyglutamine homopolymers having 8-45 residues form slablike beta-crystallite assemblies. Proteins 61:398-411.

Sieradzan KA, Mechan AO, Jones L, Wanker EE, Nukina N, Mann DM (1999) Huntington's disease intranuclear inclusions contain truncated, ubiquitinated huntingtin protein. Exp Neurol 156:92-99.

Takahashi T, Kikuchi S, Katada S, Nagai Y, Nishizawa M, Onodera O (2008) Soluble polyglutamine oligomers formed prior to inclusion body formation are cytotoxic. Hum Mol Genet 17:345-356.

Tam S, Spiess C, Auyeung W, Joachimiak L, Chen B, Poirier MA, Frydman J (2009) The chaperonin TRiC blocks a huntingtin sequence element that promotes the conformational switch to aggregation. Nat Struct Mol Biol 16:1279-1285.

Thakur AK, Wetzel R (2002) Mutational analysis of the structural organization of polyglutamine aggregates. Proc Natl Acad Sci U S A 99:17014-17019.

Thakur AK, Jayaraman M, Mishra R, Thakur M, Chellgren VM, Byeon IJ, Anjum DH, Kodali R, Creamer TP, Conway JF, Gronenborn AM, Wetzel R (2009) Polyglutamine disruption of the huntingtin exon 1 N terminus triggers a complex aggregation mechanism. Nat Struct Mol Biol 16:380-389.

Vonsattel JP, Myers RH, Stevens TJ, Ferrante RJ, Bird ED, Richardson EP, Jr. (1985) Neuropathological classification of Huntington's disease. J Neuropathol Exp Neurol 44:559-577.

Walker FO (2007) Huntington's Disease. Semin Neurol 27:143-150.

Wasmer C, Lange A, Van Melckebeke H, Siemer AB, Riek R, Meier BH (2008) Amyloid fibrils of the HET-s(218-289) prion form a beta solenoid with a triangular hydrophobic core. Science 319:1523-1526.

Williamson TE, Vitalis A, Crick SL, Pappu RV (2010) Modulation of polyglutamine conformations and dimer formation by the N-terminus of huntingtin. J Mol Biol 396:1295-1309.

Zoghbi HY, Orr HT (2000) Glutamine repeats and neurodegeneration. Annu Rev Neurosci 23:217-247.

FIGURES

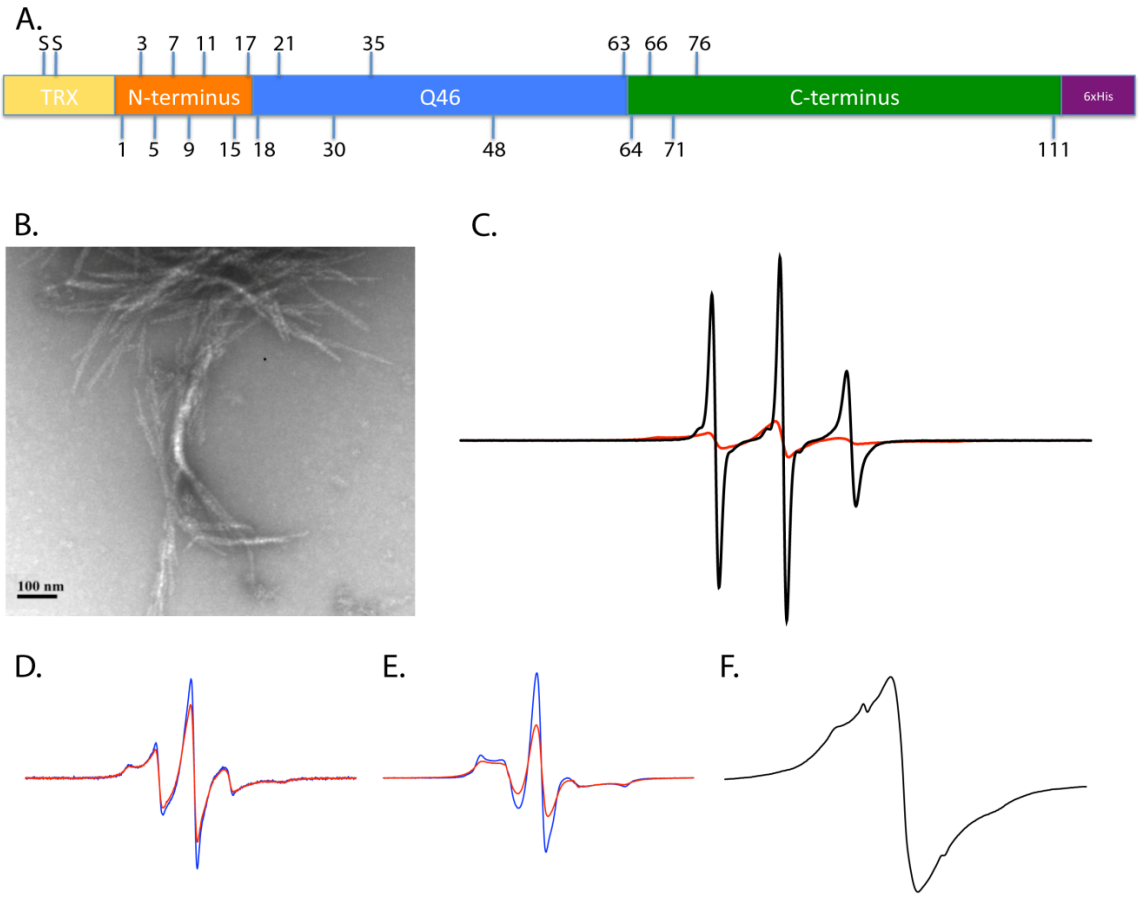

Figure 1. Outline of the experiment. Thioredoxin (TRX)-HDx1 with 46Q (thioredoxin not to scale) is labeled at various sites (A; AA position numbers) using an EPR-sensitive label. After cleavage, fibrils are formed (B) and the EPR spectrum changes from mobile to immobile (C). In HDx1 fibrils, sites are typically relatively mobile and interact only weakly, as shown by the changes from 100% labeled fibril (red) to sparsely labeled fibril (blue) (D, residue 64), or relatively immobile and interact appreciably (E, residue 48). When multiple labels come into close contact, spin exchange occurs, which is typical of parallel, in-register amyloid fibrils, such as tau (F).

Figure 2

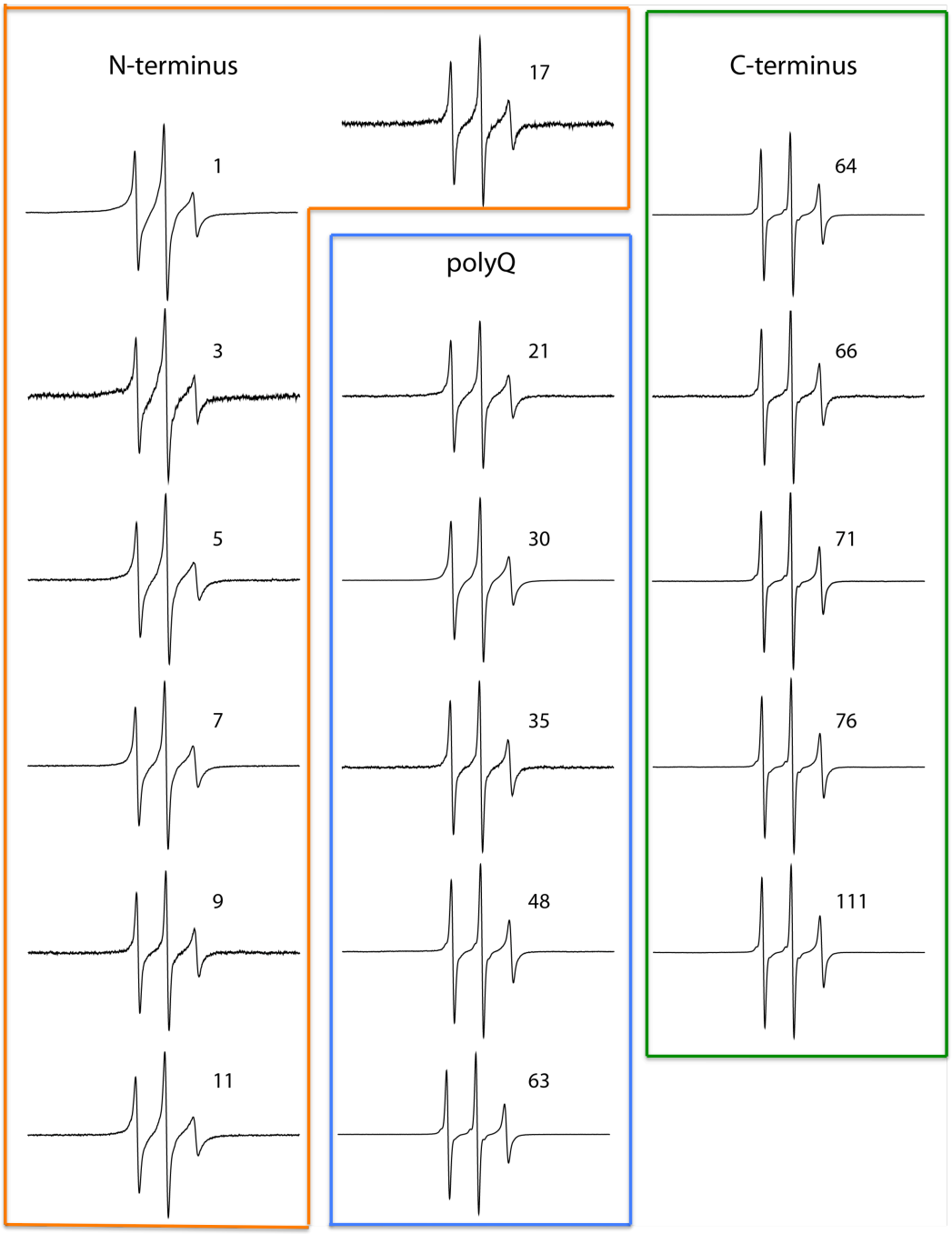

Figure 2. EPR spectra of the fusion protein. EPR spectra were collected for thioredoxin-HDx1 fusion protein. All sites are mobile and some broadening is evident in the N-terminus and polyQ region.

Figure 3

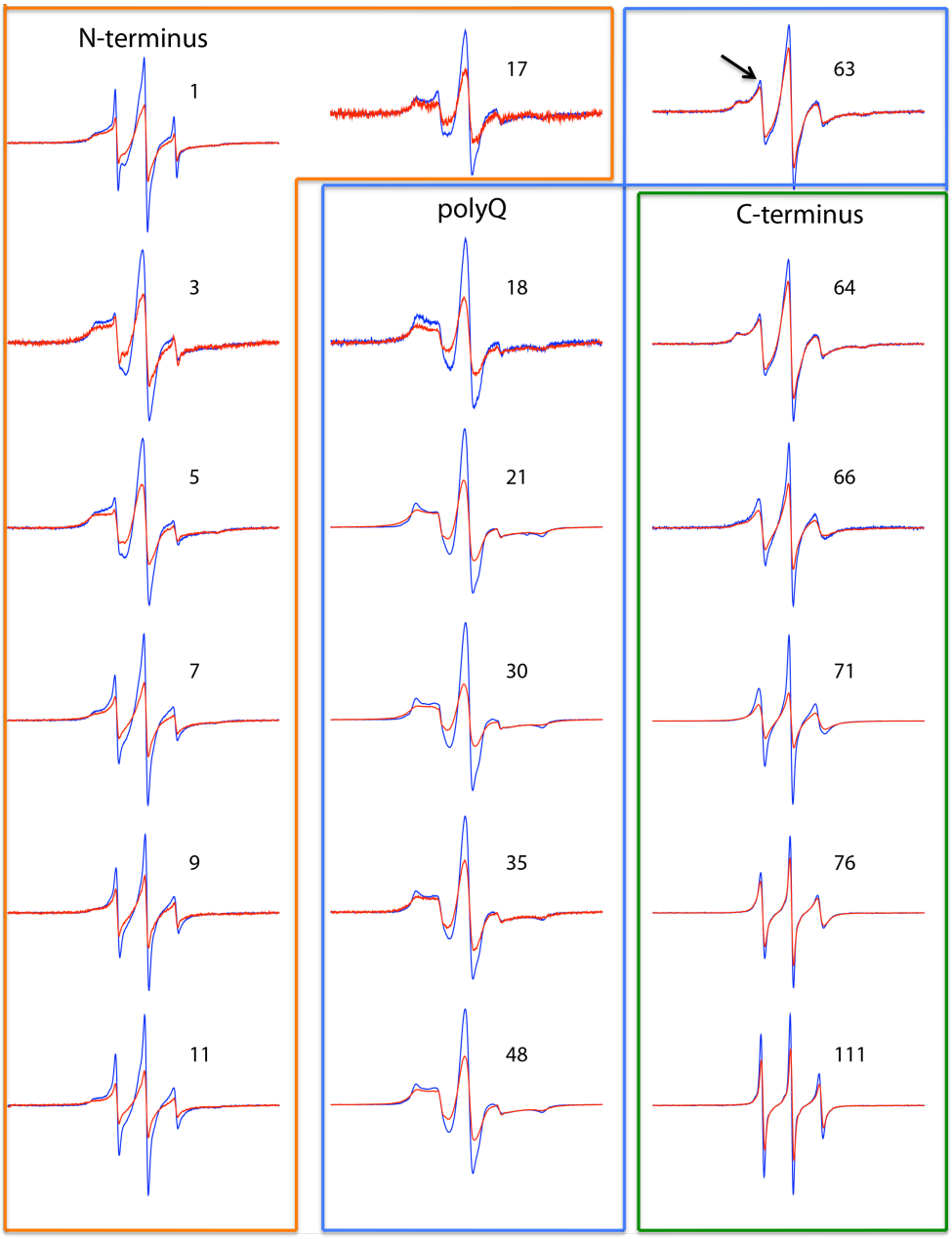

Figure 3. EPR spectra of fibrils. 100% (red) and 10% (blue) labeled fibrils for each site are overlayed. The N-terminus has complex, heterogeneous spectra, the polyQ region is largely immobilized, and the C-terminus is mobile. There are only weak spin-spin interactions between labels. The arrow denotes a mobile component in the last residue of the polyQ stretch.

Figure 4

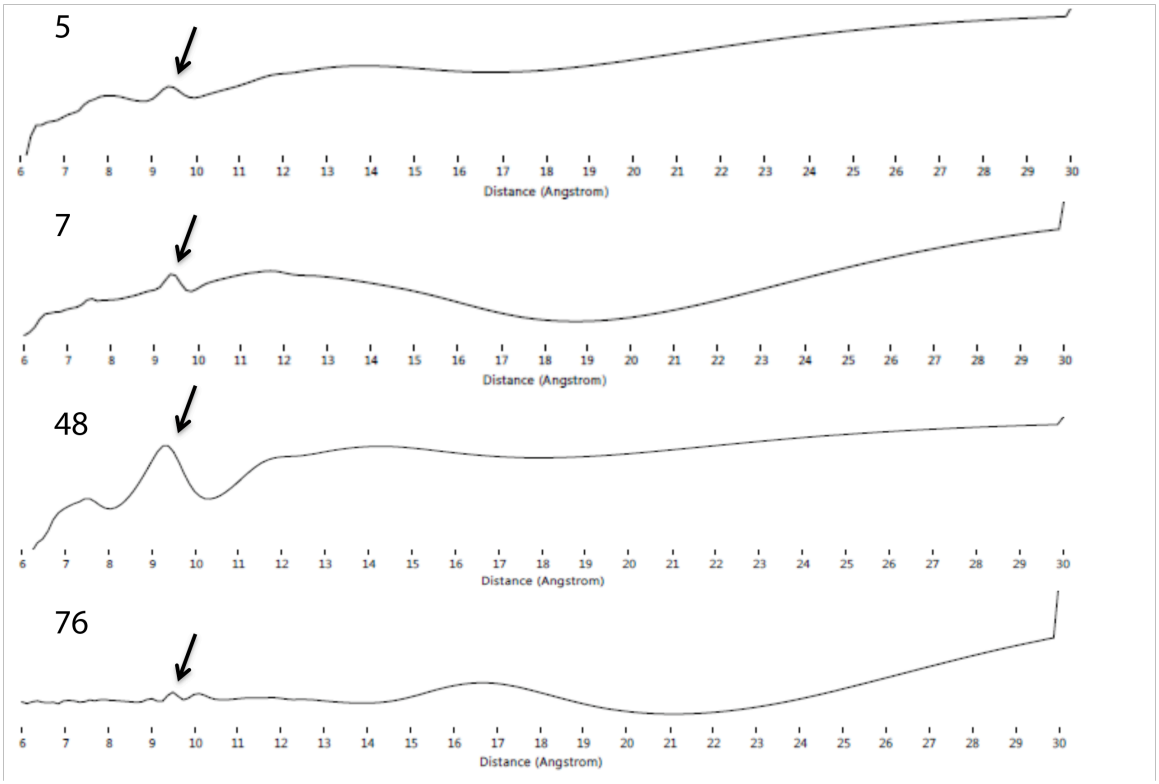

Figure 4. Distance distributions for representative sites. A peak (arrow) is present around the intersheet distance in all spectra, although it is very weak in the C-terminus (76) and particularly strong in the polyQ region (48). The remaining distances are very broad, except for in the C-terminus where there is little interaction.

Figure 5

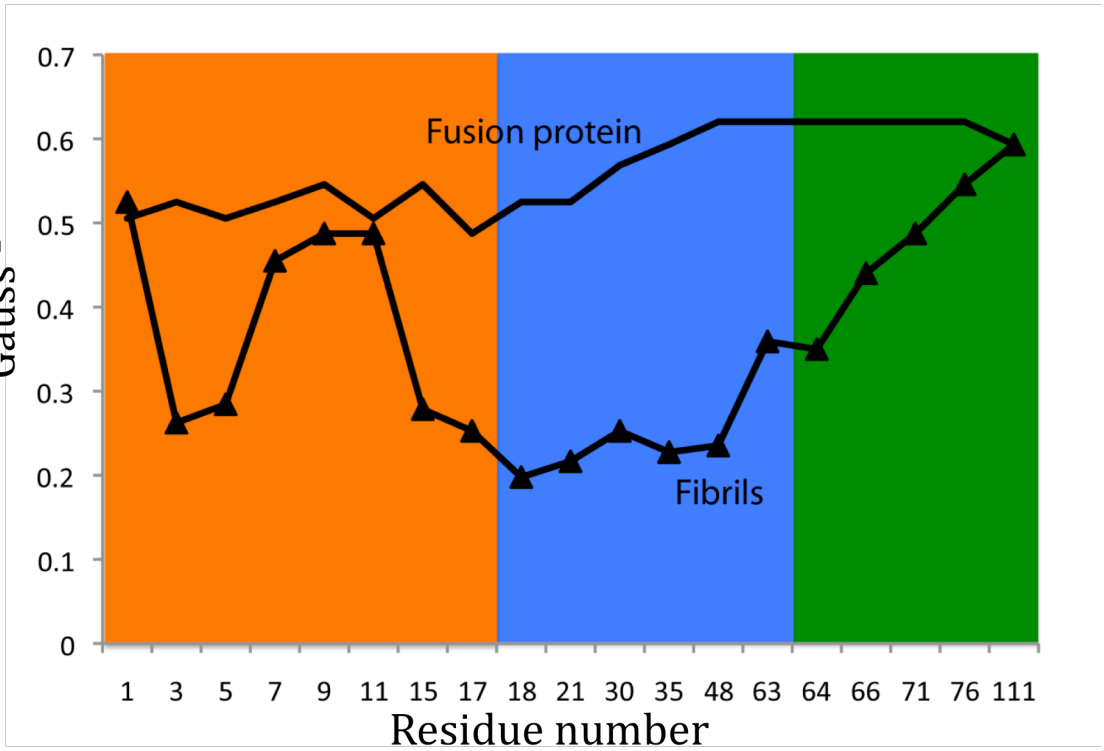

Figure 5. Inverse line width plot for HDx1 fusion protein and sparsely labeled fibrils. The inverse of the width of the central resonance line is plotted against residue number to give a measure of mobility.

Appendix A

Cell-Based Selection of Neuroprotective Intrabodies for Huntington's Disease

Charles W. Bugg, Ali Khoshnan, and Paul H. Patterson

Huntington's Disease is a one of several CAG repeat disorders, and is caused by an expansion beyond a threshold of 36 of a stretch of glutamines in exon 1 of huntingtin (Htt) (The Huntington's Disease Collaborative Research Group, 1993; Zoghbi and Orr, 2000). Cells in the affected regions have aggregates of mutant Htt (mHtt) in the nucleus and neuropil (Davies et al., 1997; DiFiglia et al., 1997), although the role of the aggregates in HD pathogenesis is not clear (Ross and Poirier, 2005).

Evidence suggests that mutant Htt exon 1 takes on a toxic conformation (Chen et al., 2002) and that monomers (Cong et al., 2006) or oligomers are the toxic species (Ross and Poirier, 2005; Cong et al., 2006), although the actual pathogenic mechanisms are unclear. There is evidence that cell death can occur autonomously (Cooper et al., 1998; Martindale et al., 1998) and non-cell autonomously (Gu et al., 2005; Kretzschmar et al., 2005). Major hypotheses include transcriptional dysregulation (Khoshnan et al., 2004; Landles and Bates, 2004), impairment of the ubiquitin-proteasome system (Venkatraman et al., 2004; Valera et al., 2005), Htt processing (Graham et al., 2006; Kim et al., 2006; Schilling et al., 2006; Tanaka et al., 2006), oxidative stress (Alexi et al., 1998; Giuliano et al., 2003; Puranam et al., 2006), disruption of intracellular transport (Li and Li, 2004; Trushina et al., 2004), excitotoxicity (Li et al., 2004; Ali and Levine, 2006) and synaptic dysfunction (Smith

et al., 2005). In addition, mHtt may depend on other molecules to misfold and exert toxicity (Meriin et al., 2002; Duennwald et al., 2006), other pathways may contribute to toxicity (Giorgini et al., 2005; Rubinsztein et al., 2005; Valenza et al., 2005; Abou-Sleymane et al., 2006; Hoshino et al., 2006), and mHtt may directly perturb or permeabilize lipid bilayers (Kayed et al., 2004; Baglioni et al., 2006; Suopanki et al., 2006). Furthermore, activation of the immune system may contribute to or protect the HD brain from neurodegeneration (Bonifati and Kishore, 2006; Pavese et al., 2006; Woodruff et al., 2006). Although much of the evidence favors a gain-of-toxic-function mechanism, loss or impairment of normal Htt function may contribute to pathogenesis (Rigamonti et al., 2000; Zuccato et al., 2003).

One recent therapeutic approach is the development of recombinant single chain intrabodies, which are intended to ameliorate HD by binding to particular epitopes of mHtt inside the cell. The first intrabodies were derived from the antigen-binding regions of full-size antibodies. These scFvs (single-chain fragment variable) were comprised of the variable regions of the heavy and light chains, containing the antigen-binding, complementarity determining regions, connected by a peptide linker. More recently, single-domain intrabodies, consisting of either the variable heavy (V_H) or variable light (V_L) domains alone have been used. Unlike scFvs, single-domain intrabodies have improved solubility and expression and do not require preselection to find those capable of folding in the reducing intracellular environment (Tanaka et al., 2003). Producing a novel intrabody usually involves selection from a naïve B-cell library or from a randomized library built on a scaffold that is stable intracellularly. The selection techniques most often involve surface

display on phage or yeast, although yeast two-hybrid screens have also been used (Stocks, 2004; Miller and Messer, 2005). A library is panned for binding to a specific antigen target and the scFvs that bind are recovered. Published mammalian selection protocols rely on display of the intrabody library on the surface of cells (Ho et al., 2006) or on a two-hybrid format. However, the mammalian two-hybrid system has only been used to confirm the binding activity of a scFv selected by yeast two-hybrid screen and remains unvalidated as a primary selection tool (Visintin et al., 1999). Retrovirally encoded display libraries have been used to select protease substrates (Buchholz et al., 1998; Schneider et al., 2003), antibody epitopes (Khare et al., 2003), and more recently, laminin-binding scFvs (Urban et al., 2005). These retroviral display techniques rely on binding of the antigen *in vitro* followed by amplification of the scFv intracellularly in mammalian cells. A recent study is of particular relevance, because it was the first unbiased selection in a mammalian cell line. In this study, an scFv library was transfected into metastatic cancer cells and a selection was performed based on the ability of the intrabody to block metastasis. A functional intrabody that could block metastasis was selected using this method. This protein was found to bind a signaling molecule involved in cell migration, but not previously specifically associated with metastasis (Inoue et al., 2007).

Three groups have created anti-Htt intrabodies. Messer's group used phage display to isolate an anti-Htt scFv intrabody specific to the 17 N-terminal residues of Htt (Lecerf et al., 2001). This intrabody, C4, reduces Htt aggregates and redox-induced morbidity in organotypic brain slice cultures expressing mutant Htt as well as in a fly model (Murphy and Messer, 2004; Wolfgang et al., 2005). Our group

made intrabodies derived from anti-Htt monoclonal antibodies that bind different domains of mutant Htt (Ko et al., 2001), and found that they have diverse effects on mutant Htt toxicity and aggregation in cell culture, depending on the epitope targeted (Khoshnan et al., 2002). One of these scFvs, MW7, protects against mutant Htt in cultured cells, acute brain slices (D. Lo, P. Reinhart, A. Khoshnan and P.H. Patterson, unpublished) and in a *Drosophila* HD model (G.R. Jackson, A. Khoshnan, and P.H. Patterson, unpublished). Most recently, Wittrup's group created a single-domain, V_L intrabody derived from a scFv isolated using yeast surface display (Colby et al., 2004a). This intrabody, V_L12.3, after removal of the disulfide bonds, reduces Htt aggregation and toxicity in *S. cerevisiae* and ST14A cells, and aggregation in several other cell lines (Colby et al., 2004b).

Such approaches may not be the best way to cure the disease, however. It is unclear whether binding mHtt is the most effective way to attack the disease, and certain anti-Htt intrabodies reliably exacerbate the toxicity of mutant Htt (Khoshnan et al., 2002). Htt is required for embryogenesis (Duyao et al., 1995; Nasir et al., 1995; Zeitlin et al., 1995); although its ablation by RNAi in adult organisms has shown therapeutic promise, it remains to be seen how toxic these agents are in the long term *in vivo* (Harper et al., 2005). Antibodies are a more versatile therapeutic option than RNAi, and have the potential to not only neutralize mHtt or perturb toxic interactions, but to preserve and stabilize beneficial interactions (Stocks, 2004). A high-throughput mammalian system that can directly select intrabodies that prevent cell death would be an advantage in development of potential therapeutics. Such a selection system would not be constrained to finding

intrabodies that bind Htt, and could potentially identify novel molecules and pathways not yet implicated in HD.

General outline of the selection system

As outlined below (Figure 1), a library of single-domain intrabodies will be transfected into a mammalian cell model expressing mHtt (Aiken et al., 2004). Induction of mHtt expression causes extensive cell death. Those cells that contain an intrabody capable of preventing cell death caused by mHtt will survive. Intrabody sequences will be rescued by RT-PCR from a lysate of the surviving cells. To ensure that cell survival is mediated by the intrabody and not a random protective mutation or insertion of the lentivirus into a key gene, the rescued intrabody sequences will be subjected to another round of the same selection. Although the probability that an inactive intrabody will survive two rounds of selection is very low, the selection can be repeated until most of the cells are protected, indicating that all nonfunctional sequences have been eliminated.

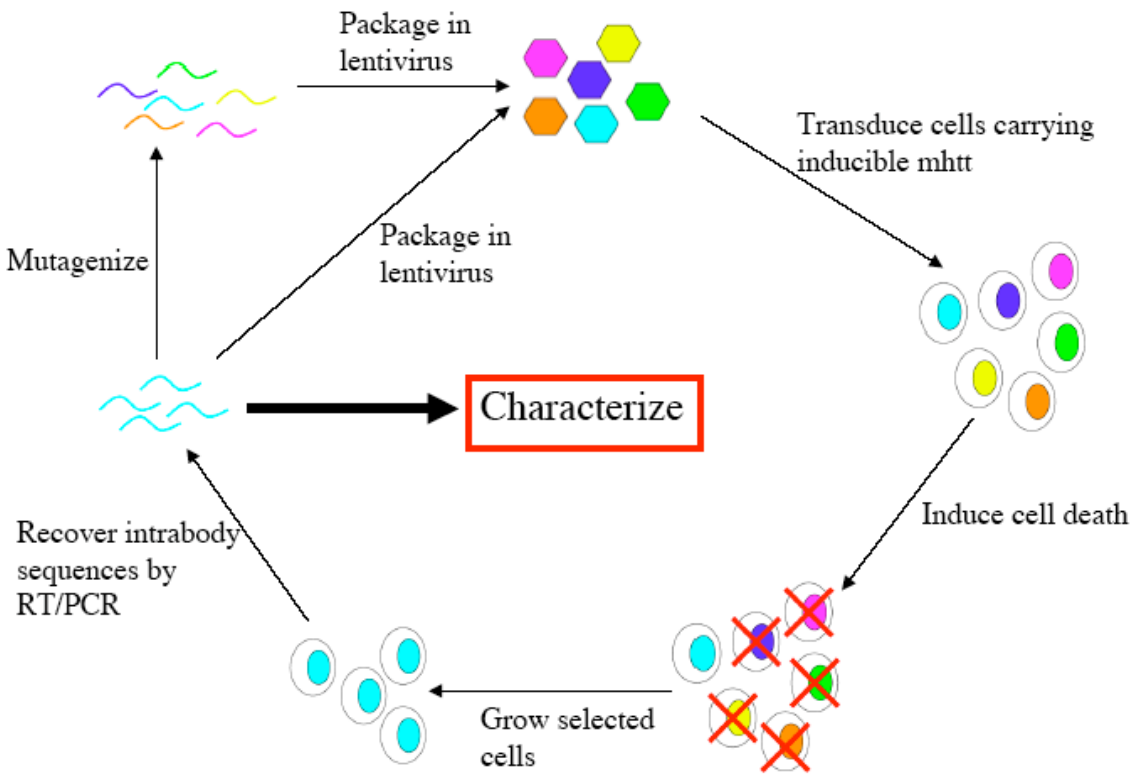

Figure 1. Iterative cell-based selection for neuroprotective intrabodies for Huntington's disease. Intrabody library sequences are packaged in lentivirus and used to transduce PC12 cells, which inducibly express mHtt. After induction, only those cells carrying a neuroprotective sequence will survive and proliferate. Sequences are recovered and recycled through the selection until a large number of cells are protected.

Selection of an appropriate cellular model

The single most important factor for the selection is the ability to control the extent of cell death in the cellular model used. Ideally, mHtt will kill all cells, unless a functional intrabody is present. PC12 cells were established from a transplantable rat adrenal pheochromocytoma (Greene and Tischler, 1976). They differentiate in

the presence of nerve growth factor (NGF) and have many characteristics of mature neurons before and after differentiation. Schweitzer PC12 cells contain mutant Htt exon 1 (103 glutamines) fused to GFP under control of the *B. mori* ecdysone-inducible promoter (Suhr et al., 1998; Kazantsev et al., 1999; Aiken et al., 2004). Addition of the ecdysone analog Muristerone A (MurA) to the culture medium induces Htt expression, leading to extensive cell death. I adjusted conditions so that the extent of cell death is dependent on the MurA concentration, as well as the incubation time. Maximal cell death of about 99% was reached by day 12 in the presence of 5 μM MurA (Figure 2A). No significant increase in death was seen when the dose of MurA is increased to 10 μM. Propidium iodide staining confirms that cell death commences rapidly after induction with MurA (Figure 2). From the lack of net cell death with 1 μM MurA at 37°C, there appears to be a threshold beyond which the MTS assay can detect cell death. Since MTS only detects metabolically active cells, this indicates that cell division is likely able to overcome cell death at low MurA concentrations. We also tested ST14A cells with low serum concentrations, as well as the proteasome inhibitor MG132. However, neither of these conditions sensitized the cells to mHtt (data not shown).

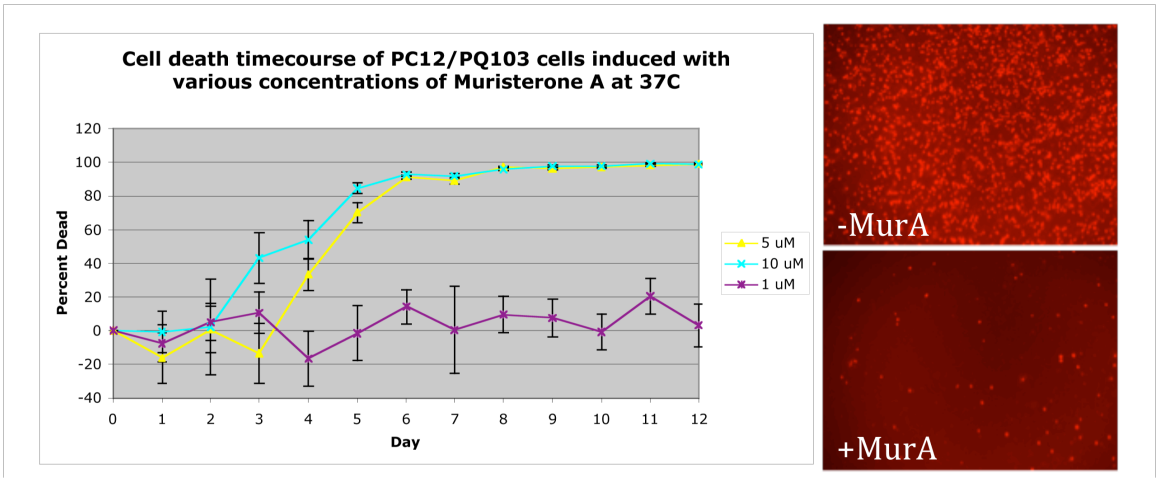

Figure 2. Cell death timecourse of Schweitzer cells induced with various concentrations of MurA at 37°C Schweitzer cells were plated on 96-well collagen I plates (~100,000 cells/well) and incubated at 37°C overnight to allow adherence. MTS assays (CellTiter 96 AQueous Non-Radioactive Cell Proliferation Assay, Promega, Madison, WI) were performed according to manufacturer instructions; the number of living cells is proportional to the A490. After establishing a baseline value, cells were induced with Muristerone A (Invitrogen, Carlsbad, CA) and MTS assays were performed daily. The fraction of living cells was calculated (compared to day 0) and cell death was inferred. Despite the lag phase apparent in the MTS assay, it is apparent from propidium iodide staining that cell death occurs rapidly, with extensive death occurring within 24 hours of induction with 5 μM MurA. Very little death occurs in uninduced cells. Propidium iodide (5 μg/ml) was added and cells incubated for 5 minutes at 37°C before fluorescence microscopy. Propidium iodide stains nuclei of dead cells red.

Validation of the selection system using a previously selected intrabody

I initially planned to establish proof of principle by engineering the MW7 V_H domain to function without the conserved disulfide bond. However, I could not detect expression of MW7 V_H, so I used intrabody V_L12.3 in the proof-of-principle selection experiment. V_L12.3 was engineered to fold stably without the conserved

disulfide bond (Colby et al., 2004b). The result is a very stable intrabody that reduces aggregation and toxicity in HEK293 and ST14A cells when cotransfected with PQ103. Thus, V_L12.3 presents an excellent candidate for a proof-of-principle selection. We attempted to express V_L12.3 from AAV and lentivirus, but it failed to significantly protect induced Schweitzer cells from death due to low expression (data not shown).

Because of the failure of the viral delivery, a transfection strategy was pursued. Since many copies of a vector are incorporated into a cell during transfection, the resulting higher expression levels were considered advantageous. In addition, incorporating multiple sequences per cell increased the total number of sequences that could be screened, potentially by an order of magnitude or more. PC12 cells, like many neuronal cell types, are difficult to transfect efficiently. I optimized transfection using CombiMag Magnetofection Reagent (Boca Scientific, Boca Raton, FL) in conjunction with Lipofectamine 2000 (Invitrogen, Carlsbad, CA) to transfect >90% of Schweitzer cells (Figure 3A). V_L12.3 in pcDNA3.1 was transfected into Schweitzer cells using the optimized transfection method and induced with 5μM MurA for four days. Significantly enhanced survival was apparent under light microscopy in cells transfected with VL12.3 (Figure 3B). Surprisingly, cells expressing DsRed Monomer as a control also showed some protection from mHtt, albeit much less than V_L12.3.

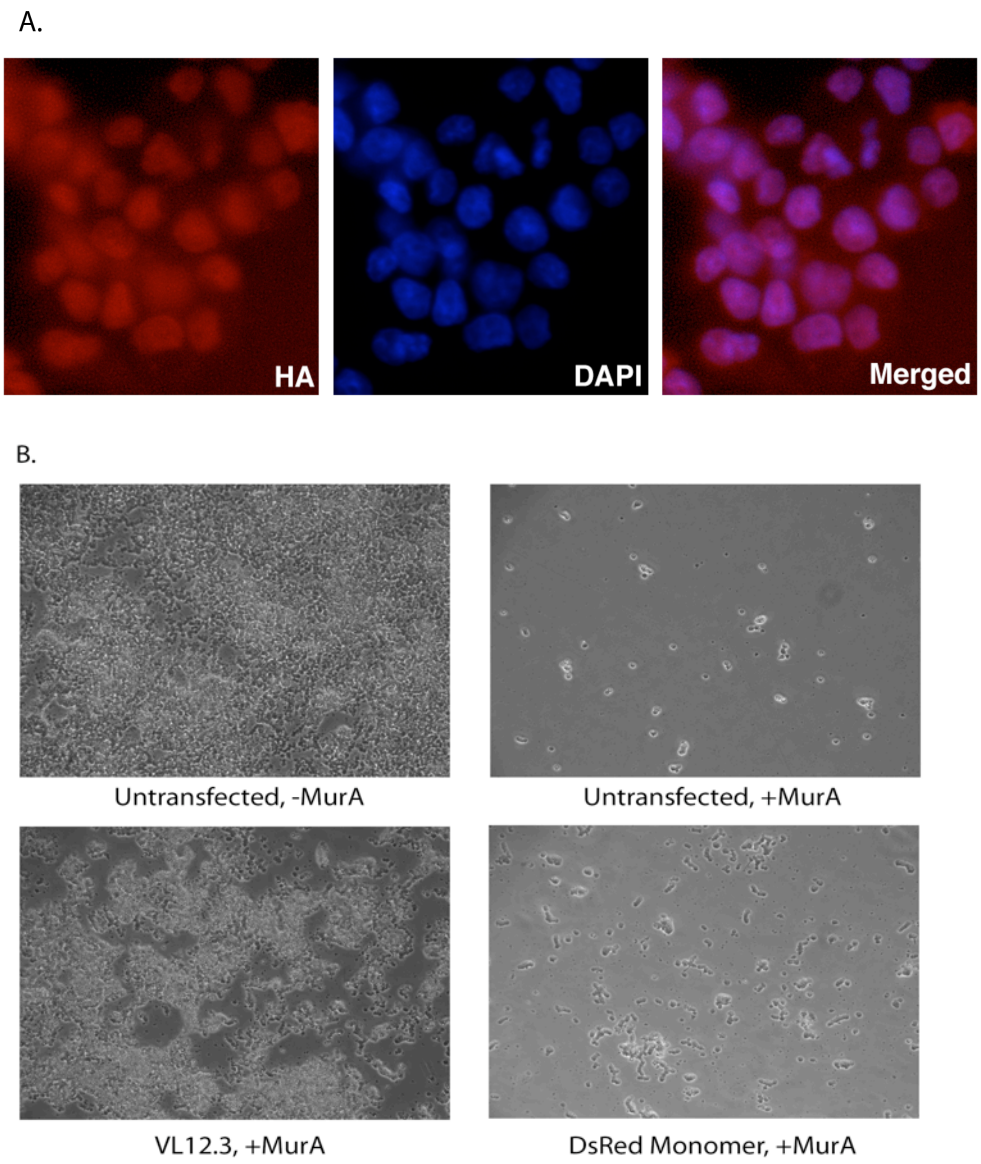

Figure 3. **Transfected VL12.3 protects from MurA-induced cell death**. (A) PC12/PQ103 cells were transfected in a 6-well poly-D-lysine coated plate with 4 μg of V_L12.3 expressed from an AAV vector using 10 μl of Lipofectamine 2000 (Invitrogen, Carlsbad, CA) in combination with 4 μl of CombiMag Magnetofection Reagent (Boca Scientific, Boca Raton, FL). Cells were fixed after 96 hours and immunostained for the presence of the HA tag on V_L12.3. Nuclei were stained with DAPI. Optimized transfection efficiency is >90%. (B) Cells were tranfected as in A. with either VL12.3 or pDsRed Monomer-N1 (Clontech, Mountain View, CA) and induced with 5 μM MurA for four days at 37°C. Cells were inspected by light microscopy.

Library construction

The Griffin.1 library (Hoogenboom et al., 1991; Winter et al., 1994) is a widely used library that had previously been used in our lab for the selection of intrabodies that bind the proline-rich repeat region of Htt (Southwell et al., 2008). Intrabodies in the Griffin.1 libraries were originally cloned as V_H and V_L domains connected by a flexible linker into the pHEN2 phagemid vector. In our experience, however, many selected clones are actually single domains. To avoid cleaving intrabodies within the coding sequence, we decided to use the established restriction sites (SfiI and NotI) that were originally used to generate the library. To find an appropriate expression vector, I digested several mammalian expression vectors containing intrabody sequences with SfiI and NotI and checked for the generation of a band on agarose gel. Of seven vectors tested, one had the appropriate restriction sites, a pcDNA3 vector expressing another scFv. Previous experiments in our laboratory had established that this vector could produce intrabody in mammalian cells. The Griffin.1 library was recovered from phage according to the instructions accompanying the library. It was subsequently amplified and cloned into the expression vector after removal of the intrabody sequence from the vector. Eight clones were sequenced and found to all be different and unlike the intrabody originally encoded in the vector. This indicated that the intrabody originally encoded in the parent vector likely did not contribute significantly to the library. Although there was no affinity tag on the proteins, expression of the library was

confirmed using a TnT Quick-Coupled T7 Transcription/Translation kit (Promega, Madison, WI) with [^{35}S]-Met included in the reaction (data not shown).

Selection

The naïve library encoded in the pcDNA3 vector—designated G.1.0—was transfected into sufficient Schweitzer cells to cover the estimated complexity of the library (10^7-10^8). The following day, 5 μM MurA was added to the plates. Fresh media and MurA were added every other day. After seven days of incubation, surviving cells were harvested after trypsinization. Total DNA was recovered using a DNeasy Blood and Tissue kit (Qiagen). The intrabody DNA was amplified by PCR using T7 promoter primer and BGH reverse primer. This yielded a band of the expected size (~1kb) corresponding to a two-domain scFv and the flanking regions derived from pcDNA3. This PCR product was then digested with SfiI and NotI in parallel with the pcDNA3 vector. It was subsequently ligated into the digested vector. The ligation was concentrated using a QiaQuick PCR Cleanup kit (Qiagen), so that the entire recovered pool could be transformed into a sufficient amount of competent cells and amplified. The amplified DNA—now designated G.1.1—was recovered using a HiSpeed Plasmid Maxiprep kit (Qiagen). This pool was subsequently put back through the selection system to generate another pool, and so on, until five rounds of selection had been completed (G.1.5).

After each cycle of killing cells, the plates were visually inspected by light microscopy in order to judge whether there was an increase in the number of surviving cells. There was no apparent increase in survival, so the experiment was

stopped before completion of the sixth round of selection. All six pools (naïve and five selected pools) were assessed for their ability to reduce aggregation and toxicity of mHtt. There was no apparent improvement on either measure (Figure 4). There was no trend that might indicate enrichment for functional sequences. While we might not expect improvement in aggregation, since our selection criterion is cell survival, no pool was markedly better than naïve library at reducing toxicity as measured by EtBr incorporation into the nucleus.

A.

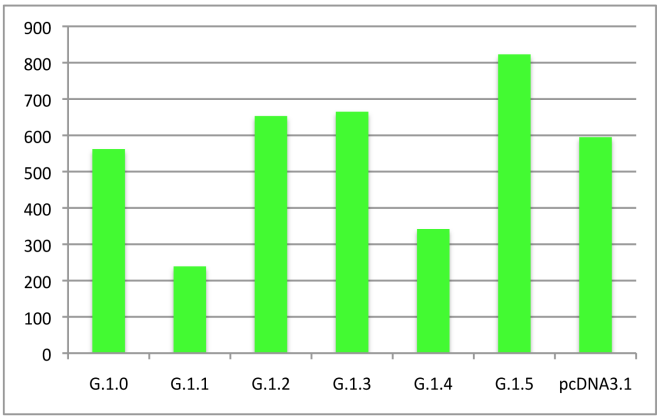

B.

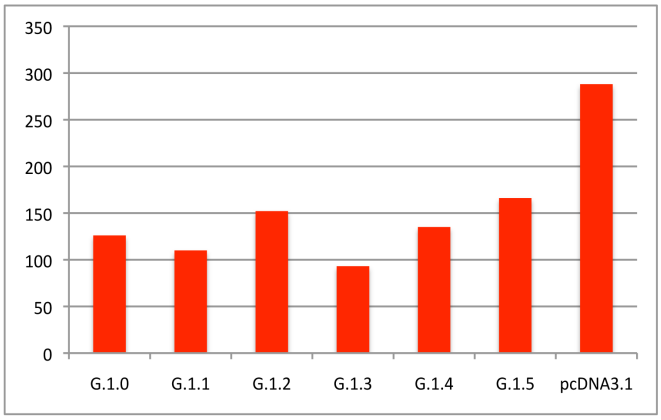

Figure 4. No enrichment is apparent after five rounds of selection. Pools from selection were cotransfected with mHtt carrying 103Q fused to GFP into HEK293 cells. (A) After 72 h, the extent of aggregation was assessed by the number of green fluorescent puncta. (B) Ethidium bromide was added to cells. Cells with intact nuclei exclude ethidium bromide, but dying and dead cells do not. Cell death was quantitated by counting red fluorescent puncta.

Repeat selection using reduced MurA

One concern with our system was that the expression levels might not be high enough to overcome induction of large amounts of mHtt, especially during the first round of selection, when only a single copy of each sequence may be represented in the library. As the lack of net cell death at low concentrations of MurA (Figure 2) was likely due to ongoing cell division at 37°C, I attempted to use lower concentrations of MurA at 33°C to inhibit cell division. I found that 1μM MurA at 33°C was as efficient as 5μM at 37°C (Figure 5), indicating that cell division had slowed sufficiently. Several rounds of selection were repeated using this condition and naïve library spiked with DNA from each selection round. After three rounds, there was no apparent enrichment and the experiment was discontinued.

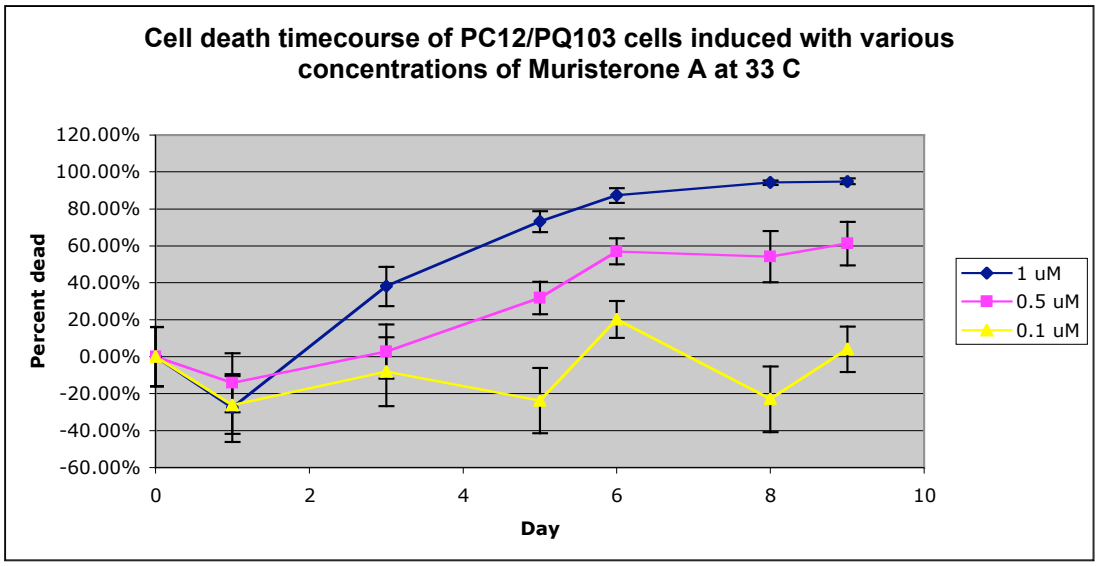

Figure 5. Cell death time course with low concentrations of MurA. 1 μM Muristerone A kills 95% of PC12/PQ103$_{ecd}$ cells in 9 days. Optimization is ongoing for lower concentrations. MTS assays were performed as above, except cells were incubated at 33°C to inhibit cell division.

Mutant Htt likely overwhelms intrabodies

It is likely that the selection failed because there is simply too much mHtt for the intrabodies to deal with, especially in the crucial first selection round. In retrospect, we should have been more wary after seeing the modest protection by V_L12.3 (Fig. 3B). It is clear from that experiment that even a well-established intrabody that reduces toxicity in several cellular models cannot completely block the toxicity induced by the large amounts of induced mHtt in the Schweitzer cells. Indeed it only rescued about 50-70% of the cells. Taking into account that during transfection, each cell can take up many copies of plasmid DNA, it seems unlikely that a single copy of any intrabody would be equal to the task. It appears that cellular models that are much more sensitive to lower concentrations of mHtt are essential to be able to select intrabodies in an unbiased fashion as originally envisioned in this project.

One way to redeem the selection using current technology might be to use a pool that is already enriched in sequences that are protective or at least bind mHtt. Although this negates one of the key advantages of the selection scheme, its unbiased approach, it may be necessary in order to work. Since there is not always a correlation between binding and reduction of toxicity, it would be advantageous to have a high-throughput system to automatically select those sequences that are protective. We had already begun generating a library based on Happ1 (Southwell et al., 2008), an intrabody directed to the proline-rich region of Htt, when the decision was made to terminate the project.

References

Abou-Sleymane G, Chalmel F, Helmlinger D, Lardenois A, Thibault C, Weber C, Merienne K, Mandel JL, Poch O, Devys D, Trottier Y (2006) Polyglutamine expansion causes neurodegeneration by altering the neuronal differentiation program. Hum Mol Genet 15:691-703.

Aiken CT, Tobin AJ, Schweitzer ES (2004) A cell-based screen for drugs to treat Huntington's disease. Neurobiol Dis 16:546-555.

Alexi T, Hughes PE, Faull RL, Williams CE (1998) 3-Nitropropionic acid's lethal triplet: cooperative pathways of neurodegeneration. Neuroreport 9:R57-64.

Ali NJ, Levine MS (2006) Changes in expression of N-methyl-D-aspartate receptor subunits occur early in the R6/2 mouse model of Huntington's disease. Dev Neurosci 28:230-238.

Baglioni S, Casamenti F, Bucciantini M, Luheshi LM, Taddei N, Chiti F, Dobson CM, Stefani M (2006) Prefibrillar amyloid aggregates could be generic toxins in higher organisms. J Neurosci 26:8160-8167.

Bonifati DM, Kishore U (2007) Role of complement in neurodegeneration and neuroinflammation. Mol Immunol 44:999-1010.

Buchholz CJ, Peng KW, Morling FJ, Zhang J, Cosset FL, Russell SJ (1998) In vivo selection of protease cleavage sites from retrovirus display libraries. Nat Biotechnol 16:951-954.

Chen S, Ferrone FA, Wetzel R (2002) Huntington's disease age-of-onset linked to polyglutamine aggregation nucleation. Proc Natl Acad Sci U S A 99:11884-11889.

Colby DW, Garg P, Holden T, Chao G, Webster JM, Messer A, Ingram VM, Wittrup KD (2004a) Development of a human light chain variable domain (V(L)) intracellular antibody specific for the amino terminus of huntingtin via yeast surface display. J Mol Biol 342:901-912.

Colby DW, Chu Y, Cassady JP, Duennwald M, Zazulak H, Webster JM, Messer A, Lindquist S, Ingram VM, Wittrup KD (2004b) Potent inhibition of huntingtin aggregation and cytotoxicity by a disulfide bond-free single-domain intracellular antibody. Proc Natl Acad Sci U S A 101:17616-17621.

Cong SY, Pepers BA, Roos RA, van Ommen GJ, Dorsman JC (2006) Small N-terminal mutant huntingtin fragments, but not wild type, are mainly present in monomeric form: Implications for pathogenesis. Exp Neurol 199:257-264.

Cooper JK, Schilling G, Peters MF, Herring WJ, Sharp AH, Kaminsky Z, Masone J, Khan FA, Delanoy M, Borchelt DR, Dawson VL, Dawson TM, Ross CA (1998) Truncated N-terminal fragments of huntingtin with expanded glutamine repeats form nuclear and cytoplasmic aggregates in cell culture. Hum Mol Genet 7:783-790.

Davies SW, Turmaine M, Cozens BA, DiFiglia M, Sharp AH, Ross CA, Scherzinger E, Wanker EE, Mangiarini L, Bates GP (1997) Formation of neuronal intranuclear inclusions underlies the neurological dysfunction in mice transgenic for the HD mutation. Cell 90:537-548.

DiFiglia M, Sapp E, Chase KO, Davies SW, Bates GP, Vonsattel JP, Aronin N (1997) Aggregation of huntingtin in neuronal intranuclear inclusions and dystrophic neurites in brain. Science 277:1990-1993.

Duennwald ML, Jagadish S, Giorgini F, Muchowski PJ, Lindquist S (2006) A network of protein interactions determines polyglutamine toxicity. Proc Natl Acad Sci U S A 103:11051-11056.

Duyao MP, Auerbach AB, Ryan A, Persichetti F, Barnes GT, McNeil SM, Ge P, Vonsattel JP, Gusella JF, Joyner AL, et al. (1995) Inactivation of the mouse Huntington's disease gene homolog Hdh. Science 269:407-410.

Giorgini F, Guidetti P, Nguyen Q, Bennett SC, Muchowski PJ (2005) A genomic screen in yeast implicates kynurenine 3-monooxygenase as a therapeutic target for Huntington disease. Nat Genet 37:526-531.

Giuliano P, De Cristofaro T, Affaitati A, Pizzulo GM, Feliciello A, Criscuolo C, De Michele G, Filla A, Avvedimento EV, Varrone S (2003) DNA damage induced by polyglutamine-expanded proteins. Hum Mol Genet 12:2301-2309.

Graham RK, Deng Y, Slow EJ, Haigh B, Bissada N, Lu G, Pearson J, Shehadeh J, Bertram L, Murphy Z, Warby SC, Doty CN, Roy S, Wellington CL, Leavitt BR, Raymond LA, Nicholson DW, Hayden MR (2006) Cleavage at the caspase-6 site is required for neuronal dysfunction and degeneration due to mutant huntingtin. Cell 125:1179-1191.

Greene LA, Tischler AS (1976) Establishment of a noradrenergic clonal line of rat adrenal pheochromocytoma cells which respond to nerve growth factor. Proc Natl Acad Sci U S A 73:2424-2428.

Gu X, Li C, Wei W, Lo V, Gong S, Li SH, Iwasato T, Itohara S, Li XJ, Mody I, Heintz N, Yang XW (2005) Pathological cell-cell interactions elicited by a

neuropathogenic form of mutant Huntingtin contribute to cortical pathogenesis in HD mice. Neuron 46:433-444.

Harper SQ, Staber PD, He X, Eliason SL, Martins IH, Mao Q, Yang L, Kotin RM, Paulson HL, Davidson BL (2005) RNA interference improves motor and neuropathological abnormalities in a Huntington's disease mouse model. Proc Natl Acad Sci U S A 102:5820-5825.

Ho M, Nagata S, Pastan I (2006) Isolation of anti-CD22 Fv with high affinity by Fv display on human cells. Proc Natl Acad Sci U S A 103:9637-9642.

Hoogenboom HR, Griffiths AD, Johnson KS, Chiswell DJ, Hudson P, Winter G (1991) Multi-subunit proteins on the surface of filamentous phage: methodologies for displaying antibody (Fab) heavy and light chains. Nucleic Acids Res 19:4133-4137.

Hoshino M, Qi ML, Yoshimura N, Miyashita T, Tagawa K, Wada Y, Enokido Y, Marubuchi S, Harjes P, Arai N, Oyanagi K, Blandino G, Sudol M, Rich T, Kanazawa I, Wanker EE, Saitoe M, Okazawa H (2006) Transcriptional repression induces a slowly progressive atypical neuronal death associated with changes of YAP isoforms and p73. J Cell Biol 172:589-604.

Huntington's Disease Collaborative Research Group (1993) A novel gene containing a trinucleotide repeat that is expanded and unstable on Huntington's disease chromosomes. Cell 72:971-983.

Inoue A, Sawata SY, Taira K, Wadhwa R (2007) Loss-of-function screening by randomized intracellular antibodies: identification of hnRNP-K as a potential target for metastasis. Proc Natl Acad Sci U S A 104:8983-8988.

Kayed R, Sokolov Y, Edmonds B, McIntire TM, Milton SC, Hall JE, Glabe CG (2004) Permeabilization of lipid bilayers is a common conformation-dependent activity of soluble amyloid oligomers in protein misfolding diseases. J Biol Chem 279:46363-46366.

Kazantsev A, Preisinger E, Dranovsky A, Goldgaber D, Housman D (1999) Insoluble detergent-resistant aggregates form between pathological and nonpathological lengths of polyglutamine in mammalian cells. Proc Natl Acad Sci U S A 96:11404-11409.

Khare PD, Rosales AG, Bailey KR, Russell SJ, Federspiel MJ (2003) Epitope selection from an uncensored peptide library displayed on avian leukosis virus. Virology 315:313-321.

Khoshnan A, Ko J, Patterson PH (2002) Effects of intracellular expression of anti-huntingtin antibodies of various specificities on mutant huntingtin aggregation and toxicity. Proc Natl Acad Sci U S A 99:1002-1007.

Khoshnan A, Ko J, Watkin EE, Paige LA, Reinhart PH, Patterson PH (2004) Activation of the IkappaB kinase complex and nuclear factor-kappaB contributes to mutant huntingtin neurotoxicity. J Neurosci 24:7999-8008.

Kim YJ, Sapp E, Cuiffo BG, Sobin L, Yoder J, Kegel KB, Qin ZH, Detloff P, Aronin N, DiFiglia M (2006) Lysosomal proteases are involved in generation of N-terminal huntingtin fragments. Neurobiol Dis 22:346-356.

Ko J, Ou S, Patterson PH (2001) New anti-huntingtin monoclonal antibodies: implications for huntingtin conformation and its binding proteins. Brain Res Bull 56:319-329.

Kretzschmar D, Tschape J, Bettencourt Da Cruz A, Asan E, Poeck B, Strauss R, Pflugfelder GO (2005) Glial and neuronal expression of polyglutamine proteins induce behavioral changes and aggregate formation in Drosophila. Glia 49:59-72.

Landles C, Bates GP (2004) Huntingtin and the molecular pathogenesis of Huntington's disease. Fourth in molecular medicine review series. EMBO Rep 5:958-963.

Lecerf JM, Shirley TL, Zhu Q, Kazantsev A, Amersdorfer P, Housman DE, Messer A, Huston JS (2001) Human single-chain Fv intrabodies counteract in situ huntingtin aggregation in cellular models of Huntington's disease. Proc Natl Acad Sci U S A 98:4764-4769.

Li L, Murphy TH, Hayden MR, Raymond LA (2004) Enhanced striatal NR2B-containing N-methyl-D-aspartate receptor-mediated synaptic currents in a mouse model of Huntington disease. J Neurophysiol 92:2738-2746.

Li SH, Li XJ (2004) Huntingtin and its role in neuronal degeneration. Neuroscientist 10:467-475.

Martindale D, Hackam A, Wieczorek A, Ellerby L, Wellington C, McCutcheon K, Singaraja R, Kazemi-Esfarjani P, Devon R, Kim SU, Bredesen DE, Tufaro F, Hayden MR (1998) Length of huntingtin and its polyglutamine tract influences localization and frequency of intracellular aggregates. Nat Genet 18:150-154.

Meriin AB, Zhang X, He X, Newnam GP, Chernoff YO, Sherman MY (2002) Huntington toxicity in yeast model depends on polyglutamine aggregation mediated by a prion-like protein Rnq1. J Cell Biol 157:997-1004.

Miller TW, Messer A (2005) Intrabody applications in neurological disorders: progress and future prospects. Mol Ther 12:394-401.

Murphy RC, Messer A (2004) A single-chain Fv intrabody provides functional protection against the effects of mutant protein in an organotypic slice culture model of Huntington's disease. Brain Res Mol Brain Res 121:141-145.

Nasir J, Floresco SB, O'Kusky JR, Diewert VM, Richman JM, Zeisler J, Borowski A, Marth JD, Phillips AG, Hayden MR (1995) Targeted disruption of the Huntington's disease gene results in embryonic lethality and behavioral and morphological changes in heterozygotes. Cell 81:811-823.

Pavese N, Gerhard A, Tai YF, Ho AK, Turkheimer F, Barker RA, Brooks DJ, Piccini P (2006) Microglial activation correlates with severity in Huntington disease: a clinical and PET study. Neurology 66:1638-1643.

Puranam KL, Wu G, Strittmatter WJ, Burke JR (2006) Polyglutamine expansion inhibits respiration by increasing reactive oxygen species in isolated mitochondria. Biochem Biophys Res Commun 341:607-613.

Rigamonti D, Bauer JH, De-Fraja C, Conti L, Sipione S, Sciorati C, Clementi E, Hackam A, Hayden MR, Li Y, Cooper JK, Ross CA, Govoni S, Vincenz C, Cattaneo E (2000) Wild-type huntingtin protects from apoptosis upstream of caspase-3. J Neurosci 20:3705-3713.

Ross CA, Poirier MA (2005) Opinion: What is the role of protein aggregation in neurodegeneration? Nat Rev Mol Cell Biol 6:891-898.

Rubinsztein DC, Ravikumar B, Acevedo-Arozena A, Imarisio S, O'Kane C J, Brown SD (2005) Dyneins, autophagy, aggregation and neurodegeneration. Autophagy 1:177-178.

Schilling B, Gafni J, Torcassi C, Cong X, Row RH, Lafevre-Bernt MA, Cusack MP, Ratovitski T, Hirschhorn R, Ross CA, Gibson BW, Ellerby LM (2006) Huntingtin Phosphorylation Sites Mapped by Mass Spectrometry: Modulation of Cleavage and Toxicity. J Biol Chem 281:23686-23697.

Schneider RM, Medvedovska Y, Hartl I, Voelker B, Chadwick MP, Russell SJ, Cichutek K, Buchholz CJ (2003) Directed evolution of retroviruses activatable by tumour-associated matrix metalloproteases. Gene Ther 10:1370-1380.

Smith R, Brundin P, Li JY (2005) Synaptic dysfunction in Huntington's disease: a new perspective. Cell Mol Life Sci 62:1901-1912.

Southwell AL, Khoshnan A, Dunn DE, Bugg CW, Lo DC, Patterson PH (2008) Intrabodies binding the proline-rich domains of mutant huntingtin increase its turnover and reduce neurotoxicity. J Neurosci 28:9013-9020.

Stocks MR (2004) Intrabodies: production and promise. Drug Discov Today 9:960-966.

Suhr ST, Gil EB, Senut MC, Gage FH (1998) High level transactivation by a modified Bombyx ecdysone receptor in mammalian cells without exogenous retinoid X receptor. Proc Natl Acad Sci U S A 95:7999-8004.

Suopanki J, Gotz C, Lutsch G, Schiller J, Harjes P, Herrmann A, Wanker EE (2006) Interaction of huntingtin fragments with brain membranes--clues to early dysfunction in Huntington's disease. J Neurochem 96:870-884.

Tanaka T, Lobato MN, Rabbitts TH (2003) Single domain intracellular antibodies: a minimal fragment for direct in vivo selection of antigen-specific intrabodies. J Mol Biol 331:1109-1120.

Tanaka Y, Igarashi S, Nakamura M, Gafni J, Torcassi C, Schilling G, Crippen D, Wood JD, Sawa A, Jenkins NA, Copeland NG, Borchelt DR, Ross CA, Ellerby LM (2006) Progressive phenotype and nuclear accumulation of an amino-terminal cleavage fragment in a transgenic mouse model with inducible expression of full-length mutant huntingtin. Neurobiol Dis 21:381-391.

Trushina E et al. (2004) Mutant huntingtin impairs axonal trafficking in mammalian neurons in vivo and in vitro. Mol Cell Biol 24:8195-8209.

Urban JH, Schneider RM, Compte M, Finger C, Cichutek K, Alvarez-Vallina L, Buchholz CJ (2005) Selection of functional human antibodies from retroviral display libraries. Nucleic Acids Res 33:e35.

Valenza M, Rigamonti D, Goffredo D, Zuccato C, Fenu S, Jamot L, Strand A, Tarditi A, Woodman B, Racchi M, Mariotti C, Di Donato S, Corsini A, Bates G, Pruss R, Olson JM, Sipione S, Tartari M, Cattaneo E (2005) Dysfunction of the cholesterol biosynthetic pathway in Huntington's disease. J Neurosci 25:9932-9939.

Valera AG, Diaz-Hernandez M, Hernandez F, Ortega Z, Lucas JJ (2005) The ubiquitin-proteasome system in Huntington's disease. Neuroscientist 11:583-594.

Venkatraman P, Wetzel R, Tanaka M, Nukina N, Goldberg AL (2004) Eukaryotic proteasomes cannot digest polyglutamine sequences and release them during degradation of polyglutamine-containing proteins. Mol Cell 14:95-104.

Visintin M, Tse E, Axelson H, Rabbitts TH, Cattaneo A (1999) Selection of antibodies for intracellular function using a two-hybrid in vivo system. Proc Natl Acad Sci U S A 96:11723-11728.

Winter G, Griffiths AD, Hawkins RE, Hoogenboom HR (1994) Making antibodies by phage display technology. Annu Rev Immunol 12:433-455.

Wolfgang WJ, Miller TW, Webster JM, Huston JS, Thompson LM, Marsh JL, Messer A (2005) Suppression of Huntington's disease pathology in Drosophila by human single-chain Fv antibodies. Proc Natl Acad Sci U S A 102:11563-11568.

Woodruff TM, Crane JW, Proctor LM, Buller KM, Shek AB, de Vos K, Pollitt S, Williams HM, Shiels IA, Monk PN, Taylor SM (2006) Therapeutic activity of C5a receptor antagonists in a rat model of neurodegeneration. Faseb J 20:1407-1417.

Zeitlin S, Liu JP, Chapman DL, Papaioannou VE, Efstratiadis A (1995) Increased apoptosis and early embryonic lethality in mice nullizygous for the Huntington's disease gene homologue. Nat Genet 11:155-163.

Zoghbi HY, Orr HT (2000) Glutamine repeats and neurodegeneration. Annu Rev Neurosci 23:217-247.

Zuccato C, Tartari M, Crotti A, Goffredo D, Valenza M, Conti L, Cataudella T, Leavitt BR, Hayden MR, Timmusk T, Rigamonti D, Cattaneo E (2003) Huntingtin interacts with REST/NRSF to modulate the transcription of NRSE-controlled neuronal genes. Nat Genet 35:76-83.

Appendix B

Recombinant Intrabodies as Molecular Tools and Potential Therapeutics for Huntington's Disease

Ali Khoshnan, Amber Southwell, Charles Bugg, Jan Ko and Paul H. Patterson

In "Neurobiology of Huntington's Disease, Applications to Drug Discovery," Edited by Don C. Lo and Robert E. Hughes (Frontiers in Neuroscience, Boca Raton, FL: CRC Press, 2011), pp. 255-266

The therapeutic potential of intracellularly expressed, recombinant or single-chain fragment variable (scFv) antibodies (intrabodies) is being explored for several diseases including cancer, HIV, and neurodegenerative disorders. Intrabodies can bind and inactivate toxic intracellular proteins, prevent misfolding, promote degradation and block aberrant protein-protein interactions with extreme molecular specificity. Neurodegenerative disorders are particularly attractive candidates for these reagents, since many of these diseases involve protein misfolding, oligomerization and aggregation (1). In particular, intrabodies have shown efficacy in blocking the toxicity of the amyloidogenic protein fragment Aβ in cell culture and mouse models of Alzheimer's disease, paving the way for clinical trials of these reagents in brain disorders (2). In addition to their therapeutic potential, intrabodies are also useful molecular tools to identify the pathogenic epitopes in toxic proteins, which can be targets for other types of therapy. In this chapter, we will review the strategies that have been used to develop intrabodies specific for the huntingtin (htt) protein, and describe their testing in models of

Huntington disease (HD) and their development as potential therapeutics for clinical use in HD.

Strategies for Intrabody Construction

Intrabodies are recombinant antibody molecules usually derived from a monoclonal antibody of interest by cDNA cloning of the antigen binding domain; the variable heavy and light chains (V_H and V_L) from the monoclonal antibody are then joined together by a synthetic cDNA encoding a flexible polypeptide linker (Fig. 1). Alternatively, naïve intrabody libraries have been constructed and cloned in phage or displayed on yeast for selection and binding to specific antigens.

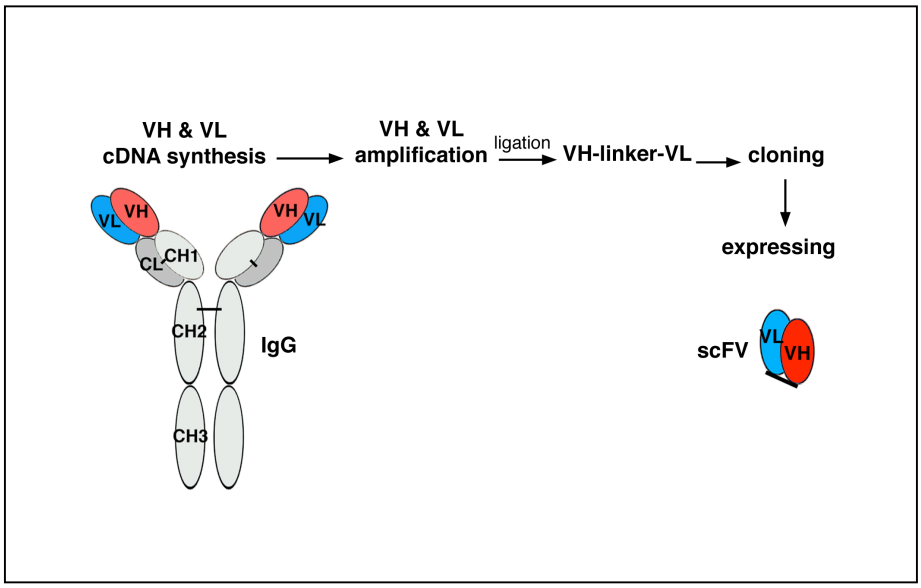

Figure. 1. Schematic representation of cloning of scFvs.

A major problem with intracellular expression of intrabodies is, however, proper folding and low solubility in the reducing cytoplamic environment ((Biocca et al., 1995). This is due to the presence of disulfide bonds in both the V_H and V_L, which are required for efficient folding. While some intrabodies are inherently

stable in the cytoplasm, selection of stable intrabody frameworks, which fold efficiently in the absence of disulfide bonds, has also been achieved (4). Additionally, a process known as *in vitro* maturation or reengineering, where the disulfide bonds are removed, can be used to correct low solubility through several rounds of random mutagenesis and antigen binding selection (5).

Single domain intrabodies. Recently, functional single domain (V_H or V_L but not both) intrabodies have also been developed and selected for specific targets. These single domain intrabodies can block protein-protein interaction and are favored for their stability and better folding (6). Moreover, *in vitro* maturation of single domain intrabodies can further enhance their folding, specificity and solubility (5).

Development of epitope-specific intrabodies against Htt

Epitopes in mutant huntingtin for intrabody development. Intrabodies recognizing a variety of epitopes within mutant huntingtin (Htt) exon-1 (HDx1) have been isolated and tested for their ability to block toxicity and aggregation (Fig. 1). Lecerf and colleagues have isolated an intrabody recognizing the 17 N-terminal AA of Htt (C4) from a synthetic phage library and tested this intrabody for efficacy in cell culture (7). C4 was found to block aggregation and interfere with malonate-enhanced toxicity of mutant HDx1 (Murphy and Messer, 2004b). Due to its modest efficacy, C4 was further matured and examined in a fly model of HD, where it was found to protect against the toxicity of HDx1 during the larval stage and significantly increase life span (Wolfgang et al., 2005a).

Surprisingly, C4 increased the level of soluble mutant HDx1 in both fly and culture models (9). This property of C4 raises the possibility that long-term exposure to this intrabody could lead to buildup of soluble HDx1 and promote oligomerization and toxicity. Recent studies suggest that mutant HDx1 monomers can acquire a toxic conformation by switching from an α-helical to a β-sheet conformation (10). Furthermore, blocking the 17 N-terminal AA of Htt may also have other undesirable consequences; for example, this motif is essential for vesicle localization as well as Htt cytoplasmic retention and turnover (11, 12) and removal of the N-terminal domain results in nuclear localization of HDx1, which has been associated with enhanced toxicity (11, 12). Therefore, long-term expression studies in transgenic HD mice will be important to examine if binding of C4 to the 17 N-terminal AA of Htt has any detrimental effects in a therapeutic setting.

Another intrabody that binds the N1-17 domain of Htt (V_L12.3) was isolated from a yeast surface display library as a single domain light chain and matured *in vitro* through random mutagenesis and selection by yeast surface display (5). V_L12.3, engineered for efficient intracellular expression and folding by removal of its disulfide bond, is a more potent inhibitor of mutant HDx1 aggregation and toxicity in cell culture than C4 (13). However, like C4, V_L12.3 increases the level of soluble mutant HDx1; moreover, V_L12.3 promotes nuclear localization of mutant HDx1 (14). This paradoxical inhibition of toxicity and aggregation together with enhancement of nuclear localization of Htt may eventually shed light on the role of nuclear Htt in toxicity. In fact, intrabodies such as V_L12.3 may have important research and clinical potential in blocking association of soluble mutant HDx1 with nuclear

targets. Examination of $V_L12.3$ in animal models of HD is crucial for validating its protective effects and further understanding of the role of N-17 AA in mutant Htt toxicity.

Figure 2. **Binding domains of different intrabodies that have been developed against the HDx-1 peptide sequence**

The polyglutamine and polyproline domains of Htt. Intrabodies recognizing the polyglutamine (polyQ) and proline-rich motifs of HDx1 have also been shown to influence toxicity. We generated a number of monoclonal antibodies using either polyQ peptides or HDx1 recombinant proteins as antigens (15). The intrabodies cloned from these antibodies display striking, epitope-specific differences in their effects on mutant HDx1 toxicity. The MW7 intrabody, which recognizes the polyproline (polyp) motifs of mutant HDx1, protects against toxicity in several models of HD, including cell culture (Fig. 2), acute brain slice culture, and *Drosophila* models (16, 17, Reinhart et al., unpublished data). This protection is correlated with reduced aggregation and increased turnover of mutant HDx1 (14, 16).

In contrast, intrabodies that bind the expanded polyQ domain exacerbate the toxicity and aggregation of mutant HDx1 in cell culture (16**).** One possible explanation for this effect is that the MW1 and MW2 intrabodies may bind and stabilize a novel confirmation in HDx1 with expanded polyQ. In fact, several anti-

polyQ antibodies bind Htt in different cellular compartments, supporting the presence of distinct conformations of expanded polyQ (15). On the other hand, anti-polyQ intrabody binding could aid in nucleation of monomeric mutant HDx1 and accelerate oligomerization**.** In a study of the crystal structure of MW1 bound to polyQ, the polyQ domain adopts an extended, coil-like structure with short sections of polyproline type II helix and b-strand. Consistent with the linear lattice model (18) for polyQ, linking MW1 intrabodies together in a multimeric form results in tighter binding to longer compared to shorter polyQ domains and, compared with monomeric Fv, binds expanded polyQ with higher apparent affinity (19). Whether the affinity of the monomeric vs. multimeric form of MW1 influences the oligomerization of mutant Htt remains unknown.

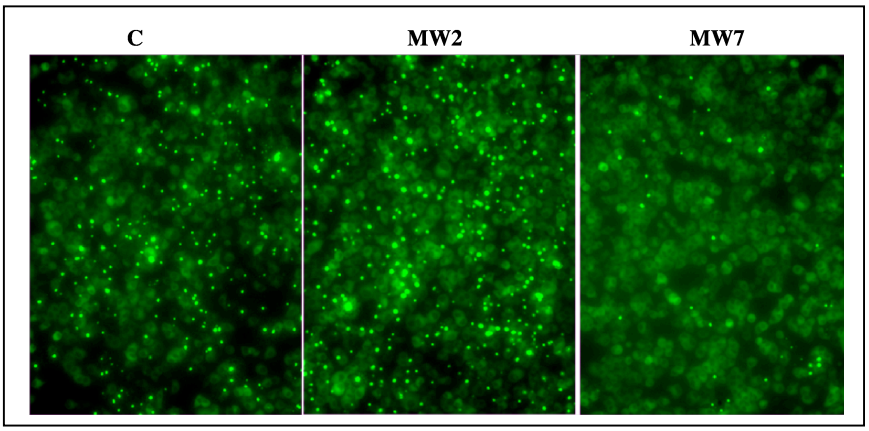

Figure 3. MW7 prevents while MW2 promotes aggregation of mutant HDx1-EGFP in PC12 cells. MW7 and MW2 cDNAs were cloned into ecdysone-inducible vectors and transfected into PC12 cells that were engineered to express HDx1 in response to ecdysone (26). Selected PC12 cell clones were then treated with ecdysone to induce simultaneous expression of HDx1 and the scFv. A luciferase construct was used as control (far left panel).

Clearly, a unified view on the role of aggregates in HD pathology will be required to understand better how anti-polyQ intrabodies could be used to regulate mutant htt toxicity. The initial studies on the effects of MW1 and MW2 on HDx1 toxicity and aggregation were done in non-neuronal cells and with 103 polyQ HDx1, which may require a high concentrations of intrabody to counteract its toxicity. Thus, reevaluation of anti-polyQ intrabodies is worthy of investigation, possibly with shorter polyQ repeats or a multimeric form of MW1 (18). Indeed, in light of recent findings that mutant HDx1 aggregation can be neuroprotective, anti-polyQ intrabodies will be ideal tools to dissect the role of aggregation and toxicity in neuronal models (20).

Conformation-specific intrabodies. Isolation of conformation specific polyQ intrabodies may help in determining whether expanded polyQ can be a potential target for intrabody therapy. This approach has recently been reported for α-synuclein oligomers (21). These oligomer-specific intrabodies inhibit both aggregation and toxicity of α-synuclein and have been useful tools for identifying the pathogenic epitopes. Our laboratory, in collaboration with Ron Wetzel's group, isolated a panel of monoclonal antibodies that specifically recognize oligomeric forms of polyQ proteins. Interestingly, some of these antibodies also react with fibrils formed by prion proteins and Aβ amyloid (22). This cross-reactivity suggests the presence of common structural motifs in the fibrils of misfolded proteins that cause neurodegeneration. A similar antiserum that also reacts with amyloid fibrils of various misfolded proteins has been reported by Glabe's laboratory (23). It will

be interesting to see if intrabodies derived from these antibodies can block oligomerization and the toxicity of these diverse proteins *in vivo*.

The proline-rich domain of Htt. Finally, we have recently isolated two V_L domain intrabodies from a human scFv phage display library (24) that specifically bind to the proline-rich epitope in HDx1 (which is between the two pure polyP domains discussed above)(14). These single-domain intrabodies (Happ1 and 3, Fig. 1) are efficient in reducing HDx1 toxicity and aggregation. A novel feature of these intrabodies, and of the anti-polyP intrabody MW7, is their reduction of soluble mutant HDx1 levels by increasing its turnover. It is intriguing that although the proline-rich epitope is identical in mutant and wild-type (WT) Htt, the Happ intrabodies have a greater effect on turnover of the mutant versus WT Htt (14). In addition, the inhibitory effects of Happ1 and 3 suggest that the proline-rich domain of Htt also contributes to Htt toxicity and may be involved in the misfolding of mutant HDx1 or in its binding to partners critical for toxicity.

Intrabodies as research tools to dissect mechanisms of Htt disease pathogenesis

While the therapeutic potential of intrabodies in mouse HD models remains to be explored, anti-Htt intrabodies are powerful molecular tools that can be used to identify and characterize the pathogenic epitopes in HDx1 that regulate oligomerization, toxicity, and interactions with other disease mechanisms and pathways. The findings that intrabodies directed against various epitopes of HDx1

can either block or enhance aggregation and toxicity underscore the importance of these domains.

For example, it is known that the first 17 amino acids of HDx1 regulate not only its nuclear targeting but also its endoplasmic reticulum and mitochondrial localization (11, 12). One hypothesis is thus that V_L12.3 reduces toxicity by blocking the localization of mutant HDx1 to mitochondria and thereby reducing mitochondrial permeability. On the other hand, consistent with the role of the first 17 AA in cytoplasmic retention of HDx1, coexpression of V_L12.3 with HDx1 also promotes HDx1 nuclear localization (14). Thus, as noted above, while studies with V_L12.3 confirm the importance of 17 N-terminal AA in cellular distribution of Htt and the contribution of this motif to aggregation and toxicity (11, 12), they also raise questions regarding whether and how nuclear localization contributes to toxicity. One possibility is that although V_L12.3 promotes nuclear localization of HDx1, it may also prevent its association with the transcriptional apparatus.

Similarly, the ability of anti-polyQ intrabodies to promote aggregation and toxicity of mutant HDx1 (16) may be relevant for understanding the mechanism of *in vivo* oligomerization. One theory is that anti-polyQ intrabodies function as nucleating centers and recruit soluble HDx1, which then forms oligomers and eventually aggregates. Alternatively, binding of anti-polyQ intrabodies may induce or stabilize a conformation in the expanded polyQ domain that enhances oligomerization. If so, this raises the question of whether there are endogenous cellular modifiers that induce such conformation changes in this domain. Understanding how MW1 and 2 promote aggregation may thus shed light on this

process *in vivo* and enable discovery of modifiers of polyQ oligomerization. In this context, it is intriguing that intracellular expression of a polyQ binding peptide (PQBP1) blocks the toxicity of mutant HDx1 in tissue culture (25); this peptide interferes with conversion of a non-toxic α-helical structure of polyQ to a toxic β-sheet conformation (10). While this conformation switch occurs *in vitro* with purified protein, the existence of an endogenous modifier of polyQ toxicity is an attractive area of investigation and intrabodies will help with the identification of these potential regulators of toxicity.

The MW7 intrabody, on the other hand, was instrumental in identifying the HDx1 polyP domain as a pathogenic epitope (16, 26). Several important signaling proteins including NEMO /IKKγ, CBP, WW domain proteins, dynamin and FIP-2 require the HDx1 polyP domain for binding to HDx1 (26-29). Therefore, the protective mechanism of the MW7 intrabody may work through its reducing the sequestration of important cellular proteins by mutant HDx1. In fact, we have shown that MW7 blocks binding of the IκB-kinase (IKK) complex to the proline-rich domain of mutant HDx1 and subsequently reduces HDx1-induced NF-κB activation (26; Fig. 3). Moreover, both MW7 and genetic inhibitors of the IKK complex have similar inhibitory effects on mutant HDx1 in cell and brain slice cultures (26). These findings underscore the importance of intrabodies as molecular tools that can lead to the identification of novel pathogenic epitopes and therapeutic targets.

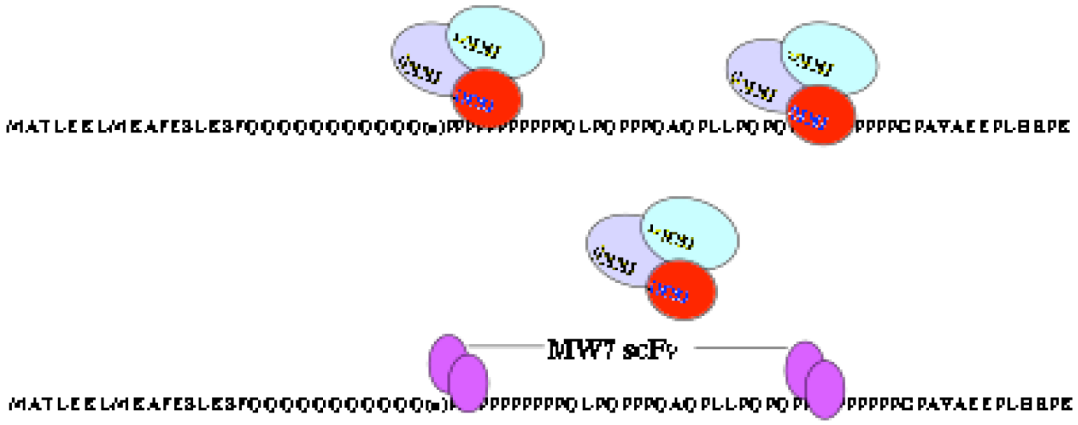

Figure 4. Schematic diagram showing the interaction of IKK complex and Htt. Binding of HDx1 to the IKK complex requires the polyP domain of Htt and the N-terminus of IKKγ. Blocking the interaction of mutant HDx1 with the IKK complex reduces the toxicity in a brain slice culture model of HD. Binding of MW7 intrabody to the poly-P domains of Htt also prevents IKK–HDx1 interaction and thereby reduces the toxicity of mutant HDx1(16).

Novel targets for intrabody therapy in HD

To date, most of the intrabodies developed to perturb Htt function have been targeted to HDx1, which is generated by proteolytic processing of full-length Htt. However, a more upstream, primary therapeutic goal would be to prevent proteolytic processing of mutant Htt using specific intrabodies. Htt is cleaved by several proteases, including caspases 3 and 6, and the calpains (30, 31). Cleaved mutant Htt fragments are precursors to oligomers, and the species that accumulate in the nucleus likely contribute to transcriptional dysregulation (2). Therefore, blocking the cleavage of full-length Htt by intrabodies may be an effective strategy to reduce the generation of fragments that misfold and induce toxicity.

Indeed, such inhibition of Htt cleavage by intrabody binding to cleavage sites may be preferred over small molecule inhibitors of the relevant proteases because of the target specificity of antibody binding, and because small molecule inhibitors can have systemic side effects. This technology has already been applied to reduce production of β-amyloid in AD models. Intracellular expression of an intrabody that binds an epitope in close proximity to the β-secretase cleavage site of amyloid precursor protein (APP) blocks production of amyloidogenic fragments and promotes cleavage with α-secretase, which generates non-amyloidogenic Aβ (32). For HD, intrabodies specific to Htt cleavage sites can readily be isolated from phage display libraries and tested in tissue culture for their effects on Htt processing. This approach could be used to validate the role of these caspases on Htt processing and toxicity and, importantly, would generate potential therapeutics for HD.

Delivery of intrabodies to the HD brain

In principle, viral vector-based gene therapy is the ideal method for the delivery of therapeutic intrabodies to the brain. Optimal delivery of gene therapy vectors into the diseased brain remains an important research area and represents the best mode of delivery for long-term expression. Among these, adeno-associated viruses (AAV) are the most promising vectors, since they are largely non-pathogenic and the virus is already widespread and non-toxic in human populations. AAV is capable of infecting both dividing and non-dividing cells and generating long-term expression of transgenes. The existence of several serotypes offers varied tropism allowing expression in a wide range of cell and tissue types. AAV vectors also

appear to be safe and well tolerated, as no obvious side effects have been reported following a phase 1 clinical trial of AAV-mediated delivery of glutamic acid decoarboxylase (GAD) to the brains of human Parkinson's disease patients (Kaplitt et al., 2007). Intracerebral delivery may also avoid systemic complications outside of the CNS.

In animal models of AD, several successful approaches have been reported for delivery of anti-Aβ intrabodies (2, 34). Intracranial delivery of AAV encoding anti-Aβ scFvs, which can be secreted and enter the circulation, has been effective in reducing amyloid plaque loads, neurotoxicity and correcting behavioral abnormalities (2). Viral injections in this model were performed at P0, which allowed widespread distribution and expression. Intrabody delivery to HD models may be more challenging, since the toxic protein remains intracellular, in contrast to Aβ, which is secreted. Nonetheless, success has been obtained with systemic vaccination approaches in mouse models of Parkinson's disease, in which the targeted antigen, a-synuclein, is also thought to be intracellular (35). Moreover, we find that anti-Htt antibodies display specific binding to the surfaces of live cells expressing mutant HDx1, suggesting that systemic and/or extracellular delivery of intrabodies may also be beneficial in combating Htt toxicity (Fig. 5).

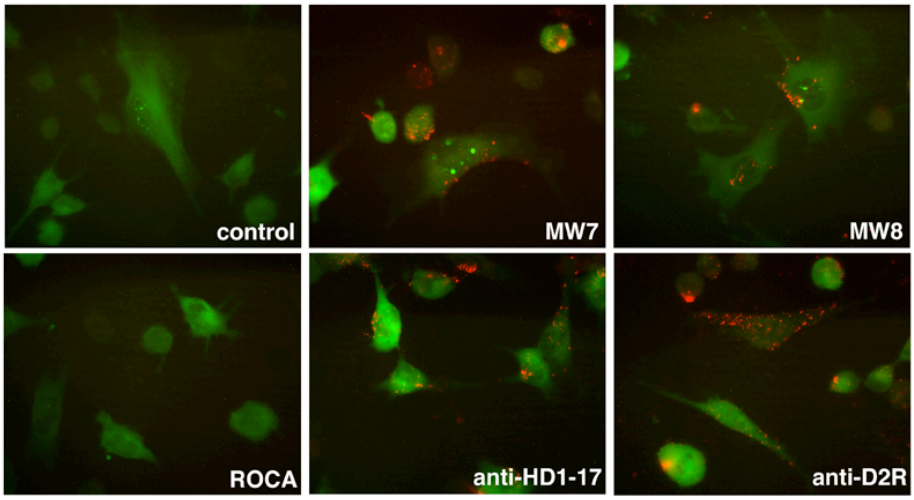

Figure 5. The anti-huntingtin antibodies/intrabodies, anti-N1-17, MW7 and MW8, stain living striatal cells with a punctate pattern (red) similar to an anti-dopamine D2 receptor (D2R) antibody. The striatal ST-14 cell line was transduced with HDx1-EGFP (PQ103) lentivirus and live cells were incubated with either control antibodies (mouse Ig2b, and a non-neuronal anti-CD9 (ROCA), or anti-Htt antibodies/intrabodies as indicated. A polyclonal antibody against D2R was used as positive control for cell surface staining. Alexa 568-conjugated secondary antibody was used to visualize staining (red); the green fluorescence is native HDx1-EGFP.

Direct viral delivery to the striatum has also proven to be effective. A single injection of an AAV vector encoding an RNAi targeted against Htt results in extensive spread, reduced HDx1 oligomerization, enhanced DARPP-32 expression in striatal neurons, and amelioration of HD neuropathology (36, 37). Significant neuroprotection by AAV-mediated delivery of the neurotrophins GDNF and BDNF to striatum has also been demonstrated in the quinolinic acid model of HD (38). Thus, direct delivery of intrabody viral vectors to the striatum may be realistic and it is

expected that intrabodies will have fewer off-target effects than either RNAi or neurotrophins, due to the high degree of specificity of antibodies. In fact, an intrabody constructed from the EM48 monoclonal antibody, which targets the C-terminus of HDx1 provides significant protection against mutant HDx1 *in vivo* (39). Injection of an adenvovirus expressing EM48 intrabody in the striatum of N-171-82Q HD mice reduces the overall toxicity and decreases the aggregation of mutant Htt in the neuropil. Moreover, expression of EM48 in the striatum improves some of the behavioral deficits in the HD mice. EM48 does not, however, extend the life span (39). In a lentiviral model of mutant HDx1, which causes substantial degeneration in the striatum of injected mice, coinjection with an AAV expressing V_L12.3- or Happ1 reduces aggregation and ameliorates the loss of DARP-32 expression in the adult. Preliminary results indicate that AAV-V_L12.3 and AAV-HAPP-1 also improve the amphetamine-induced rotation bias seen with unilateral mHtt lentivirus injection (40).

Future directions for intrabodies in HD therapy

Development of intrabodies for therapeutic purposes and as novel molecular tools to perturb protein function *in vivo* is an exciting emerging field. Some intrabodies have already reached clinical trials and others have been used as novel diagnostic tools (40). As optimization of delivery vehicles progesses, anti-Htt intrabodies will hold great promise for HD therapy in the future. However, many milestones, including the identification of the best targets, the most potent and

effective intrabodies, and the most effective methods to ensure a widespread delivery to the CNS must first be achieved. With rapid progress in proteomics, intrabodies can also serve as excellent tools for *in vivo* functional knock-down, for inactivating specific protein domains, and for inhibiting interactions between particular proteins. The HD field can also benefit from intrabody technology for inactivating other intracellular targets that enhance Htt toxicity such as caspases, p53, and IKKs.

References

1. Ross CA, Poirier MA (2005) What is the role of protein aggregation in neurodegeneration? *Nat Rev Mol Cell Biol* 6:891-8.

2. Levites Y, Jansen K, Smithson LA, l Dakin R, Holloway VM, Das P, Golde TE (2006) Intracranial adeno-associated virus-mediated delivery of anti-pan amyloid beta, amyloid beta40, and amyloid beta42 single-chain variable fragments attenuates plaque pathology in amyloid precursor protein. *J Neurosci,* 26:11923 -8.

3. Biocca S, Ruberti, F, Tafani, M, Pierandrei-Amaldi, P, Cattaneo A (1995) Redox state of single chain Fv fragments targeted to the endoplasmic reticulum, cytosol and mitochondria. *Biotechnology* 13:1110-5.

4. Tanaka T, Rabbitts TH (2003) Intrabodies based on intracellular capture frameworks that bind the RAS protein with high affinity and impair oncogenic transformation. *EMBO J* 22:1025-35.

5. Colby DW, Garg P, Holden T, Chao G, Webster JM, Messer A, Ingram VM, Wittrup KD (2004) Development of a human light chain variable domain (V(L)) intracellular antibody specific for the amino terminus of huntingtin via yeast surface display. *J Mol Biol* 342:901-12.

6. Tanaka T, Lobato MN, Rabbitts TH (2003) Single domain intracellular antibodies: a minimal fragment for direct in vivo selection of antigen-specific intrabodies. *J Mol Biol* 331:1109-20.

7. Lecerf JM, Shirley TL, Zhu Q, Kazantsev A, Amersdorfer P, Housman DE, Messer A, Huston JS (2001) Human single-chain Fv intrabodies counteract in situ

huntingtin aggregation in cellular models of Huntington's disease. *Proc Natl Acad Sci* 98:4764-9.

8. Murphy RC, Messer A (2004) A single-chain Fv intrabody provides functional protection against the effects of mutant protein in an organotypic slice culture model of Huntington's disease. *Molec Brain Res* 121: 141-5.

9. Wolfgang WJ, et al. (2005) Suppression of Huntington's disease pathology in Drosophila by human single-chain Fv antibodies. *Proc Natl Acad Sci* 102: 11563-8.

10. Nagai Y, Inui T, Popiel HA, Fujikake N, Hasegawa K, Urade Y, Goto Y, Naiki H, Toda T (2007) A toxic monomeric conformer of the polyglutamine protein. *Nat Struct Mol Biol* 14:332-40.

11. Rockabrand E, Slepko N, Pantalone A, Nukala VN, Kazantsev A, Marsh JL, Sullivan PG, Steffan JS, Sensi SL, Thompson LM (2007) The first 17 amino acids of Huntingtin modulate its sub-cellular localization, aggregation and effects on calcium homeostasis. *Hum Mol Genet* 16:61-77.

12. Atwal RS, Xia J, Pinchev D, Taylor J, Epand RM, Truant R (2007) Huntingtin has a membrane association signal that can modulate huntingtin aggregation, nuclear entry and toxicity. *Hum Mol Genet* 16:2600-15.

13. Colby DW, et al. (2004) Potent inhibition of huntingtin aggregation and cytotoxicity by a disulfide bond-free single-domain intracellular antibody. *Proc Natl Acad Sci* 101:17616-21.

14. Southwell, AL, Khoshnan A, Dunn D, Bugg C, Lo D, and Patterson PH. Novel intrabodies block aggregation and toxicity of mutant huntingtin by increasing its turnover. *J. Neurosci.* 28:9013-20.

15. Ko J, Ou S, Patterson PH (2001) New anti-huntingtin monoclonal antibodies: implications for huntingtin conformation and its binding proteins. *Brain Res Bull.* 56:319-29.

16. Khoshnan A, Ko J, Patterson PH (2002) Effects of intracellular expression of anti-huntingtin antibodies of various specificities on mutant huntingtin aggregation and toxicity. *Proc Natl Acad S*ci 99:1002-7.

17. Jackson GR, Sang TK, Ko J, Khoshnan A, Patterson PH (2004) Inhibition of mutant huntingtin-induced neurodegeneration in vivo by expression of a polyproline-binding single chain antibody. *Soc Neurosci* abstr 938.5.

18. Bennett MJ, Huey-Tubman KE, Herr AB, West AP Jr, Ross SA, Bjorkman PJ (2002) A linear lattice model for polyglutamine in CAG-expansion diseases. *Proc Natl Acad Sci* 99:11634-9.

19. Li P, Huey-Tubman KE, Gao T, Li X, West AP Jr, Bennett MJ, Bjorkman PJ (2007) The structure of a polyQ-anti-polyQ complex reveals binding according to a linear lattice model. *Nat Struct Mol Biol* 14:381-7.

20. Arrasate M, Mitra S, Schweitzer ES, Segal MR, Finkbeiner S (2004) Inclusion body formation reduces levels of mutant huntingtin and the risk of neuronal death. *Nature* 431:805-10.

21. Emadi S, Barkhordarian H, Wang MS, Schulz P, Sierks MR (2007) Isolation of a human single chain antibody fragment against oligomeric alpha-synuclein that

inhibits aggregation and prevents alpha-synuclein-induced toxicity. *J Mol Biol* 368:1132-44.

22. Geva M, Wetzel R et al. (2005) Monoclonal antibodies that bind different polyglutamine aggregate conformations. The Protein Society, abstr B165.

23. Kayed R, Head E, Thompson JL, McIntire TM, Milton SC, Cotman CW, Glabe CG (2003) Common structure of soluble amyloid oligomers implies common mechanism of pathogenesis. *Science* 300:486-9.

24. Griffiths AAD, et al. (1994) Isolation of high affinity human antibodies directly from large synthetic repertoires. *EMBO J* 13: 3245-60.

25. Popiel HA, Nagai Y, Fujikake N, Toda T (2007) Protein transduction domain-mediated delivery of QBP1 suppresses polyglutamine-induced neurodegeneration in vivo. *Mol Ther* 15:303-9.

26. Khoshnan A, Ko J, Watkin EE, Paige LA, Reinhart PH, Patterson PH (2004) Activation of the IkappaB kinase complex and nuclear factor-kappaB contributes to mutant huntingtin neurotoxicity. *J Neurosci* 24:7999-8008.

27. Qin ZH, Wang Y, Sapp E, Cuiffo B, Wanker E, Hayden MR, Kegel KB, Aronin N, DiFiglia M (2004) Huntingtin bodies sequester vesicle-associated proteins by a polyproline-dependent interaction. *J Neurosci* 24:269-81.

28. Steffan JS, Bodai L, Pallos J, Poelman M, McCampbell A, Apostol BL, Kazantsev A, Schmidt E, Zhu YZ, Greenwald M, Kurokawa R, Housman DE, Jackson GR, Marsh JL, Thompson LM (2001) Histone deacetylase inhibitors arrest polyglutamine-dependent neurodegeneration in Drosophila. *Nature* 413:739-43.

29. Faber PW, Barnes GT, Srinidhi J, Chen J, Gusella JF, MacDonald ME (1998)

Huntingtin interacts with a family of WW domain proteins. *Hum Mol Genet.* 7:1463-74.

30. Gafni J, Hermel E, Young JE, Wellington CL, Hayden MR, Ellerby LM (2004) Inhibition of calpain cleavage of huntingtin reduces toxicity: accumulation of calpain/caspase fragments in the nucleus. *J Biol Chem* 279:20211-20.

31. Graham RK, Deng Y, Slow EJ, Haigh B, Bissada N, Lu G, Pearson J, Shehadeh J, Bertram L, Murphy Z, Warby SC, Doty CN, Roy S, Wellington CL, Leavitt BR, Raymond LA, Nicholson DW, Hayden MR (2006) Cleavage at the caspase-6 site is required for neuronal dysfunction and degeneration due to mutant huntingtin. *Cell* 125:1179-91.

32. Paganetti P, Calanca V, Galli C, Stefani M, Molinari M (2005) Beta-site specific intrabodies to decrease and prevent generation of Alzheimer's Abeta peptide. *J Cell Biol* 168:863-8.

33. Kaplitt MG, Feigin A, Tang C, Fitzsimons HL, Mattis P, Lawlor PA, Bland RJ, Young D, Strybing K, Eidelberg D, During MJ (2007). Safety and tolerability of gene therapy with an adeno-associated virus (AAV) borne GAD gene for Parkinson's disease: an open label, phase I trial. Lancet. 369(9579):2097-2105.

34. Fukuchi K, Tahara K, Kim HD, Maxwell JA, Lewis TL, Accavitti-Loper MA, Kim H, Ponnazhagan S, Lalonde R (2006) Anti-Abeta single-chain antibody delivery via adeno-associated virus for treatment of Alzheimer's disease. *Neurobiol Dis* 23:502-11.

35. Masliah E, Rockenstein E, Adame A, Alford M, Crews L, Hashimoto M, Seubert P, Lee M, Goldstein J, Chilcote T, Games D, Schenk D (2005) Effects of alpha-

synuclein immunization in a mouse model of Parkinson's disease. *Neuron* 46:857-68.

36. Harper, SQ, et al. (2005) RNA interference improves motor and neuropathological abnormalities in a Huntington's disease mouse model. *Proc Natl Acad Sci* 102: 5820-5.

37. Machida Y, Okada T, Kurosawa M, Oyama F, Ozawa K, Nukina N (2006) rAAV-mediated shRNA ameliorated neuropathology in Huntington disease model mouse. *Biochem Biophys Res Commun* 343:190-7.

38. Kells AP, Fong DM, Dragunow M, During MJ, Young D, Connor B (2004) AAV-mediated gene delivery of BDNF or GDNF is neuroprotective in a model of Huntington disease. *Mol Ther* 9:682-8.

39. Wang CE, Zhou H, McGuire JR, Cerullo V, Lee B, Li SH, Li XJ (2008) Suppression of neuropil aggregates and neurological symptoms by an intracellular antibody implicates the cytoplasmic toxicity of mutant huntingtin. *J Cell Biol.* 181:803-816.

40. Amber L. Southwell AL, Ali Khoshnan A, Denise Dunn D, Donald C. Lo DC, Paul H. Patterson PH. (2008) Intrabodies binding the proline-rich domains of mutant huntingtin increase turnover and reduce neurotoxicity.

Appendix C

Intrabodies binding the proline-rich domains of mutant huntingtin increase its turnover and reduce neurotoxicity

Southwell AL, Khoshnan A, Dunn DE, Bugg CW, Lo DC, Patterson PH

J Neurosci. 2008, 28(36): 9013-20.

Introduction

Huntington's disease is an autosomal dominant, progressive, neurodegenerative disorder that results from the expansion of a polyglutamine (polyQ) tract in HDx1 (The Huntington's Disease Collaborative Research Group, 1993). At least nine other neurodegenerative diseases are caused by the expansion of a polyQ tract, including several types of spinocerebellar ataxia (Orr et al., 1993; Kawaguchi et al., 1994; Imbert et al., 1996; David et al., 1997), dentatorubral pallidoluysian atrophy (Koide et al., 1994), and spinobulbar muscular atrophy (Spada et al., 1991). In each case, the polyQ expansion is in a different protein, and although the mutant protein is expressed widely, only a specific subset of neurons unique to each disease die. Although expression of pure polyQ is sufficient to cause toxicity (Marsh et al., 2000; Yang et al., 2002b), it is the protein context surrounding the polyQ expansion that makes particular neurons susceptible in each disease. In HD, the mutant protein exhibits toxic gain of function, which includes aggregation, sequestering of important cellular proteins such as transcription factors, and aberrant protein-protein interactions, including disruption of the ubiquitin proteasome (Duyao et al., 1995a; Ross, 1997; Wanker, 2000; Jana et al., 2001;

Ramaswamy et al., 2007). This leads to chorea, dementia and loss of medium spiny striatal as well as some cortical neurons (Reddy et al., 1999a; Zoghbi and Orr, 2000b; Nakamura and Aminoff, 2007). HDx-1 consists of 17 N-terminal amino acids followed by the polyQ tract, the PRR, which consists of two polyP stretches that are separated by a P-rich domain, and 13 additional AAs (Fig.1A). The non-polyQ domains in HDx-1 are known to modulate the toxicity of the mutant protein, although the mechanisms by which this occurs are not well understood (Duennwald et al., 2006a). Understanding how these non-polyQ domains contribute to the toxicity and specificity of mHtt could lead to new therapeutic strategies.

Classically, the function of a protein domain would be studied by removal of that domain followed by functional testing. Although a great deal of knowledge has been acquired through such methods, the deletion of a domain may cause altered folding of the remaining protein or otherwise generate effects not related directly to the function of the missing domain. Perturbation of a protein domain by intrabody binding is a more specific method for exploring function. Intrabodies are intracellular, recombinant, single chain antibody fragments (scFv) that contain the heavy and light antigen-binding domains (V_H and V_L) connected by a linker. Alternatively, single domain antibody fragments consist of either V_H or V_L. Intrabodies are highly specific reagents that can be targeted to subcellular compartments, distinct protein conformations, posttranscriptional modifications, as well as to non-protein targets such as oligosaccharides (Biocca and Cattaneo, 1995; Stocks, 2005; Messer and McLear, 2006; Lo et al., 2008). Intrabodies thus have great

potential to increase our understanding of the functions of individual protein domains in living cells.

We sought to use intrabodies to better understand the role of the polyP and P-rich domains (the PRR) of Htt in HD pathology. The PRR is known to be important for mHtt toxic gain of function (Passani et al., 2000; Steffan et al., 2000; Modregger et al., 2002; Khoshnan et al., 2004a; Qin et al., 2004), and although a number of binding partners, including WW domain-containing proteins, vesicle-associated proteins, P53, and IKKg, have been identified, the mechanism of the modulation of mHtt toxicity by these domains remains unclear. The role of the P-rich domain is not known. To investigate this aspect of PRR function we used MW7, a scFv intrabody that binds polyP. MW7 reduces mutant Htt (mHtt)-induced aggregation and promotes cell survival in culture (Khoshnan et al., 2002a). It also inhibits mHtt-induced neurodegeneration in a *Drosophila* HD model (Jackson et al., 2004). However, the specificity of this intrabody for pure polyP could allow binding to other cellular proteins containing a polyP domain, although there is no evidence of the latter binding to date. To characterize the role of the PRR, we produced novel intrabodies (Happs) against the P-rich domain of Htt. Happ1 and 3 are single domain, light chain intrabodies (V_Ls) that bind mHtt in a PRR-dependent manner. We then tested the Happs, MW7 and V_L12.3, a single domain light chain intrabody that binds the 17 N terminal AAs of Htt (Colby et al., 2004b), for efficacy in blocking mHDx-1 aggregation and toxicity, as well as their effects on sub-cellular localization and mHDx-1 protein levels. The most striking findings are that both the anti-polyP and anti-P-rich intrabodies reduce toxicity by increasing mHtt turnover and

lowering the mHtt levels, while the anti-N-terminal intrabody appears to reduce mHtt toxicity by a different mechanism.

Materials and Methods

Cell culture. HEK 293 (ATCC, Manassas, VA.) or ST14A striatal precursor (Elena Cattaneo, 1998) cells were grown in DMEM (Invitrogen, Carlsbad, CA.) supplemented with 10% heat-inactivated fetal bovine serum, 2 mM glutamine, 1 mM streptomycin and 100 international units of penicillin (Invitrogen). Cells were maintained in 37°C (293) or 33°C (ST14A) incubators with 5% CO_2 unless otherwise stated. Transfections were performed using lipofectamine 2000 transfection reagent (Invitrogen) according to the manufacturer's protocol.

Immunoblotting. Protein concentration was determined using a BCA assay (Pierce, Rockford IL.). Seventy five milligram total protein/sample in a volume of 30 ml was combined with 6 ml 6X protein loading buffer (Ausubel F.M., 1993), and boiled for 5 minutes. Samples were separated by sodium dodecyl sulfate polyacrylamide gel electrophoresis (SDS/PAGE) using 4-20% criterion precast gels (Biorad, Hercules, CA.) and precision plus protein kaleidoscope molecular weight standard (BioRad). Samples were then transferred overnight to nitrocellulose membranes for immunoblotting. Appropriate primary and horseradish peroxidase (HRP)-conjugated secondary antibodies were then applied as described in (Ausubel F.M., 1993). Super signal west dura (Pierce) substrate was applied to membranes according to the manufacturer's protocol. Chemiluminescence was detected and

densitometry was performed using a Fluorchem 8900 (Alpha Innotech, San Leandro CA.) gel doc system.

Selection of phage display library for binding to P-rich epitope of Htt. Intrabodies were selected from the Griffin.1 human recombinant, scFv phage display library (Griffiths et al., 1994). One well of a six-well plate was coated with a synthetic peptide (200 μg /ml) derived from the P-rich epitope of Htt (PQLPQPPPQAQP) located between the two poly P stretches by incubating at 4°C overnight**.** The coated well was then used to select phage expressing intrabodies specific for this epitope according to the provider's instructions. After the fourth round of selection, the P-rich enriched phage library was purified by PEG/NaCl precipitation and suspended in 2 ml PBS.

Generation of bait peptide for isolation of Happ intrabodies. A plasmid encoding PQ50-GST (Scherzinger et al., 1997a) was transformed into XL-10 gold ultracompetent bacteria (Stratagene, La Jolla, CA.) according to the manufacturer's protocol. Cells were grown to an OD of 0.6 at 600 nm and induced with 1 mM Isopropyl β-D-1-thiogalactopyranoside (IPTG) for 4 hours. Bacteria were collected by centrifugation, and GST fusion proteins were isolated in 1 ml 50% Glutathione Sepharose bead slurries containing bound peptide (Ausubel F.M., 1993). 25 ml of each bead slurry was added to 10 ml protein loading buffer, boiled for 5 minutes and separated by SDS/PAGE. Peptide expression was verified by Coomassie staining of PAGE gels and comparison to a protein molecular weight marker (data not shown).

Selection of Happ intrabodies from P-rich-specific phage display library. One milliliter of the preselected P-rich-specific phage was selected with PQ50-GST as described in the library provider's instructions. Briefly, GST-fusion bait peptide bound to glutathione agarose beads was incubated with replication deficient phage displaying preselected, P-rich scFvs and then washed in PBS with 0.1% triton X-100 to remove any unbound phage particles. Bound phage were allowed to infect log phase bacteria. To repeat selection, M13 helper phage, which do not display scFvs but enable the replication of scFv displaying phage from pre-infected bacteria, were used to recover selected phage. This selection was repeated an additional two times. After the final round of selection, individual clones were selected and screened for inserts by the polymerase chain reaction (PCR)(Griffiths et al., 1994). Six clones with inserts were identified (Happ1-6). Inserts were sequenced and analyzed for open reading frames (ORFs). Three clones were found to contain ORFs, two of which were redundant. The two unique ORFs (Happ1 and 3) were amplified by PCR using primers designed to add both appropriate restriction sites and a C-terminal hemaglutinin (HA) epitope tag, and cloned into the AAV (adeno-associated virus genome plasmid)(Stratagene) mammalian expression vector for characterization in cell culture, and into the pGEX-6p1 GST fusion (Amersham Biosciences, Piscataway, NJ.) bacterial expression vector for protein purification. A control intrabody that does not bind HDx-1 (CV_L) was also isolated from the library and cloned into these vectors. Cloning was performed according to the Invitrogen One-shot top 10 competent cell protocol.

Htt aggregation and toxicity assays. HEK 293 cells were cotransfected with HDx-1-GFP and intrabody in poly-D-lysine-coated 24-well plates at ~60% confluency. Each well received 0.2 mg PQ103 DNA in pcDNA3.1 vector and intrabody (V_L12.3, MW7, Happ1, Happ3, or CV_L) DNA in AAV vector at various ratios to HDx-1 (0.5:1, 1:1, 2:1, 3:1, 4:1). DNA levels were normalized to 1 mg per well using CV_L in AAV vector. Non-transfected wells were used as a negative control, and each condition was performed in triplicate. Cultures were moved to a 33°C incubator 8 hours posttransfection to slow cell division and maintain a monolayer. At 40 hours posttransfection, cells were incubated in medium containing 1 mM ethidium homodimer-2 (EthD-2)(Invitrogen) for 15 minutes at 33°C for detection of dead cell nuclei. Cells were then fixed in 4% PFA at 4°C for 30 minutes and permeabilized with PBS containing 0.1% triton for 15 minutes. For detection of all nuclei, cells were treated with PBS containing 0.5 mg/ml DAPI. Fluorescence microscopy was used to visualize dead cells (red channel), large Htt aggregates (green channel), and total cell number (blue channel). Three representative microscope fields were analyzed for each well (9 per condition). Dead cells and aggregates were counted for each field and normalized to the total cell number. P values were computed using Student's t-test.

Brain slice neurodegeneration assay. All animal experiments were performed in accordance with the institutional Animal Care and Use Committee and Duke University Medical Center Animal Guidelines. Brain slice preparation and biolistic transfection were performed as previously described (Lo et al., 1994; Khoshnan et al., 2004a). Briefly, brain tissue was dissected from euthanized

postnatal day 10 (P10) CD Sprague-Dawley rats (Charles River Laboratory, Raleigh, NC) and placed in ice-cold culture medium containing 15% heat-inactivated horse serum, 10 mM KCl, 10 mM HEPES, 100 U/ml penicillin/streptomycin, 1 mM MEM sodium pyruvate, and 1 mM L-glutamine in Neurobasal A (Invitrogen). Brain tissue was cut into 250 mm thick coronal slices using a Vibratome (Vibratome, St. Louis, MO) and incubated for 1 hr at 37^{o}C under 5.0% CO_2 prior to biolistic transfection. Gold particles (1.6 mm gold microcarriers; Bio-Rad, Hercules, CA) were coated with the appropriate DNAs (see below) as per manufacturer's instructions and loaded into Tefzel tubing (McMaster-Carr, Atlanta, GA) for use with the Helios biolistic device (Bio-Rad) which was used at a delivery pressure of 95 psi. Gold particles were coated with expression constructs encoding yellow fluorescent protein (YFP) as a morphometric marker, cyan fluorescent protein (CFP)-tagged mHDx-1 Q-73, and the relevant intrabody; for control transfections, particles were coated with YFP + CV_L, YFP + mHDx-1Q73 and vector backbone DNA, or YFP + mHDx-1Q73 + CV_L. For each condition, transfections were done on 12 brain slices and numbers of healthy medium spiny neurons (MSNs) expressing the YFP reporter were assessed 4-5 days after brain slice preparation and transfection using fluorescence microscopy. MSNs with normal-sized cell bodies, even and continuous expression of YFP in the cell body and dendrites, and having >2 discernable primary dendrites > 2 cell bodies long were scored as healthy. P values were computed using Student's t-test.

Immunohistochemical HDx-1 localization. ST14A cells were grown in 6-well plates containing coverslips and cotransfected with HDx-1-GFP and intrabody

in 6 well plates at ~60% confluency. Each well received 1 mg PQ103 and intrabody DNA at optimal ratios. Non-transfected wells were used as a negative control. At 48 hours posttransfection, cells were fixed and permeabilized as described above. Intrabodies were then labeled using M2 anti-Flag for MW7 and 3F10 anti-HA for V_L12.3, Happ1, and Happ3. Secondary antibodies were conjugated to Alexa fluor 568 (Molecular Probes)(S. Hockfield, 1993). Cells were processed for microscopy as above. Mean fluorescence intensity for whole cell and nuclear HDx-1 (green channel) and intrabody (red channel) was measured in 3 microscope fields per well. The ratio of nuclear HDX-1 or intrabody to cellular HDx-1 or intrabody was determined by (mean intensity of nucleus/mean intensity of whole cell). P values were computed using Student's t-test.

HDx-1 immunoblot assay. HEK 293 cells were cotransfected with HDx-1-GFP and intrabody in 10 cm dishes at ~80% confluency. Each dish received 4 mg of PQ103 or PQ25 DNA in pcDNA3.1 vector and intrabody DNA in AAV vector at the optimal ratio for each intrabody (4 mg V_L12.3, 16 mg MW7, 8 mg Happ1 and Happ3). A non-transfected dish was used as a negative control. Cells were dislodged by mechanical dissociation and pipetting 48 hours posttransfection, harvested by centrifugation, washed with PBS and lysed by sonication in 500 ml lysis buffer (25 mM Hepes, 50 mM NaCl, 1 mM $MgCl_2$, 0.5 % triton) containing 1 Complete, Mini, EDTA-free; Protease Inhibitor Cocktail tablet (Roche) per 7 ml buffer. The soluble protein fraction was collected by centrifugation for 20 min at 4^o C at 20,000x g. The insoluble pellet was sonicated in 150 ml 6 M urea and incubated for 20 min at RT. Immunoblots were then performed using rabbit anti-GFP (1:1000

Molecular Probes, Carlsbad CA) as primary antibody and HRP-conjugated, goat anti-rabbit (1:10,000 Santa Cruz Biotechnology, Santa Cruz, CA) as secondary antibody to detect HDx-1-GFP. For a loading control, membranes were stripped using Restore Western blot stripping buffer (Pierce) and reprobed with mouse anti-b-tubulin (1:1000 Sigma) as primary and HRP-conjugated, goat anti-mouse (1:10,000 Santa Cruz Biotechnology) as secondary antibody. Densities of HDx-1 and b-tubulin bands were determined. Each HDx-1 band was normalized to the level of the b-tubulin band for that sample. The ratio of HDx-1 level in the presence of intrabody to HDx-1 level alone was determined by (density of intrabody plus HDX-1/density of intrabody plus HDx-1 tubulin)/(density of HDx-1 alone/density of HDx-1 alone tubulin). The experiment was repeated three additional times giving an N of 4. P values were computed using Student's t-test.

HDx-1 turnover assay. ST14A cells were grown in 6 well plates containing coverslips and cotransfected with HDx-1-SNAP and intrabody at ~60% confluency. Each well received 1 mg of either PQ97-SNAP (97Q-HDx-1 fused to the SNAP tag) or PQ25-SNAP (25Q-HDx-1 fused to the SNAP tag) DNA in pSEMXT-26m vector (Covalys Witterswil, Switzerland) and intrabody DNA in AAV vector at optimal ratios (1 mg V_L12.3, 4 mg MW7, 2 mg Happ1 and Happ3). Non-transfected wells were used as a negative control, and each condition was performed twice. To covalently label HDx-1 present at 24 hours posttransfection, cells were treated with DAF green fluorescent SNAP-substrate (Covalys) according to the manufacturer's protocol. After labeling, cells were handled in low light conditions to avoid photobleaching the DAF substrate. One well of each condition was then fixed and

permeabilized as described above. For detection of all nuclei, cells were treated with blocking solution (3% BSA w/v, 10% NGS, 0.1% Triton X-100 in PBS) containing 1:2000 Toto-3 iodide (Molecular Probes). Coverslips were then mounted with Prolong gold anti-fade reagent (Molecular Probes). The remaining well of each condition was incubated for an additional 24 hours (48 hours posttransfection) to allow turnover of labeled HDx-1, and processed for microscopy as above. Mean fluorescence intensity of individual cells was observed in 3 microscope fields per well using LCS software (Leica Wetzlar, Germany). Mean cellular fluorescence intensities were computed for both 24 and 48 hour conditions. The percentage of labeled HDx-1 at 24 hours and remaining at 48 hours was determined by ((mean intensity at 48 hours/mean intensity at 24 hours) x 100). The experiment was repeated three additional times giving an N of 4. P values were computed using Student's t-test.

Results

Isolation of Happ intrabodies. Novel intrabodies against the PRR domain were selected in a two-stage protocol. First, a non-immune, human recombinant scFv phage library (Griffin.1)(Griffiths et al., 1994) was used to select clones that bind a unique, P-rich sequence between the two polyP domains in mHDx-1. The second stage involved three rounds of selection using PQ50 (HDx-1 containing 50 Q and the PRR)(Scherzinger et al., 1997a). Following the second stage, individual clones were analyzed for inserts containing ORFs. Although the Griffin.1 library consists of full scFv fragments, the two clones selected had only the V_L ORFs. A

control V_L that does not bind Htt (CV_L) was also isolated from the library. These three V_Ls (Happ1, Happ3 and CV_L) were then inserted into a mammalian expression vector for cell culture and brain slice studies. To verify the specificity of these intrabodies, they were expressed as GST fusion proteins and used as primary antibodies to stain membranes containing the lysates of 293 cells transfected with HDx1 or HDx1DPRR. The lysates of non-transfected cells were used to test for binding non-Htt cellular proteins. As expected, MW7 and the Happs bind only to HDx1 containing the PRR while V_L12.3 binds both forms of HDx1. None of the intrabodies bind the non-transfected lysates. These results confirm that the Happs require the Htt PRR epitope for binding.

The intrabodies reduce mHDx-1 aggregation and toxicity. Each of the intrabodies was tested at various ratios to mHDx-1 (0.5:1, 1:1, 2:1, 3:1, and 4:1) for effects on mHDx-1 toxicity by counting EthHD-2-positive dead cell nuclei (Fig. 1B), and aggregation by counting green foci of the HDx-1-GFP fusion protein (Fig. 1C). While V_L12.3, Happ1 and Happ3 demonstrate dose-dependent, saturable beneficial effects on aggregation, MW7 demonstrates a threshold effect requiring a 4:1 ratio for benefit. This may be the result of its specificity for pure polyP. As there are two polyP stretches that can each accommodate binding of two intrabody molecules, reduction of aggregation by polyP binding may require complete blockade of these epitopes. Interestingly, this does not appear to be the case for the toxicity induced by mHDx-1. The V_L12.3 intrabody is the most effective in reducing toxicity, with an optimal ratio to mHDx-1 of 1:1. MW7 is optimal at a ratio of 4:1, while Happ1 and 3 each show an optimal ratio of 2:1, with significant beneficial effects at 1:1. Similar

effects on mHDx-1-induced toxicity were seen when measuring lactate dehydrogenase (LDH) activity (data not shown). These results confirm previous findings with the N-17 AA epitope and further demonstrate that the PRR also regulates HDx1 toxicity. As CV_L shows no dose-dependent effects (data not shown), the median ratio of 2:1 was used as a baseline level of mHDx-1-induced toxicity or aggregation (Fig 1B, zero point).

The intrabodies reduce mHDx-1-induced neurodegeneration in a cortico-striatal brain slice model of HD. Rat brain slices, which preserve much of the intrinsic circuitry, were biolistically cotransfected with YFP, mHDx-1-CFP and an intrabody. The number of morphologically healthy, transfected medium spiny neurons (MSNs) in the striatum of each slice was then assessed using YFP fluorescence as an independent reporter of cell type and vitality 4-5 days after slice preparation and transfection (Fig. 2). The number of healthy MSNs per brain slice was compared between a positive control (brain slices transfected with YFP + CV_L), a negative control (transfected with YFP + mHDx-1 + vector backbone DNA), and the test condition transfected with YFP + mHDx-1 + anti-Htt intrabody). Cotransfection of mHDx-1 with CV_L, results in significantly reduced numbers of healthy MSNs, as is seen in slices transfected with mHDx-1 and vector. In contrast, cotransfection of mHDx-1 with V_L12.3 or Happ1 results in numbers of healthy MSNs that are similar to slices transfected with YFP + CV_L. Cotransfection of slices with mHDx-1 + MW7 yields intermediate results, with significantly greater numbers of healthy MSNs than with mHDx-1 + CV_L, but fewer than with YFP + CV_L. These results extend the findings from 293 cells to MSNs in a semi-intact milieu.

V_L12.3 alters cytoplasmic vs. nuclear trafficking of mHDx-1. To evaluate the effect of the intrabodies on HDx-1 intracellular trafficking, ST14A striatal neuronal precursor cells were cotransfected with mHDx-1-GFP and intrabody and incubated for 48 hours. Cells were fixed, stained for both intrabody and nuclei, and then mounted for analysis by confocal microscopy. GFP fluorescence intensity was used to compare levels of mHDx-1 in the whole cell vs. the nucleus (Fig. 3). The PRR-binding intrabodies do not alter the cytoplasmic/nuclear mHDx-1 ratio, while V_L12.3 causes a dramatic increase of nuclear Htt. In terms of localization of the intrabodies themselves, V_L12.3, Happ1 and Happ3 display a slight preference for the nucleus while MW7 is slightly more cytoplasmic (Fig. S2). This could be the result of the larger size of the MW7 scFv compared to the single domain intrabodies. No significant differences are seen between V_L12.3, Happ1 and Happ3, and the slight preference of V_L12.3 for the nucleus is too small to account for the increased nuclear HDx-1 in the presence of V_L12.3, indicating that this change in localization is not the result of intrabody localization. Thus, intrabody binding to the N-terminus of Htt disrupts cytoplasmic vs. nuclear trafficking of Htt, which may influence its nuclear functions. Since the amount of nuclear mHtt correlates with toxicity (Truant et al., 2007), this result suggests that V_L12.3 may not be ideal as a therapeutic intrabody despite its clear effects on blocking mHtt toxicity.

The intrabodies differentially alter the level of soluble mHDx-1. To determine the effects of the intrabodies on mHDx-1 levels, 293 cells were cotransfected with intrabody and either wtHDx-1 or mHDx-1, using each intrabody at its optimal ratio to HDx-1, and incubated for 48 hr. Soluble and insoluble cell

fractions were then assayed for HDx-1 by immunoblotting and densitometery (Fig. 4). Each of the intrabodies dramatically reduces the level of insoluble mHDx-1. However, the three PRR-binding intrabodies (MW7, Happ1, Happ3) also significantly reduce the level of soluble mHDx-1, while V_L12.3 has no significant effect on soluble m- or wtHDx-1 levels. From a therapeutic standpoint, it is important that only a slight reduction of wtHDx-1 protein is seen, indicating that anti-PRR intrabodies are selective for the mutant form. Although these intrabodies bind wtHDx-1, their preference for the mutant form is not unexpected as the interaction of endogenous Htt PRR-binding partners with Htt is known to increase with increasing polyQ repeat length (Passani et al., 2000; Holbert et al., 2001).

The PRR-binding intrabodies increase mHDx-1 turnover. To further investigate the reduction of soluble mHDx-1 a SNAP tag fusion labeling experiment was performed (Jansen et al., 2007). A traditional pulse chase experiment was not used because mHDx-1 is known to affect transcriptional regulation. This property of mHDx-1 could conceivably be altered by intrabody binding leading to variable transcription rates of HDx-1 in the presence of the various intrabodies. Traditional pulse-chase experiments require equal transcription and translation of the target protein in all conditions within the labeling period. The SNAP tag fusion system allows labeling of all preexisting HDx-1. By measuring the amount of Htt at the time of labeling and again at a later time point, we are able to measure a rate of turnover independent of transcription or translation rate. This system also offers greater specificity as only the SNAP tag fusion protein is labeled as opposed to all cellular

proteins translated during the labeling period as with traditional pulse-chase experiments.

To investigate HDx-1 turnover using the SNAP tag fusion system, 293 cells were cotransfected with intrabody and HDX-1 fused to the SNAP tag. Twenty-four hours posttransfection, HDx-1 was labeled using a fluorescent, cell permeable SNAP substrate. This substrate undergoes a covalent binding reaction with the SNAP tag and remains fluorescent until the SNAP-tag fusion protein is broken down. Some cultures were immediately examined for HDx-1 levels while others were incubated for 48 hours posttransfection to allow turnover of labeled HDx-1. Fluorescence intensity of HDx-1-SNAP was used to determine the percentage of HDx-1 labeled at 24 hours that is still intact at 48 hours (Fig. 5). Cells transfected with HDx-1-SNAP alone were used to determine a baseline level of turnover. While the percentage of mHDx-1 remaining in the presence of V_L12.3 is equivalent to that in the control, this percentage is significantly reduced in the presence of MW7, Happ1 or Happ3, indicating an increase in the rate of mHDx-1 turnover specifically in the presence of the PRR-binding intrabodies (Fig. 5B). The lack of effect of V_L12.3 provides a convenient control for non-specific effects of intrabody binding to mHDx-1. Although the mechanism by which this increase in mHtt turnover occurs is not yet clear, the levels of intrabody protein are increased in the presence of mHtt (data not shown), suggesting that mHtt is not broken down as a part of a complex with intrabody. This novel ability of PRR-binding intrabodies to increase turnover of mHtt suggests that this region of the protein is important for stability. Further

evidence of the specificity of the intrabody effects is shown by the fact that none of the anti-Htt intrabodies significantly changes the rate of wtHDx-1 turnover (Fig 5C).

Discussion

While anti-N-terminal and anti-PRR intrabodies ameliorate the negative effects of mHtt in cell culture and brain slice models of HD, they do so with different efficacy and by different mechanisms. These different mechanisms offer clues to the specific functions of their target domains.

The V_L12.3 intrabody was isolated from a yeast surface display library and initially required a 5:1 ratio to mHtt to reduce aggregation (Colby et al., 2004a). It was then reengineered, including removal of the disulfide bonds, which do not form in the reducing environment of the mammalian cytoplasm (and can cause mis-folding of intrabodies (Biocca et al., 1995)), and mutated for greater binding affinity to Htt (Colby et al., 2004c). In addition to inhibiting mHtt-induced toxicity and aggregation, we find that V_L12.3 also alters cytoplasmic vs. nuclear trafficking of HDx-1.

Modulation of Htt intracellular targeting by the N-terminus has been recently characterized. Removal of this amphipathic alpha helix causes an increase in the level of nuclear Htt, indicating that it functions as a cytoplasmic retention signal (Rockabrand et al., 2007). Mutation of hydrophobic residues, or the introduction of a helix breaking proline residue in the N-terminal domain results in increased nuclear Htt, suggesting that cytoplasmic retention by the N-terminus is the result of association with organelle and vesicle membranes (Atwal et al., 2007b). Although

the N-terminus is not a dimerization domain, disruption of the helical structure also prevents the aggregation of mHtt, which is accompanied by an increase in the toxicity of the protein. Thus, the N-terminus of Htt is required for cytoplasmic localization and the formation of aggregates. The effect on toxicity seen in these experiments may be related to the prevention of aggregation, since mHtt-expressing neurons without aggregates exhibit more toxicity than those with aggregates (Arrasate et al., 2004b). Toxicity related to the N-terminus may also involve altered Htt localization, as the addition of a nuclear localization signal to mHtt increases its toxicity in both cell culture and mouse models of HD (Peters et al., 1999; Schilling et al., 2004). Interestingly, while removal or mutation of the N-terminus results in increased toxicity, V_L12.3 binding results in reduced toxicity, suggesting that V_L12.3 may inhibit formation of a toxic conformation or an oligomerization seed molecule. Thus, this intrabody may ameliorate toxicity regardless of mHtt localization or aggregation state.

The polyP and P-rich domains of mHtt are implicated in a number of aberrant protein interactions. These domains are required for mHtt binding to, and sequestering of, several SH3 domain-containing proteins, including proteins associated with vesicle function (Modregger et al., 2002; Qin et al., 2004). The PRR of Htt is required for interaction with WW domain-containing proteins (Staub and Rotin, 1996; Faber et al., 1998). These include transcription factors, and these interactions are enhanced with increased polyQ repeat length (Passani et al., 2000; Holbert et al., 2001). These domains are the site of interaction with IKKg, a regulatory subunit of the IkB kinase complex. Activation of this complex is known

to promote aggregation and nuclear localization of mHtt (Khoshnan et al., 2004a). The PRR of Htt is also the site of P53 interaction and is required for transcriptional repression of P53-regulated genes (Steffan et al., 2000). Again, this interaction is enhanced by increased polyQ repeat length.

MW7, an intrabody recognizing pure polyP, reduces mHtt-induced aggregation and toxicity in cell culture and in *Drosophila* models of HD (Khoshnan et al., 2002a; Jackson et al., 2004). We find that it is also effective in an acute brain slice model of HD, and that it increases the turnover of HDx-1, with greater effect on the mutant than the wild type form. We also produced novel intrabodies, Happ1 and 3, which recognize the unique, P-rich epitope between the two polyP domains of Htt. The Happ intrabodies exhibit beneficial properties similar to those of MW7 such as preferential effects on the mutant form of Htt and increasing turnover without altering localization, but the Happs are effective at lower ratios to Htt than MW7. We found no evidence that the anti-PRR intrabodies bind to previously aggregated mHtt, suggesting that the observed reduction in aggregation is the indirect result of increased turnover of the soluble form of the protein, causing a shift away from the aggregated state. The increased turnover of HDx-1 in the presence of either anti-polyP or anti-P-rich intrabodies suggests that this effect is a direct result of blocking these epitopes and therefore that this domain has a role in modulating stability of the mutant protein.

Disruption of mHtt stability by Happ binding could have therapeutic potential. The success of RNAi experiments show that reduction of mHtt levels is an effective therapeutic strategy (Harper et al., 2005a; Rodriguez-Lebron et al., 2005;

Machida et al., 2006). Unlike RNAi however, these intrabodies can distinguish between the wildtype and mutant forms of Htt, which is preferable, as the loss of normal Htt function can have negative effects (Dragatsis et al., 2000; Leavitt et al., 2001; Zuccato et al., 2001). The ability of the Happ intrabodies to increase turnover of mHtt may ameliorate the disruption of the ubiquitin proteasome seen in HD, although it is presently unclear if this increased turnover occurs through a ubiquitin-dependent pathway. As the levels of intrabody protein are increased in the presence of Htt, it is likely that the intrabodies direct the breakdown of mHtt without themselves being degraded. Moreover, the Happs, although significantly more effective than the original intrabody isolated and matured to become V_L12.3, have yet to undergo any reengineering and could potentially be improved by removal of disulfide bonds and mutation for greater Htt binding affinity. In addition, the present results with the Happ intrabodies highlight the importance of the unique, P-rich domain in mHtt toxicity.

References

The Huntington's Disease Collaborative Research Group (1993) A novel gene containing a trinucleotide repeat that is expanded and unstable on Huntington's disease chromosomes. Cell 72:971-983.

Arrasate M, Mitra S, Schweitzer ES, Segal MR, Finkbeiner S (2004) Inclusion body formation reduces levels of mutant huntingtin and the risk of neuronal death. Nature 431:805-810.

Atwal RS, Xia J, Pinchev D, Taylor J, Epand RM, Truant R (2007) Huntingtin has a membrane association signal that can modulate huntingtin aggregation, nuclear entry and toxicity. Hum Mol Genet:ddm217.

Ausubel F.M. RB, R.E. Kingston, D.D. Moore, J.G. Seidman, J.A. Smith, K. Struhl (1993) Current Protocols in Molecular Biology: Greene Publishing Associates and Wiley Interscience

Biocca SS, Cattaneo AA (1995) Intracellular immunization: antibody targeting to subcellular compartments. Trends in cell biology 5:248-252.

Biocca SS, Ruberti FF, Tafani MM, Pierandrei-Amaldi PP, Cattaneo AA (1995) Redox state of single chain Fv fragments targeted to the endoplasmic reticulum, cytosol and mitochondria. Bio/technology 13:1110-1115.

Colby DW, Garg P, Holden T, Chao G, Webster JM, Messer A, Ingram VM, Wittrup KD (2004a) Development of a Human Light Chain Variable Domain (VL) Intracellular Antibody Specific for the Amino Terminus of Huntingtin via Yeast Surface Display. Journal of Molecular Biology 342:901-912.

Colby DW, Chu Y, Cassady JP, Duennwald M, Zazulak H, Webster JM, Messer A, Lindquist S, Ingram VM, Wittrup KD (2004b) Potent inhibition of huntingtin aggregation and cytotoxicity by a disulfide bond-free single-domain intracellular antibody. PNAS 101:17616-17621.

David G, Abbas N, Stevanin G, Durr A, Yvert G, Cancel G, Weber C, Imbert G, Saudou F, Antoniou E, Drabkin H, Gemmill R, Giunti P, Benomar A, Wood N, Ruberg M, Agid Y, Mandel J-L, Brice A (1997) Cloning of the SCA7 gene reveals a highly unstable CAG repeat expansion. Nat Genet 17:65-70.

Dragatsis I, Levine MS, Zeitlin S (2000) Inactivation of Hdh in the brain and testis results in progressive neurodegeneration and sterility in mice. Nat Genet 26:300-306.

Duennwald ML, Jagadish S, Muchowski PJ, Lindquist S (2006) Flanking sequences profoundly alter polyglutamine toxicity in yeast. Proceedings of the National Academy of Sciences 103:11045-11050.

Duyao MP, Auerbach AB, Ryan A, Persichetti F, Barnes GT, McNeil SM, Ge P, Vonsattel J-P, Gusella JF, Joyner AL, MacDonald ME (1995) Inactivation of the Mouse Huntington's Disease Gene Homolog Hdh. Science 269:407-410.

Elena Cattaneo LC (1998) Generation and characterization of embryonic striatal conditionally immortalized ST14A cells. Journal of Neuroscience Research 53:223-234.

Faber PW, Barnes GT, Srinidhi J, Chen J, Gusella JF, MacDonald ME (1998) Huntingtin interacts with a family of WW domain proteins. Hum Mol Genet 7:1463-1474.

Griffiths AAD, Williams SSC, Hartley OO, Tomlinson IIM, Waterhouse PP, Crosby WWL, Kontermann RRE, Jones PPT, Low NNM, Allison TTJ (1994) Isolation of high affinity human antibodies directly from large synthetic repertoires. The EMBO journal 13:3245-3260.

Harper SQ, Staber PD, He X, Eliason SL, Martins IH, Mao Q, Yang L, Kotin RM, Paulson HL, Davidson BL (2005) From the Cover: RNA interference improves motor and neuropathological abnormalities in a Huntington's disease mouse model. PNAS 102:5820-5825.

Holbert S, Denghien I, Kiechle T, Rosenblatt A, Wellington C, Hayden MR, Margolis RL, Ross CA, Dausset J, Ferrante RJ, Neri C (2001) The Gln-Ala repeat transcriptional activator CA150 interacts with huntingtin: Neuropathologic and genetic evidence for a role in Huntington's disease pathogenesis. PNAS 98:1811-1816.

Imbert G, Saudou F, Yvert G, Devys D, Trottier Y, Garnier J-M, Weber C, Mandel J-L, Cancel G, Abbas N, Durr A, Didierjean O, Stevanin G, Agid Y, Brice A (1996) Cloning of the gene for spinocerebellar ataxia 2 reveals a locus with high sensitivity to expanded CAG/glutamine repeats. Nat Genet 14:285-291.

Jackson GR, Sang T, Khoshnan A, Ko J, Patterson PH (2004) Inhibition of mutant huntingtin-induced neurodegeneration In vivo by expression of a polyproline-binding single chain antibody. SFN abstract 938.5.

Jana NR, Zemskov EA, Wang G-h, Nukina N (2001) Altered proteasomal function due to the expression of polyglutamine-expanded truncated N-terminal

huntingtin induces apoptosis by caspase activation through mitochondrial cytochrome c release. Hum Mol Genet 10:1049-1059.

Jansen LET, Black BE, Foltz DR, Cleveland DW (2007) Propagation of centromeric chromatin requires exit from mitosis. J Cell Biol:jcb.200701066.

Kawaguchi Y, Okamoto T, Taniwaki M, Aizawa M, Inoue M, Katayama S, Kawakami H, Nakamura S, Nishimura M, Akiguchi I, Kimura J, Narumiya S, Kakizuka A (1994) CAG expansions in a novel gene for Machado-Joseph disease at chromosome 14q32.1. Nat Genet 8:221-228.

Khoshnan A, Ko J, Patterson PH (2002) Effects of intracellular expression of anti-huntingtin antibodies of various specificities on mutant huntingtin aggregation and toxicity. PNAS 99:1002-1007.

Khoshnan A, Ko J, Watkin EE, Paige LA, Reinhart PH, Patterson PH (2004) Activation of the I{kappa}B Kinase Complex and Nuclear Factor-{kappa}B Contributes to Mutant Huntingtin Neurotoxicity. J Neurosci 24:7999-8008.

Koide R, Ikeuchi T, Onodera O, Tanaka H, Igarashi S, Endo K, Takahashi H, Kondo R, Ishikawa A, Hayashi T, Saito M, Tomoda A, Miike T, Naito H, Ikuta F, Tsuji S (1994) Unstable expansion of CAG repeat in hereditary dentatorubral-pallidoluysian atrophy (DRPLA). Nat Genet 6:9-13.

Leavitt BBR, Guttman JJA, Hodgson JJG, Kimel GGH, Singaraja RR, Vogl AAW, Hayden MMR (2001) Wild-type huntingtin reduces the cellular toxicity of mutant huntingtin in vivo. American journal of human genetics 68:313-324.

Lo ASY, Zhu Q, Marasco WA (2008) Intracellular Antibodies (Intrabodies) and Their Therapeutic Potential. In: Therapeutic Antibodies, pp 343-373.

Lo DDC, McAllister AAK, Katz LLC (1994) Neuronal transfection in brain slices using particle-mediated gene transfer. Neuron 13:1263-1268.

Machida Y, Okada T, Kurosawa M, Oyama F, Ozawa K, Nukina N (2006) rAAV-mediated shRNA ameliorated neuropathology in Huntington disease model mouse. Biochemical and Biophysical Research Communications 343:190-197.

Marsh JL, Walker H, Theisen H, Zhu Y-Z, Fielder T, Purcell J, Thompson LM (2000) Expanded polyglutamine peptides alone are intrinsically cytotoxic and cause neurodegeneration in Drosophila. Hum Mol Genet 9:13-25.

Messer AA, McLear JJ (2006) The therapeutic potential of intrabodies in neurologic disorders: focus on Huntington and Parkinson diseases. BioDrugs 20:327-333.

Modregger J, DiProspero NA, Charles V, Tagle DA, Plomann M (2002) PACSIN 1 interacts with huntingtin and is absent from synaptic varicosities in presymptomatic Huntington's disease brains. Hum Mol Genet 11:2547-2558.

Nakamura KK, Aminoff MJMJ (2007) Huntington's disease: clinical characteristics, pathogenesis and therapies. Medicamentos de actualidad 43:97-116.

Orr HT, Chung M-y, Banfi S, Kwiatkowski TJ, Servadio A, Beaudet AL, McCall AE, Duvick LA, Ranum LPW, Zoghbi HY (1993) Expansion of an unstable trinucleotide CAG repeat in spinocerebellar ataxia type 1. Nat Genet 4:221-226.

Passani LA, Bedford MT, Faber PW, McGinnis KM, Sharp AH, Gusella JF, Vonsattel J-P, MacDonald ME (2000) Huntingtin's WW domain partners in Huntington's

disease post-mortem brain fulfill genetic criteria for direct involvement in Huntington's disease pathogenesis. Hum Mol Genet 9:2175-2182.

Peters MF, Nucifora FC, Kushi J, Seaman HC, Cooper JK, Herring WJ, Dawson VL, Dawson TM, Ross CA (1999) Nuclear Targeting of Mutant Huntingtin Increases Toxicity. Molecular and Cellular Neuroscience 14:121-128.

Qin Z-H, Wang Y, Sapp E, Cuiffo B, Wanker E, Hayden MR, Kegel KB, Aronin N, DiFiglia M (2004) Huntingtin Bodies Sequester Vesicle-Associated Proteins by a Polyproline-Dependent Interaction. J Neurosci 24:269-281.

Ramaswamy SS, Shannon KMKM, Kordower JHJH (2007) Huntington's disease: pathological mechanisms and therapeutic strategies. Cell transplantation 16:301-312.

Reddy PH, Williams M, Tagle DA (1999) Recent advances in understanding the pathogenesis of Huntington's disease. Trends in Neurosciences 22:248-255.

Rockabrand E, Slepko N, Pantalone A, Nukala VN, Kazantsev A, Marsh JL, Sullivan PG, Steffan JS, Sensi SL, Thompson LM (2007) The first 17 amino acids of Huntingtin modulate its sub-cellular localization, aggregation and effects on calcium homeostasis. Hum Mol Genet 16:61-77.

Rodriguez-Lebron E, Denovan-Wright EM, Nash K, Lewin AS, Mandel RJ (2005) Intrastriatal rAAV-mediated delivery of anti-huntingtin shRNAs induces partial reversal of disease progression in R6/1 Huntington's disease transgenic mice. Mol Ther 12:618-633.

Ross CA (1997) Intranuclear neuronal inclusions: a common pathogenic mechanism for glutamine-repeat neurodegenerative diseases? Neuron 19:1147-1150.

S. Hockfield SC, C. Evans, P. Levitt, J. Pintar, L. Silberstein (1993) Selected methods for antibody and nucleic acid probes: Cold Spring Harbor Laboratory press.

Scherzinger E, Lurz R, Turmaine M, Mangiarini L, Hollenbach B, Hasenbank R, Bates GP, Davies SW, Lehrach H, Wanker EE (1997) Huntingtin-encoded polyglutamine expansions form amyloid-like protein aggregates in vitro and in vivo. Cell 90:549-558.

Schilling G, Savonenko AV, Klevytska A, Morton JL, Tucker SM, Poirier M, Gale A, Chan N, Gonzales V, Slunt HH, Coonfield ML, Jenkins NA, Copeland NG, Ross CA, Borchelt DR (2004) Nuclear-targeting of mutant huntingtin fragments produces Huntington's disease-like phenotypes in transgenic mice. Hum Mol Genet 13:1599-1610.

Spada ARL, Wilson EM, Lubahn DB, Harding AE, Fischbeck KH (1991) Androgen receptor gene mutations in X-linked spinal and bulbar muscular atrophy. Nature 352:77-79.

Staub OO, Rotin DD (1996) WW domains. Structure 4:495-499.

Steffan JS, Kazantsev A, Spasic-Boskovic O, Greenwald M, Zhu Y-Z, Gohler H, Wanker EE, Bates GP, Housman DE, Thompson LM (2000) The Huntington's disease protein interacts with p53 and CREB-binding protein and represses transcription. Proceedings of the National Academy of Sciences 97:6763-6768.

Stocks MM (2005) Intrabodies as Drug Discovery Tools and Therapeutics. Curr Opin Chem Biol 9:359-365.

Truant R, Atwal RS, Burtnik A (2007) Nucleocytoplasmic trafficking and transcription effects of huntingtin in Huntington's disease. Progress in Neurobiology In Press, Corrected Proof.

Wanker EEE (2000) Protein aggregation and pathogenesis of Huntington's disease: mechanisms and correlations. Biological chemistry 381:937-942.

Yang W, Dunlap JR, Andrews RB, Wetzel R (2002) Aggregated polyglutamine peptides delivered to nuclei are toxic to mammalian cells. Hum Mol Genet 11:2905-2917.

Zoghbi HY, Orr HT (2000) Glutamine repeats and neurodegeneration. Annual Review of Neuroscience 23:217-247.

Zuccato C, Ciammola A, Rigamonti D, Leavitt BR, Goffredo D, Conti L, MacDonald ME, Friedlander RM, Silani V, Hayden MR, Timmusk T, Sipione S, Cattaneo E (2001) Loss of huntingtin-mediated BDNF gene transcription in huntington's disease. Science 293:493-498.

Figures

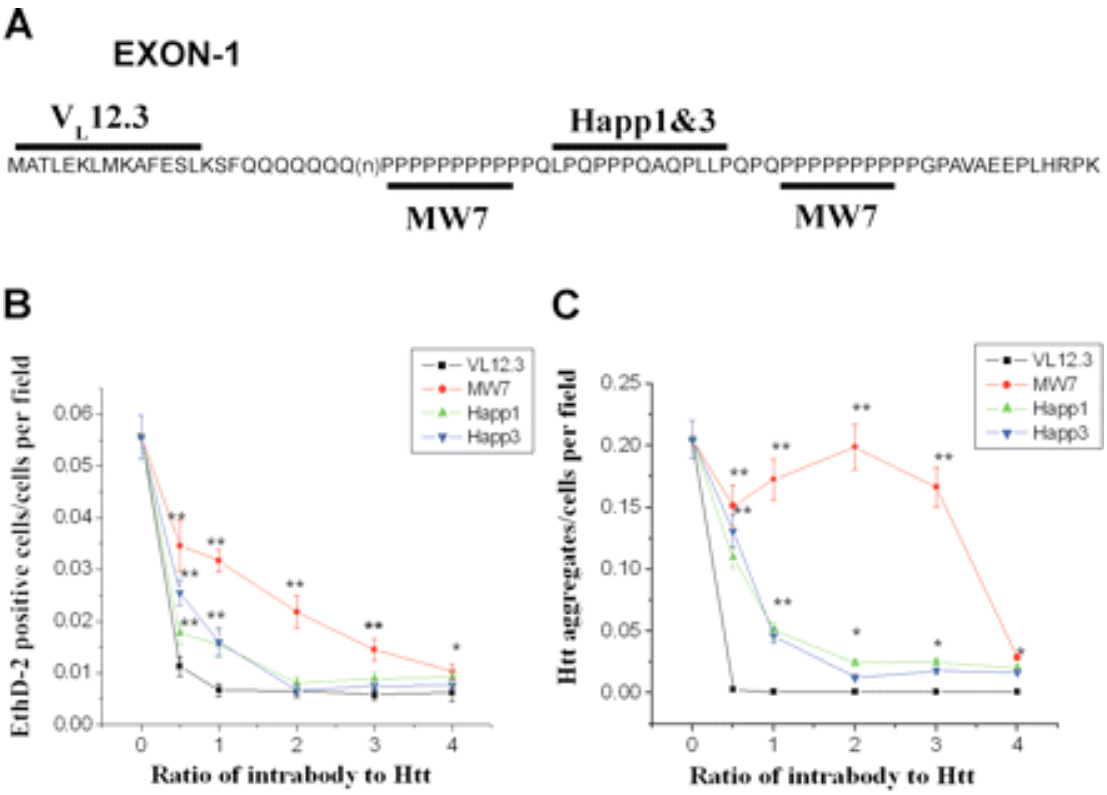

Figure 1. The anti-Htt intrabodies reduce mHDx-1-induced toxicity and aggregation in cell culture. (A) The epitopes in HDx-1 for the various intrabodies are depicted. (B) To quantify mHtt toxicity, 293 cells were cotransfected with mHDx-1-GFP and intrabody at various intrabody/Htt ratios and incubated for 48 hours. Cells were stained with EthD-2 to identify dead cell nuclei, fixed, and stained with DAPI to identify all cell nuclei. The number of dead cells was normalized to total cell number. All of the intrabodies reduce mHDx-1-induced cell death in a saturable, dose-dependent manner, with maximal effects at different intrabody/Htt ratios (1:1 for V_L12.3, 2:1 for Happ1 and 3, and 4:1 for MW7). (C) Aggregation was determined by counting GFP foci and normalizing to total cell number. * = Differ

from V_L12.3 at $p<0.05$, **=$p<0.01$. The point labeled as 0 on the intrabody:Htt axis corresponds to the value for HDX-1 + CV_L.

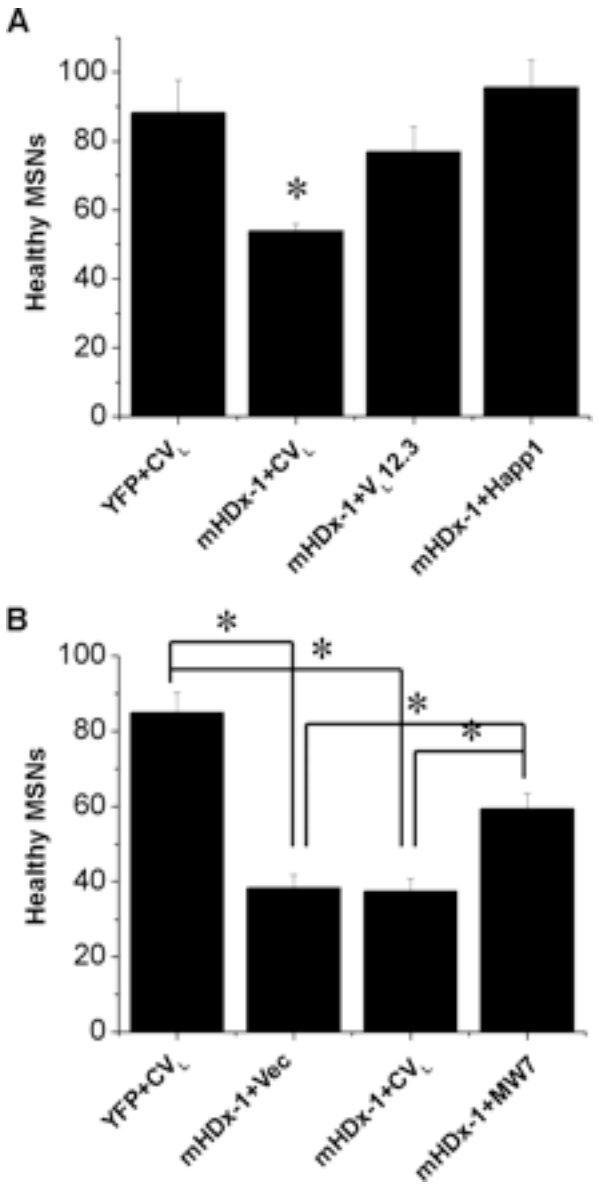

Figure 2. Protective effects of anti-Htt intrabodies against mHDx-1-induced neurodegeneration in cortico-striatal brain slice explants. Cortico-striatal brain slices were biolistically transfected with plasmid expression constructs encoding YFP, mHDx1(N1-66 with 148 Q), and the indicated intrabody. The number of healthy medium spiny neurons in the striatal region of each slice was scored visually 4-5 days after slice preparation and transfection. (A) Slices were

transfected with either YFP + CV_L; YFP + CV_L + mHDx1; YFP + mHDx1 + V_L12.3; or YFP + mHDx1 + Happ1. * = Differ from YFP at p<.01. (B) Slices were transfected with YFP + CV_L; YFP + vector + mHDx-1; YFP + CV_L + mHDx1 or YFP + mHDx1 + MW7. * = p<0.01. The data in A and B are from independent experiments.

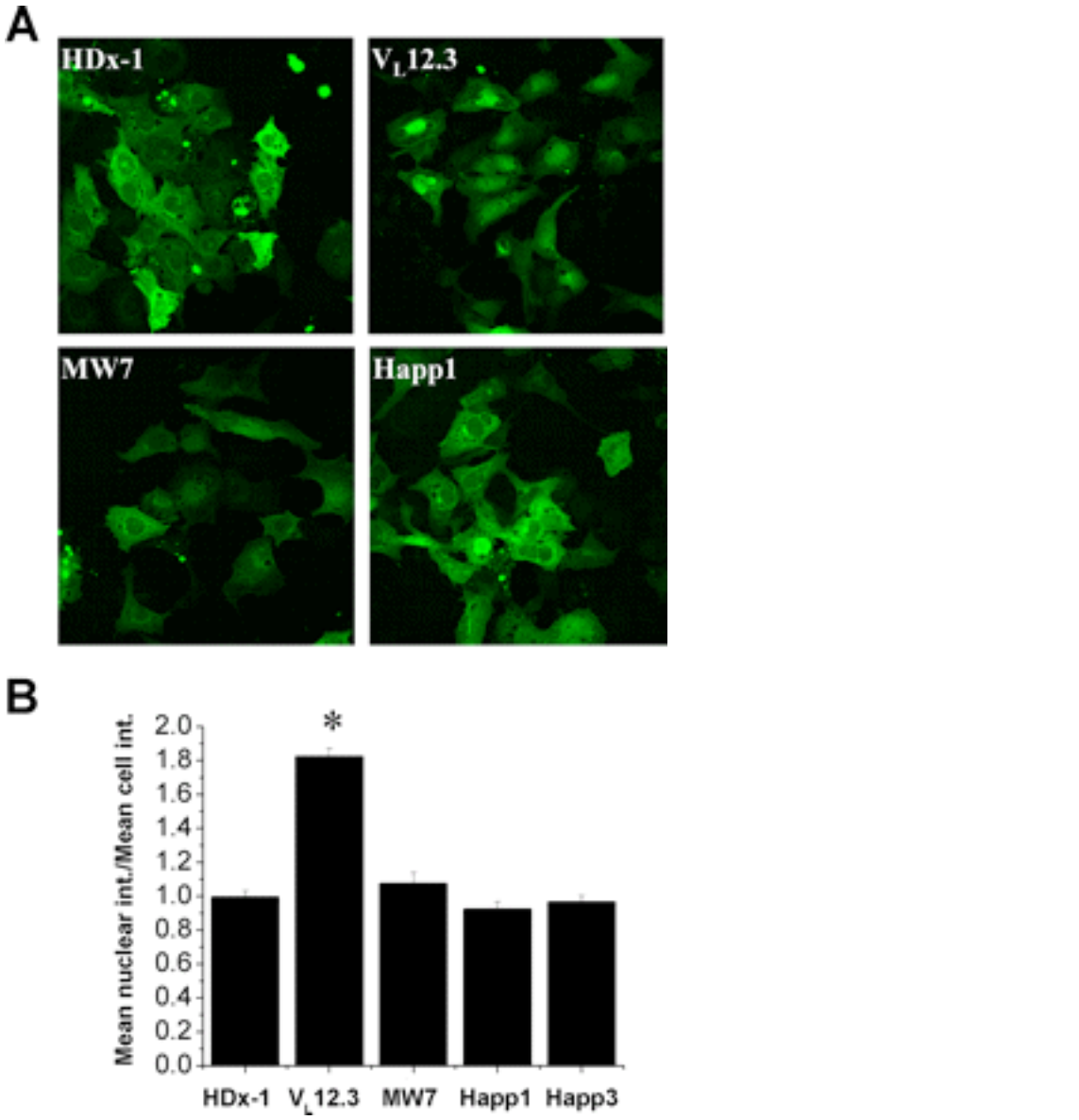

Figure 3. VL12.3 increases the level of nuclear HDx-1. ST14A cells were cotransfected with mHDx-1-GFP with 103Q and intrabody at optimal ratios. (A) At 48 hours posttransfection, cells were fixed, stained for the appropriate intrabody and cell nuclei, and analyzed by confocal microscopy. (B) Mean whole cell fluorescence intensity (int.) and mean nuclear fluorescence intensity of HDx-1 were compared. While MW7, Happ1 and Happ3 have no effect on HDx-1 localization, V_L12.3 significantly increases nuclear HDx-1. *=Differ from HDx-1 at $p<0.01$

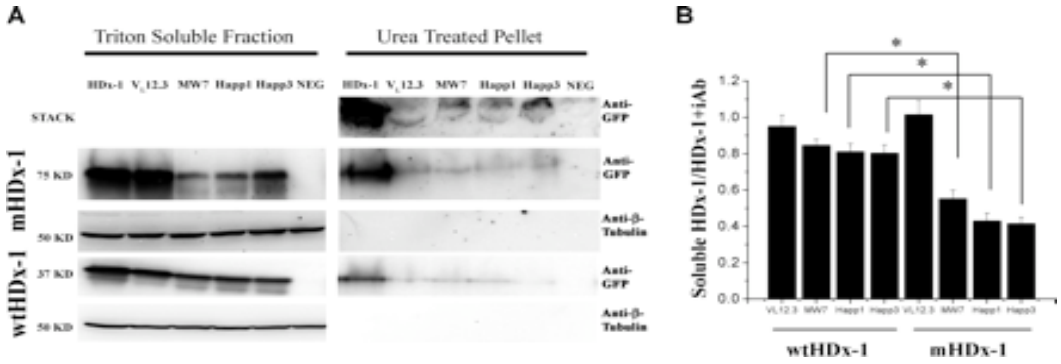

Figure 4. All of the anti-Htt intrabodies reduce insoluble HDx-1, while only the anti-PRR intrabodies also reduce soluble HDx-1. 293 cells were cotransfected with intrabody and mHDx-1 (76 kD) or wtHDx-1 (40 kD) at the optimal ratio for each intrabody. (A) At 48 hours posttransfection, cells were lysed with detergent. The soluble protein fraction was recovered and the insoluble fraction was treated with urea. Samples were then separated by SDS-PAGE and blotted for HDx-1. Non-transfected cells (NEG) were used as a negative control. (B) Quantification of bands shows that reduction of HDx-1 by PRR-binding intrabodies is significantly greater for the mutant form of Htt. Chemiluminescence densitometry was used to compare the levels of soluble m- and wtHDx-1. Each band was normalized to the level of b-tubulin (54 kD) in that sample. Bands for HDx-1+intrabody (iAb) were then normalized to the level of soluble HDx-1 for that blot. N = 4 independent experiments, and values for each blot were used to compile a mean. * = $p<0.01$

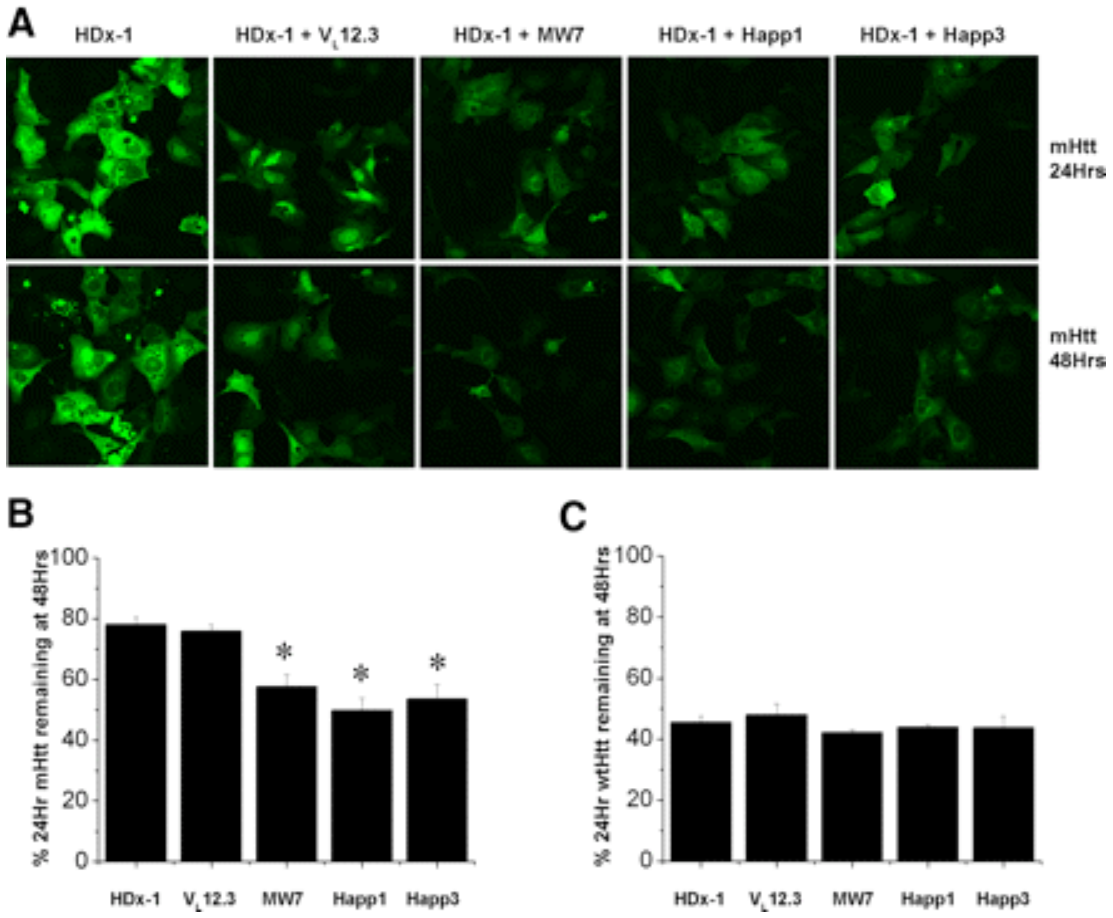

Figure 5. Anti-PRR intrabodies increase mHDx-1 turnover. ST14A cells were transfected with mHDx-1-SNAPtag 97Q (A and B) or wtHDx-1-SNAPtag 25Q (C) and intrabody at the optimal ratio for each intrabody. DAF green fluorescent SNAP substrate was added to cultures at 24 hr posttransfection. Some cultures were then fixed and stained with Toto-3 iodide nuclear marker while others were incubated an additional 24 hr to allow turnover of labeled HDx-1. Mean fluorescence intensity of cells at 24 hr was compared to intensity at 48 hr to determine the percentage of labeled HDx-1 remaining. V_L12.3 has no effect on m- or wtHDx-1 turnover while MW7, Happ1 and Happ3 significantly increase the rate of mHDx-1 turnover. N = 4, * = $p<0.01$

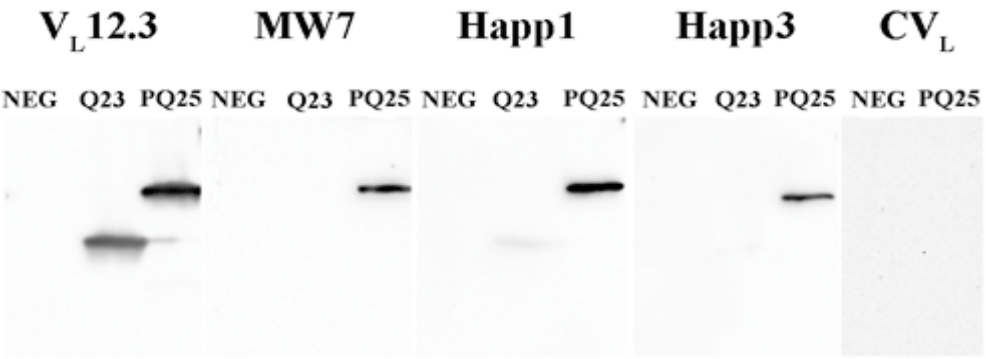

Figure S1. MW7, Happ1 and Happ3 bind Htt in a PRR-dependent manner. 293 cells were transfected with HDx-1 (PQ25) or HDx-1DPRR (Q23). After 48 hours, cell lysates were separated by SDS/PAGE and blotted with intrabodies. Non-transfected cells (NEG) were used as a negative control. While V_L12.3 binds both forms of HDx-1, MW7, Happ1 and Happ3 bind only the form containing the PRR. CV_L does not bind HDx-1.

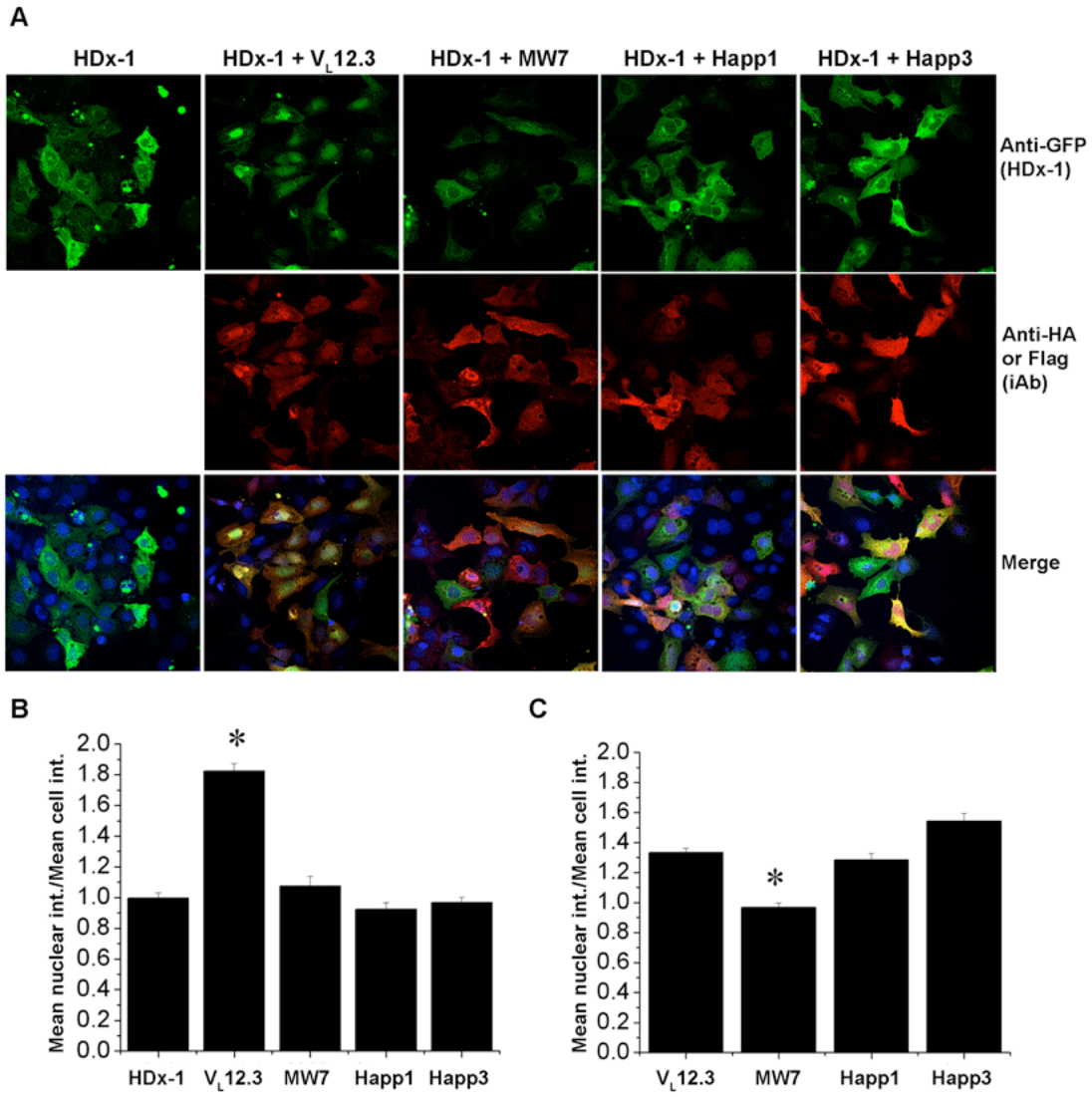

Figure S2. VL12.3 increases the level of nuclear HDx-1. ST14A cells were cotransfected with mHDx-1-GFP and intrabody at optimal ratios. (A) At 48 hours posttransfection, cells were fixed, stained for the appropriate intrabody (iAb) and cell nuclei, and analyzed by confocal microscopy. (B) Mean whole cell fluorescence intensity (int.) and mean nuclear fluorescence intensity of HDx-1 were compared. While MW7, Happ1 and Happ3 have no effect on HDx-1 localization, V_L12.3 significantly increases nuclear HDx-1. * = Differs from HDx-1 at $p<0.01$. (C) Mean

whole cell fluorescence intensity and mean nuclear fluorescence intensity of the intrabodies themselves were compared. MW7 is slightly more cytoplasmic than the other intrabodies, possibly due to its larger size.

Supplemental methods

Expression and purification of intrabody proteins. Intrabodies in pGEX-6p1 vector were transformed into ArcticExpress competent bacteria (Stratagene), and cells induced according to the manufacturer's protocol. GST fusion proteins were harvested from bacterial cultures as described above. Intrabody protein was verified by Coomassie staining of PAGE gels and comparison to protein molecular weight standards (data not shown). Relative expression levels of intrabodies were determined by intensity of Coomassie staining, and slurry volumes normalized to obtain approximately equal concentrations of intrabody protein. Intrabodies were eluted from glutathione beads and suspended in 1 ml PBS (Ausubel F.M., 1993).

Intrabody binding assays. HEK 293 cells in 10 cm dishes at ~80% confluency were transfected with 10 mg 23Q-HDx-1-CFP lacking the PRR (Q23) or 25Q-HDx-1-GFP (PQ25) in pcDNA3.1 vector (Invitrogen). A non-transfected dish was used as a negative control. Cells were dislodged by mechanical dissociation and pipetting 48 hours posttransfection, harvested by centrifugation, washed with PBS and lysed by sonication in 500 ml whole cell lysis buffer (0.2 M Tris-HCl, 140 mM SDS, 50% glycerol). Samples were analyzed by SDS/PAGE and immunoblotting. Intrabody protein eluates dissolved in 15 ml 3% milk were used as primary antibody. Secondary antibodies were HRP-conjugated M2 anti-flag (1:1000 Sigma,

St. Louis, MO.) for detecting MW7, and HRP-conjugated 3F10 anti-HA (1:1000

Roche, Indianapolis, IN.) for detecting V_L12.3, Happ1, Happ3 and CV_L.

Appendix D

Perturbation with intrabodies reveals that calpain cleavage is required for degradation of huntingtin exon 1

Southwell AL, Bugg CW, Kaltenbach L, Dunn D, Butland S, Weiss A, Paganetti P, Lo DC, Patterson PH

(Submitted)

Introduction

Huntington's disease (HD) is caused by the expansion of a polyglutamine (polyQ) tract in the first exon (HDx-1) of the large protein, huntingtin (Htt) (Huntington's Disease Collaborative Research Group, 1993). Mutant Htt protein (mHtt) perturbs many cellular processes by both gain of toxic function and loss of normal function. These include axonal transport, mitochondrial metabolism, transcriptional regulation and the ubiquitin proteasome system (UPS) (Imarisio et al., 2008). There is an age-dependent accumulation of mHtt protein in HD (Gil and Rego, 2008), which may be partially responsible for the adult onset of symptoms despite the lifelong expression of mHtt. Increasing the clearance of mHtt could prevent this accumulation and thereby delay or prevent the onset of symptoms.

Degradation of mHtt occurs through several mechanisms, suggesting a number of potential therapeutic opportunities for enhancing removal. Caspases and calpains cleave Htt, generating N-terminal fragments, some of which are more toxic than the full-length protein (Qin and Gu, 2004). Increasing polyQ tract length leads

to increased caspase and calpain activation and enhanced production of toxic N-terminal fragments in the HD brain (Majumder et al., 2007). These fragments are degraded by additional protease cleavage, the UPS and autophagy, which can involve isolation in an autophagosome and introduction to the lysosome by fusion, macroautophagy, or delivery to the lysosome by chaperone proteins (chaperone-mediated autophagy, CMA) (Todde et al., 2009). Certain cleavage events generate toxic fragments, and selective prevention of these events dramatically reduces the toxicity of mHtt by the generation of other, less toxic N-terminal cleavage products (Gafni et al., 2004; Graham et al., 2006). Posttranslational modifications such as phosphorylation also play a role in regulating Htt proteolysis (Thompson et al., 2009; Warby et al., 2009), and phosphorylated mHtt can be more toxic than unphosphorylated mHtt (Thompson et al., 2009). Thus, the dichotomy of mHtt processing: while some modifications increase the toxicity of the protein, these more toxic forms are intermediates in the process leading to total degradation. Since enhancing total degradation represents a powerful therapeutic strategy, a better understanding of this process is warranted. As the site of the disease-causing mutation, insight into the clearance of HDx-1 is particularly salient.

We have used intrabodies (iAbs), intracellularly expressed antibody fragments directed against various sites in HDx-1 to gain such insight. Intrabodies retain the high target specificity of antibodies but lack the immunogenic constant domains. These reagents have shown significant promise as therapeutics for proteinopathies including HD (Southwell and Patterson, 2010). Moreover, iAbs are

also powerful molecular tools for probing the functions and interactions of their targets when expressed in living cells.

We have previously shown that binding of the iAb Happ1, which recognizes the proline rich region of HDx-1, results in a selective increase in the turnover of the mutant form (mHDx-1) (Southwell et al., 2008). Here we report on the mechanism of Happ1-induced turnover of mHDx-1.

Methods

Cell culture. HEK 293 cells (ATCC) and ST14A cells (Elena Cataneo, Milan, Italy) were grown in DMEM (Invitrogen) supplemented with 10% heat inactivated fetal bovine serum, 2 mM glutamine, 1 mM streptomycin and 100 international units of penicillin (Invitrogen). Cells were maintained in 37°C (293) or 33°C (ST14A) incubators with 5% CO_2. Transfections utilized calcium phosphate.

Ubiquitination of Htt. HEK 293 cells were transfected with mHDx-1-GFP plus iAb (HDx-1:iAb = V_L12.3, 1:1; Happ1, 1:2). Thirty-six hours posttransfection, cells were collected for Western blotting and immunoprecipitation (IP) as in Southwell et al., 2008. Briefly, cells were dislodged by pipetting, pelleted by centrifugation, rinsed with PBS, and lysed by sonication in lysis buffer. Insoluble material was removed by additional centrifugation, and the protein concentration was determined by BCA assay (Pierce). Htt protein was immunoprecipitated from the lysate by combining 400 mg lysate protein with 50 mg anti-GFP antibody (Invitrogen) conjugated to protein G sepharose beads and rocking for 4 hr at room temperature. Beads were washed 4 times in PBS containing 0.1% Triton X100 to

remove unbound protein. Seventy-five milligram total lysate protein samples and bound IP samples were boiled in 6X protein loading buffer containing 20% b-mercaptoethanol (BME), separated by polyacrylamide gel electrophoresis (PAGE), transferred to nitrocellulose membrane, and immunoblotted for ubiquitin. Membranes were then stripped with Restore Western blot stripping buffer (Pierce) and reblotted for Htt. Membranes were stripped a second time and immunoblotted for b-tubulin, used as a loading control. The ratio of immunoprecipitated ubiquitin (ubiquitinated Htt) to immunoprecipitated Htt (total Htt) was assessed using chemiluminescence densitometry. Each band was first normalized to the density of the b-tubulin band for that sample. Immunoprecipitated Htt and ubiquitin levels were compared by computing the ratio of the density of the band in the presence of Happ1 to the density of the band in the presence of V_L12.3. The ratio of immunoprecipitated ubiquitin:Htt in the presence of Happ1 vs. V_L12.3 was then compared. The experiment was repeated two additional times.

Htt levels. HEK 293 cells were transfected with mHDx-1-GFP plus iAb (V_L12.3, 1:1; Happ1, 2:1) or mHDx-1DPRR (lacking the proline-rich region) plus iAb as a control for non-specific effects of Happ1. Inhibitors of proteolytic processing were added to the culture medium 24 hr posttransfection in the following concentrations: lactacystin (Sigma), 10 mM; epoxomicin (Sigma), 10 mM; 3-MA (Sigma), 10 mM; bafilomycin A1 (Sigma), 100 nM; caspase inhibitor I (NBD Biosciences), 50 mM; calpain inhibitor I (Sigma), 50 mM. Cell lysates were prepared for Western blotting 48 hr posttransfection as described above. Membranes were blotted for Htt, and stripped and blotted for b-tubulin as a loading control. Htt levels

were compared by chemiluminescence densitometry. The density of each band was normalized to the density of the b-tubulin band for that sample. The ratio of Htt levels in the presence of Happ1 to Htt levels in the presence of V_L12.3 was then compared. The experiment was repeated 3 times, giving an N of 4.

Htt turnover. Htt turnover was assayed using the SNAP-tag fusion system for *in vivo* protein labeling (NEB) as described by Southwell et al., 2008. Briefly, ST14A cells were transfected with mHDx-1-SNAP alone or with iAb. To control for non-specific effects of Happ1, mHDx-1DPRR–SNAP alone or with iAb was used. Green fluorescent SNAP-substrate was added to cells 24 hr posttransfection to label all mHDx-1. Immediately after labeling, some samples were fixed in 4% PFA, stained for cell nuclei (topro-3-iodide, Invitrogen) and mounted for confocal microscopy. Inhibitors of proteolytic processing were then added to the medium of the remaining cultures. At 48 hr posttransfection, these cells were fixed, stained and mounted as above. Mean intensity of green fluorescence in cells in three microscope fields per well and three wells for each condition was used to determine average Htt levels. The ratio of mean cell intensity at 24 hr to mean cell intensity at 48 hr was computed to determine rate of Htt turnover. The experiment was repeated twice, giving an N of 3.

Calpain cleavage site prediction in HDx-1. Calpain 1 and calpain 2 cleavage sites in HDx-1 were predicted using the SitePrediction tool with the pre-computed cleavage site profiles "calpain-1_Homo_sapiens_4_2" and "calpain-2_Homo_sapiens_4_2" (Verspurten et al., 2009). The HDx-1 sequence was obtained from the February 2009 human reference sequence (GRCh37) through the UCSC

Genome Browser (Kent et al., 2002). PolyQ tract lengths of 17 and 42 AAs were used to determine if cleavage is modified by polyQ length.

***In vitro* calpain cleavage of HDx-1.** HDx-1 Q46 fused to a thioredoxin tag (TRX) to promote solubility (mHDx-1-TRX) was purified as reported previously (Bennett et al., 2002) and exchanged into diluent (20mM Tris-HCl, pH 7.4 containing 150 mM NaCl and 2 mM $Ca2^{+}$) using a disposable PD10 desalting column (GE Healthcare). 20 μg purified mHDx-1-TRX was incubated with 1 μg calpain 1 (Sigma) at 37^{o}C for 1 hour. As a control for possible calpain cleavage in the TRX tag or linker sequence, mHDx-1-TRX was cleaved with enterokinaseMax (EKMax) (Invitrogen), a peptidase known to remove the entire TRX-linker sequence from mHDx-1-TRX according to the manufacturer's specifications. Cleavage reactions were separated byPAGE and stained with coomassie to visualize protein bands. Molecular weight of protein bands was determined by comparison to precision plus dual protein molecular weight standard (Biorad) using a FluorChem 8900 (Alpha Innotech) gel documentation system and AlphaImager software. A reaction containing only mHDx-1-TRX and diluent was used to assess uncleaved protein and reactions containing either calpain 1 or EKMax and diluent in the absence of mHDx-1-TRX were used to visualize bands corresponding to these proteins.

Peptide array mapping of the V_L12.3 binding site. A 14-mer 7-peptide array covering Htt N1-32 in steps of three AAs was purchased from Mimotopes. Peptides were dissolved in 80% DMSO/20% water to an average concentration of 5 mg/ml. Peptides were further diluted 100-fold in water and 2 ml of each peptide was blotted onto nitrocellulose and allowed to dry. Nitrocellulose membranes were

blocked with 1% milk in PBS for one hour at room temperature. GST-V_L12.3 generated as previously described (Southwell et al., 2008) was added as primary antibody and incubated overnight at 4°C. After washing in PBS with 0.1% Tween, anti-HA tag antibody 3F10 coupled to HRP (Roche) was added for 1 hour at room temperature. Dot blots were developed by exposure to X-ray film.

Organotypic brain slice cultures. Brain tissue was removed from euthanized postnatal day 10 (P10) CD Sprague-Dawley rats (Charles River Laboratory, Raleigh, NC) in accordance with Duke University Medical Center Institutional Animal Care and Use Committee guidelines and approvals, and as described previously (Lo et al., 1994; Southwell et al., 2008). 250 μm thick coronal slices containing both striatum and cortex were cut using Vibratomes (Vibratome, St. Louis, MO) in ice-cold culture medium containing 15% heat-inactivated horse serum, 10 mM KCl, 10 mM HEPES, 100 U/ml penicillin/streptomycin, 1 mM MEM sodium pyruvate, and 1 mM L-glutamine in Neurobasal A (Invitrogen). Corticostriatal brain slices were then incubated at 37°C under 5% CO_2 for 1 hr before biolistic transfection with 1.6 μm gold particles coated with DNA constructs expressing yellow fluorescent protein (YFP) as a vital marker, mHDx-1 Q-73, and either V_L12.3 or the CV_L non-targeting intrabody. For control transfections, gold particles were coated with YFP alone plus vector backbone DNA. For time-resolved Förster resonance energy transfer (TR-FRET) analysis, brain slices were triturated 10x through 26-gauge needles in ice-cold lysis buffer (50 mM Tris-HCl, 150 nM NaCl, 2 mM EDTA, 1% NP-40, 0.1% SDS + Roche protease inhibitor cocktail tablet) and centrifuged at 12,000 g for 10 min. at 4°C. The supernatants were collected and

stored at -80^{o}C until TR-FRET analysis. Experimental conditions were run in triplicate using a single brain slice per lysate.

Primary neuron co-culture. Cortico-striatal cocultures were prepared as described in (Kaltenbach et al., 2010). Briefly, cortices and striata from embryonic day 18 (E18) rat brains were dissected then separately dissociated with papain/DNase (Worthington biochemicals). Dissociated striatal and cortical neurons were counted and $5x10^6$ cells each were separately cotransfected by nucleofection (Amaxa, Lonza AG) with plasmids encoding Httexon1 carrying 73 CAG repeats or empty vector and either V_L12.3 or the preimmune control CV_L. After electroporation, striatal and cortical cells were combined and 60,000 cells/well were plated onto an established bed of astroglia in 96-well plates. Astroglial feeder layers were generated by dissection of E18 cortices followed by three serial passages to establish an enriched population of astroglia. Astroglia were plated into 96-well plates at a density of 2000 cells/well three days before neuron plating. Neurons were cultured in Neurobasal media (Invitrogen, Carlsbad, CA) supplemented with 5% fetal calf serum (Sigma-Aldrich, St. Louis, MO), 2 mM glutamine (Glutamax, Invitrogen), 10 mM potassium chloride, and 5 μg/mL gentamicin at 37°C in 95% 0_2/5%CO_2 for 4-6 days before analysis.

For TR-FRET analysis, cells were harvested by scraping from wells and triturating as described above for brain slice explants

Soluble mHtt-TR-FRET assay. TR-FRET detection of soluble mHtt was previously described (Weiss et al., 2009). In brief, samples were lysed in PBS, 0.4% TritonX100 and Complete Protease Inhibitor (Roche). 5 μl sample plus 1 μl antibody

mix diluted in assay buffer (50 mM NaH_2PO_4, 400 mM NaF, 0.1% BSA and 0.05% Tween) were pipetted per well of a low-volume 384 microtiter plate (Sigma). Final antibody amount per well was 1 ng 2B7-terbium cryptate-labeled antibody and 10 ng MW1-D2-labeled antibody. Plates were incubated for 1 hr at 4°C and measured with a Xenon-lamp Envision Reader (PerkinElmer) after excitation at 320 nm. Signal measured at 620 nm resulted from the emission of the terbium cryptate-labeled antibody and was used as a normalization signal for possible assay artifacts due to scattering, quenching, absorption or sample turbidity. Mutant Htt specific signal which resulted from the time-delayed excitation of the D2-labeled MW1 antibody after excitation by the terbium cryptate was detected at 665 nm. 665/620 nm signal ratio was calculated as "TR-FRET signal" specific for soluble mutant Htt.

Results

Happ1 does not increase mHDx-1 ubiquitination. To assess the effects of Happ1 on ubiquitination of mHDx-1, HEK 293 cells were cotransfected with mHDx-1-GFP plus Happ1 or V_L12.3. V_L12.3 was used as a control for non-specific iAb effects as we have previously shown that this iAb binds mHDx-1 but has no effect on its levels in this system (Southwell et al., 2008). Huntingtin was immunoprecipitated from transfected cell lysates and immunoblotted for both Htt and ubiquitin. Densitometry was used to determine the ratio of ubiquitinated mHDx-1 to total mHDx-1 in the presence of Happ1 versus V_L12.3 (Fig. 1). There is no differential effect of iAb treatment on this ratio, indicating that Happ1 does not increase mHDx-

1 ubiquitination and therefore likely does not work through a UPS-dependent mechanism.

Happ1-induced reduction of mHtt levels requires calpain activity and maintenance of lysosomal pH. We previously showed that Happ1 stimulates mHDx-1 turnover (Southwell et al., 2008). To determine which proteolytic pathway is involved, soluble lysates of HEK 293 cells cotransfected with mHDx-1 plus iAb, or mHDx-1DPRR plus iAb, and treated with various inhibitors of proteolytic processing were immunoblotted for Htt. The ratio of the Htt level in the presence of Happ1 to the Htt level in the presence of V_L12.3 was compared among the various inhibitors. In unperturbed cells, or in the presence of DMSO vehicle, the level of Htt in the presence of Happ1 is reduced compared to the level of Htt in the presence of V_L12.3. This ratio is unchanged by the addition of various inhibitors: lactacystin, a proteasome inhibitor that also affects cathepsin A of lysosomes; epoxomicin, a proteasome inhibitor; 3-MA, an inhibitor of autophagosome formation; or caspase inhibitor I, an irreversible pan-caspase inhibitor. In contrast, the addition of bafilomycin A1, an inhibitor of the vacuolar-type H(+)-ATPase that is known to inhibit autophagosome/lysosome fusion as well as lysosomal pH; or calpain inhibitor I, a pan-calpain inhibitor, significantly increases the ratio of Htt in the presence of Happ1 to Htt in the presence of V_L12.3 (Fig. 2). Thus, these latter two inhibitors interfere with the mechanism by which Happ1 reduces the level of mHtt. The levels of HDx-1 in the presence of calpain inhibitor I or bafilomycin A1 are quantitatively very similar to those found using the HDx-1 construct lacking the proline-rich region to which Happ1 binds. Thus, it appears that these inhibitors

completely abolish the effect of Happ1 on mHDx-1 clearance. The effect of bafilomycin A1 is likely due to disrupted lysosomal pH rather than inhibition of autophagosome/lysosome fusion as evidenced by the lack of effect by 3-MA, which should act upstream of bafilomycin A1 in the macro-autophagy pathway. Therefore, we infer that Happ1 reduces mHDx-1 level by a calpain-CMA-dependent mechanism.

Happ1-induced stimulation of mHtt turnover requires calpain activity and maintenance of lysosomal pH. In another approach to defining how Happ1 stimulates mHDx-1 clearance, mHDx-1 was labeled with the SNAP reagent and the loss of the label followed over time (Jansen et al., 2007). A traditional pulse chase experiment was not used because mHDx-1 is known to affect transcriptional regulation. This property of mHDx-1 could conceivably be altered by iAb binding, leading to variable transcription rates of HDx-1 in the presence of the various iAbs. The SNAP tag fusion system allows labeling of all preexisting HDx-1. By measuring the amount of Htt at the time of labeling and again at a later time point, we are able to measure a rate of turnover independent of transcription or translation rate. This system also offers greater specificity, because only the SNAP tag fusion protein is labeled as opposed to all cellular proteins translated during the labeling period as with traditional pulse-chase experiments. ST14A cells were transfected with mHDx-1-SNAP alone or with iAb, as well as mHDx-1DPRR-SNAP alone or with iAb. Green fluorescent SNAP substrate was used to label mHDx-1 protein 24 hr posttransfection. Cells were allowed to incubate an additional 24 hr in the presence of various inhibitors of proteolytic processing or vehicle. The mean fluorescence intensity of cells at 24 hr and at 48 hr was compared to determine the amount of

mHDx-1 labeled at 24 hr that still remained at 48 hr.

Compared to that in the presence of V_L12.3, there is significantly less mHDx-1 remaining at 48hr in the presence of Happ1 (Fig. 3). Addition of epoxomicin or 3-MA has no effect on the turnover rate of mHDx-1 in the presence of Happ1, reinforcing the conclusion that Happ1 does not increase mHDx-1 turnover by enhancing proteasome or macroautophagy function. On the other hand, addition of bafilomycin A1 or calpain inhibitor I completely blocks the Happ1 stimulation of mHDx-1 turnover, leading to turnover levels equivalent to those with mHDx-1 alone or in the presence of V_L12.3 (Fig. 3). These results support the finding with total HDx-1 levels (above) that Happ1 increases turnover of mHtt by enhancing calpain cleavage and CMA.

A turnover rate could not be assessed for mHDx-1DPRR due to the increased toxicity and aggregation of this construct, leading to a paucity of morphologically normal cells or soluble HDx-1 at 48 hr (Fig. 4). There is still significant soluble HDx-1 in the presence of V_L12.3 at this time point, indicating that, as expected from our previous work, this iAb inhibits aggregation of this modified HDx-1, while Happ1 does not.

There are putative calpain cleavage sites at AA 15 and AA 8 of HDx-1. To identify the site of calpain action, human HDx-1 amino acid sequence was analyzed for potential calpain 1 and 2 cleavage sites using the web application SitePrediction (Verspurten et al., 2009). Using this program, AAs 12-17 with cleavage between 15 and 16, (ESLK.SF), is predicted to be the most likely site for both proteases, with greater than 99.9% specificity for calpain 1 and greater than 99% specificity for

calpain 2. A secondary site at AAs 5-10, with cleavage between 8 and 9, (EKLM.KA), is predicted to have greater than 99% specificity for calpain 1 and greater than 95% specificity for calpain 2 (Fig. 5).

Calpain 1 cleaves mHDx-1 *in vitro*. To determine if calpain directly or indirectly promotes clearance of mHDx-1 we incubated purified, recombinant calpain 1 and mHDx-1 protein *in vitro*. A thioredoxin tag (TRX) was fused to mHDx-1 to promote solubility. Cleavage at the predicted calpain recognition sites would result in N-terminal fragments consisting of the TRX tag and linker and N1-8 or N1-15 (Fig. 6a) As a control for cleavage within the TRX tag, mHDx-1 was also incubated with EKMax, which removes the entire tag and linker sequence. Reactions containing either no protease or no HDx-1 were used as controls. Reactions were separated by PAGE and visualized with coomassie to evaluate cleavage. In the absence of protease, mHDx-1 protein appears as a single band of approximately 46 kDa. In the presence of calpain 1, mHDx-1 is cleaved resulting in three smaller products (Fig. 6b). The smallest of these are 15.2 and 16.0 kDa which are very close to the predicted sizes for N1-8-TRX and N1-15-TRX of 15.1 and 15.9 kDa supporting cleavage at the predicted sites. These products are larger than those generated by EKMax cleavage indicating that calpain cleavage is occurring within mHDx-1.

V_L12.3 binds to the putative calpain cleavage site at AA 15. The iAb V_L12.3 was selected for binding to an N1-20 AA fragment of HDx-1 (Colby et al., 2004), a domain that encompasses but is not limited to the predicted calpain cleavage sites. To determine the exact location of V_L12.3 binding we used a 3 AA stepped peptide array binding assay. The results show that V_L12.3 binds to peptides 3, 4 and 5 which

are N7-20, N10-23 and N13-26, respectively (Fig. 7). This demonstrates that V_L12.3 requires AAs 15-18 at the minimum and 13-20 at the maximum for binding. Thus, V_L12.3 binding would be expected to interfere with cleavage at AA 15 and possibly sterically hinder cleavage at AA 8.

Blocking cleavage at AA 15 by V_L12.3 binding prevents clearance of soluble mHDx-1. To determine the effect of compromising cleavage at AA 15 on mHDx-1 clearance, we performed a TR-FRET assay to measure soluble mHDx-1 levels in lysates of organotypic brain slice cultures biolistically transfected with mHDx-1 alone or with either V_L12.3 or CV_L, a control iAb. Soluble mHtt levels were compared 1, 2 and 3 days posttransfection by measuring the TR-FRET signal between a donor fluorophore-labeled antibody, 2B7, recognizing N1-17 of HDx-1, and an acceptor fluorophore-labeled antibody, MW1, recognizing polyQ (Weiss et al., 2009). This system is more suited to the measurement of reduced mHDx-1 turnover than the SNAP-tag fusion system described above, in which we observed no effect of V_L12.3 on turnover rate. The brain slice culture system allows for longer experimental time frames during which, unlike the SNAP-tag system, significant normal mHDx-1 clearance is observed. As expected, the level of soluble mHDx-1 in the presence of CV_L declines over time, reflecting normal clearance. In the presence of V_L12.3, there is no change in mHDx-1 levels over time indicating a complete block of clearance (Fig. 8a). To extend our observation period even further, we have utilized a primary neuronal coculture system consisting of striatal and cortical neurons as well as glia (Kaltenbach et al., 2010). Primary neurons were transfected with iAb or mHDx-1 plus iAb and plated on a previously generated glial bed. Lysates were collected 4, 5

or 6 days later, and mHDx-1 protein level was assessed by TR-FRET. At these later time points, there is dramatically more mHDx-1 protein in the presence of V_L12.3 than in the presence of CV_L (Fig. 8b). This suggests that clearance of mHDx-1 requires calpain cleavage at AA15, and that this cleavage event likely occurs upstream of CMA degradation.

Discussion

Huntington's disease is a devastating neurodegenerative disease for which there is currently no disease modifying therapy. One of the difficulties with HD therapy development is the complex web of dysfunction resulting from the presence of the mutant protein that affects a great many processes and pathways in susceptible neurons. As a result, lowering the levels of mHtt protein either by silencing expression or increased clearance remains the most promising therapeutic approach for HD. For this reason, understanding the mechanism of mHtt degradation is important.

Huntingtin degradation involves numerous pathways, with differential toxicity regulated by posttranslational modifications. Transgenic mice expressing mHtt that is resistant to caspase-6 cleavage at amino acid (AA) 586 do not develop the HD-like symptoms seen in their caspase-6 sensitive counterparts, despite the presence of other caspase cleavage products in the brain (Graham et al., 2006). Phosphorylation of serine 421 shifts processing toward these less toxic products by inhibiting cleavage at AA 586 (Warby et al., 2009). Moreover, calpain-resistant mHtt lacking the AA 469 and AA 536 cleavage sites is less toxic and aggregation-prone

than calpain cleavage-sensitive mHtt (Gafni et al., 2004). Phosphorylation of serine 536 inhibits cleavage at AA 536, which also results in reduced toxicity (Schilling et al., 2006). Modifications of mHtt can also regulate non-protease degradation events. Phosphorylation of serines 13 and 16 increases proteasomal and lysosomal degradation of Htt in turn reducing toxicity. In *Drosophila*, presumably due to the absence of mammalian degradative machinery and mechanisms, this modification leads to increased toxicity due to accumulation of the more toxic phosphorylated form of mHtt (Thompson et al., 2009). A better understanding of the complex process of mHtt proteolysis could eventually lead to the development of therapeutics that shift processing toward less toxic pathways and/or enhance removal. Although the generation of N-terminal mHtt fragments by caspase and calpain cleavage has been previously characterized, the subsequent degradation of the highly toxic HDx-1 fragment has remained unclear.

With their high target specificity, iAbs are an ideal molecular tool for elucidating protein interactions and functions. For example, the 17 N-terminal AAs of HDx-1 are required for aggregate seeding and cytoplasmic retention (Atwal et al., 2007; Rockabrand et al., 2007). Blockade of this region by the binding of the iAb V_L12.3 results in nuclear translocation and a potent inhibition of aggregation of HDx-1, illustrating the informative relationship between iAb effects and target function (Colby et al., 2004; Southwell et al., 2008). Happ1 recognizes the proline rich region of HDx-1 and increases clearance of mutant but not wildtype HDx-1 (Southwell et al., 2008). We have exploited this effect of Happ1 binding to gain insight into the mechanism of HDx-1 proteolysis.

Htt undergoes a variety of proteolytic processing steps including protease cleavage, proteasomal degradation, and lysosomal/autophagic degradation. In order to determine the initiating or rate-limiting step in mHDx-1 degradation, we tested inhibitors of each of these pathways in the presence and absence of Happ1. An important control in our experiments is the use of mHDx-1DPRR, which lacks the Happ1 binding site. Levels of this protein are not affected by Happ1, indicating that the reduced mHDx-1 levels in the presence of Happ1 do not result from non-specific iAb actions such as activation of the unfolded protein response (Schroder and Kaufman, 2005).

The proteasome inhibitors epoxomicin and lactacystin do not disrupt Happ1 stimulation of HDx-1 turnover, and Happ1 does not increase ubiquitination of HDx-1. These results indicate that Happ1 does not accelerate proteasomal degradation of Htt. We also find that 3-MA, an inhibitor of autophagosome formation and the macroautophagy pathway, does not interfere with Happ1-accelerated mHDx-1 degradation. In contrast, bafilomycin A1, a vacuolar-type H(+)-ATPase inhibitor that hinders lysosome-autophagosome fusion as well as disrupting lysosomal pH, prevents Happ1-induced changes in mHDx-1 clearance rate. Due to the lack of effect of 3-MA, it is unlikely that the action of bafilomycin A1 on autophagosome/ lysosome fusion is responsible for disrupting Happ1 function. It is more likely that bafilomycin A1 disrupts Happ1 function by disrupting lysosomal pH. This indicates a role for CMA, which is an autophagosome-independent lysosomal degradation process, in Happ1-enhanced mHDx-1 clearance.

We next evaluated the sensitivity of the Happ1 effects to the caspase and calpain proteases. While caspase inhibition has no effect on Happ1 function, calpain inhibition is effective in blocking the ability of Happ1 to both decrease the level of soluble mHDx-1 and increase its turnover. These results indicate that Happ1 likely increases mHDx-1 clearance through enhanced calpain cleavage, which is particularly interesting because of the lack of a known calpain cleavage site in HDx-1. Calpain inhibitor I has, however, been reported to cause accumulation and increased aggregation of N-terminal Htt fragments including HDx-1, and calpain 1 is known to increase degradation of these fragments in the lysates of transfected PC12 cells (Ratovitski et al., 2007). These results indicate that calpains participate either directly or indirectly in the degradation of mHDx-1. Analysis of the AA sequence of human HDx-1 using the web application SitePrediction identifies AAs 12-17 as having the highest degree of specificity for both calpain 1 and calpain 2 with a secondary recognition site at AA 5-10. Cleavage at these sites, which is not predicted to be modulated by increasing polyQ length, would result in the removal of 15 of the 17 N-terminal AAs of Htt, effectively removing the N-terminus. The N-terminus of Htt is the site of many posttranslational modifications including phosphorylation, acetylation and sumoylation (Steffan et al., 2004; Aiken et al., 2009). It is interesting to note that phosphorylation of this putative calpain cleavage site is known to increase mHDx-1 nuclear localization followed by degradation (Thompson et al., 2009) and that removal of the N-terminus is known to increase nuclear localization (Atwal et al., 2007; Rockabrand et al., 2007).

Calpain I cleaves purified mHDx-1 *in vitro* generating cleavage products of the expected sizes showing that this protease can act directly on HDx-1 and supporting the site prediction. We employed iAb blockade of the N-terminal 12-17 AA site to determine the importance of cleavage here in the degradative process. V_L12.3 was raised against a peptide of AAs 1-20 of Htt and therefore binds somewhere in this region (Colby et al., 2004), which includes but is not limited to the putative calpain cleavage sites identified here. Peptide array epitope mapping shows that V_L12.3 binding requires at a minimum, AAs 15-18 of HDx-1 for binding, a region that includes the putative calpain cleavage site at AA 15. As V_L12.3 binding is known to prevent interactions of HDx-1 that require this domain, such as aggregate seeding and cytoplasmic retention (Southwell et al., 2008), it is reasonable to postulate that V_L12.3 would also compromise cleavage here. If calpain cleavage at this site is involved in the degradation of mHDx-1, V_L12.3 binding would be expected to reduce turnover. We have previously shown that V_L12.3 binding has no effect on mHDx-1 protein level or turnover rate in cultured 293 and ST14A cells respectively (Southwell et al., 2008). These systems are, however, temporally constrained by the toxicity of transfection reagents and mHDx-1 as well as cell proliferation. These factors limit our experimental time frame to 24 hr, an interval in which we observe very little normal mHDx-1 clearance, and any decreases in clearance may be below the sensitivity threshold of the assays. As a result, these systems, though sufficient for evaluating increased turnover, are inadequate for evaluating decreased turnover. Moreover, these systems lack differentiated neurons and connectivity, which are integral to HD pathology**.** In an effort to overcome these

caveats, we used a TR-FRET assay to evaluate the effect of V_L12.3 on mHDx-1 clearance in biolistically cotransfected brain slice explants and in primary corticostriatal neuronal cocultures, which allow longer experimental time frames of up to 3 and 6 days respectively, in more relevant, partially intact neuronal systems. In these systems in the presence of CV_L, an iAb that does not bind HDx-1, the level of mHDx-1 protein appears to decline over the first three days, reaching a plateau that is maintained for the subsequent 3 days, reflecting normal turnover. Conversely, during the observed time period there is no change in mHDx-1 level in the presence of V_L12.3, demonstrating a lack of normal turnover when the putative calpain cleavage site is bound by the iAb. These results suggest that calpain-mediated removal of the N-terminus of mHDx-1, which is likely followed by CMA degradation, is required for clearance of this toxic protein and that selective regulation of this cleavage event could prove beneficial in the treatment or prevention of HD.

References

Aiken CT, Steffan JS, Guerrero CM, Khashwji H, Lukacsovich T, Simmons D, Purcell JM, Menhaji K, Zhu Y-Z, Green K, LaFerla F, Huang L, Thompson LM, Marsh JL (2009) Phosphorylation of Threonine 3: Implications for huntingtin aggregation and neurotoxicity. J Biol Chem 284:29427-29436.

Atwal RS, Xia J, Pinchev D, Taylor J, Epand RM, Truant R (2007) Huntingtin has a membrane association signal that can modulate huntingtin aggregation, nuclear entry and toxicity. Hum Mol Genet 16:2600-2615.

Bennett MJ, Huey-Tubman KE, Herr AB, West AP, Ross SA, Bjorkman PJ (2002) A linear lattice model for polyglutamine in CAG-expansion diseases. PNAS 99:11634-11639.

Colby DW, Garg P, Holden T, Chao G, Webster JM, Messer A, Ingram VM, Wittrup KD (2004) Development of a human light chain variable domain (VL) intracellular antibody specific for the amino terminus of huntingtin via yeast surface display. J Mol Bio 342:901-912.

Gafni J, Hermel E, Young JE, Wellington CL, Hayden MR, Ellerby LM (2004) Inhibition of calpain cleavage of huntingtin reduces toxicity: accumulation of calpain/caspase fragments in the nucleus. J Biol Chem 279:20211-20220.

Gil JM, Rego AC (2008) Mechanisms of neurodegeneration in Huntington's disease. Eur J Neurosci 27:2803-2820.

Graham RK, Deng Y, Slow EJ, Haigh B, Bissada N, Lu G, Pearson J, Shehadeh J, Bertram L, Murphy Z, Warby SC, Doty CN, Roy S, Wellington CL, Leavitt BR,

Raymond LA, Nicholson DW, Hayden MR (2006) Cleavage at the caspase-6 site Is required for neuronal dysfunction and degeneration due to mutant huntingtin. Cell 125:1179-1191.

Huntington's Disease Collaborative Research Group. (1993) A novel gene containing a trinucleotide repeat that is expanded and unstable on Huntington's disease chromosomes. Cell 72:971-983.

Imarisio S, Carmichael J, Korolchuk V, Chen C-W, Saiki S, Rose C, Krishna G, Davies JE, Ttofi E, Underwood BR, Rubinsztein DC (2008) Huntington's disease: from pathology and genetics to potential therapies. Biochem J 412:191-209.

Jansen LET, Black BE, Foltz DR, Cleveland DW (2007) Propagation of centromeric chromatin requires exit from mitosis. J Cell Biol 176:795-805.

Kaltenbach LS, Bolton MM, Shah B, Kanju PM, Lewis GM, Turmel GJ, Whaley JC, Trask OJ, Lo DC (2010) Composite primary neuronal high-content screening assay for Huntington's disease incorporating non-cell-autonomous interactions. J Biomol Screen 15:806-819.

Kent WJ, Sugnet CW, Furey TS, Roskin KM, Pringle TH, Zahler AM, Haussler aD (2002) The human genome browser at UCSC. Genome Res 12:996-1006.

Majumder P, Raychaudhuri S, Chattopadhyay B, Bhattacharyya NP (2007) Increased caspase-2, calpain activations and decreased mitochondrial complex II activity in cells expressing exogenous huntingtin exon 1 containing CAG repeat in the pathogenic range. Cell Mol Neurobiol 27:1127-1145.

Qin Z-H, Gu Z-L (2004) Huntingtin processing in pathogenesis of Huntington disease. Acta Pharm Sinic 25:1243-1249.

Ratovitski T, Nakamura M, D'Ambola J, Chighladze E, Liang Y, Wang W, Graham RK, Hayden MR, Borchelt DR, Hirschhorn RR, Ross CA (2007) N-terminal proteolysis of full-length mutant huntingtin in an inducible PC12 cell model of Huntington's disease. Cell Cycle 6:12.

Rockabrand E, Slepko N, Pantalone A, Nukala VN, Kazantsev A, Marsh JL, Sullivan PG, Steffan JS, Sensi SL, Thompson LM (2007) The first 17 amino acids of Huntingtin modulate its sub-cellular localization, aggregation and effects on calcium homeostasis. Hum Mol Genet 16:61-77.

Schilling B, Gafni J, Torcassi C, Cong X, Row RH, LaFevre-Bernt MA, Cusack MP, Ratovitski T, Hirschhorn R, Ross CA, Gibson BW, Ellerby LM (2006) Huntingtin phosphorylation sites mapped by mass spectrometry: modulation of cleavage and toxicity. J Biol Chem 281:23686-23697.

Schroder M, Kaufman RJ (2005) The mammalian unfolded protein response. Ann Rev Biochem 74:739-789.

Southwell AL, Patterson PH (2010) Antibody therapy in Neurodegenerative disease. Rev Neurosci.

Southwell AL, Khoshnan A, Dunn DE, Bugg CW, Lo DC, Patterson PH (2008) Intrabodies binding the proline-rich domains of mutant huntingtin increase its turnover and reduce neurotoxicity. J Neurosci 28:9013-9020.

Steffan JS, Agrawal N, Pallos J, Rockabrand E, Trotman LC, Slepko N, Illes K, Lukacsovich T, Zhu Y-Z, Cattaneo E, Pandolfi PP, Thompson LM, Marsh JL (2004) SUMO modification of duntingtin and Huntington's disease pathology. Science 304:100-104.

Thompson LM, Aiken CT, Kaltenbach LS, Agrawal N, Illes K, Khoshnan A, Martinez-Vincente M, Arrasate M, O'Rourke JG, Khashwji H, Lukacsovich T, Zhu Y-Z, Lau AL, Massey A, Hayden MR, Zeitlin SO, Finkbeiner S, Green KN, LaFerla FM, Bates G, Huang L, Patterson PH, Lo DC, Cuervo AM, Marsh JL, Steffan JS (2009) IKK phosphorylates huntingtin and targets it for degradation by the proteasome and lysosome. J Cell Biol 187:1083-1099.

Todde V, Veenhuis M, van der Klei IJ (2009) Autophagy: Principles and significance in health and disease. Biochim Biophys Acta 1792:3-13.

Verspurten J, Gevaert K, Declercq W, Vandenabeele P (2009) SitePredicting the cleavage of proteinase substrates. Trends Biochem Sci 34:319-323.

Warby SC, Doty CN, Graham RK, Shively J, Singaraja RR, Hayden MR (2009) Phosphorylation of huntingtin reduces the accumulation of its nuclear fragments. Mol Cell Neurosci 40:121-127.

Weiss A, Abramowski D, Bibel M, Bodner R, Chopra V, DiFiglia M, Fox J, Kegel K, Klein C, Grueninger S, Hersch S, Housman D, Régulier E, Rosas HD, Stefani M, Zeitlin S, Bilbe G, Paganetti P (2009) Single-step detection of mutant huntingtin in animal and human tissues: A bioassay for Huntington's disease. Anal Biochem 395:8-15.

Figures

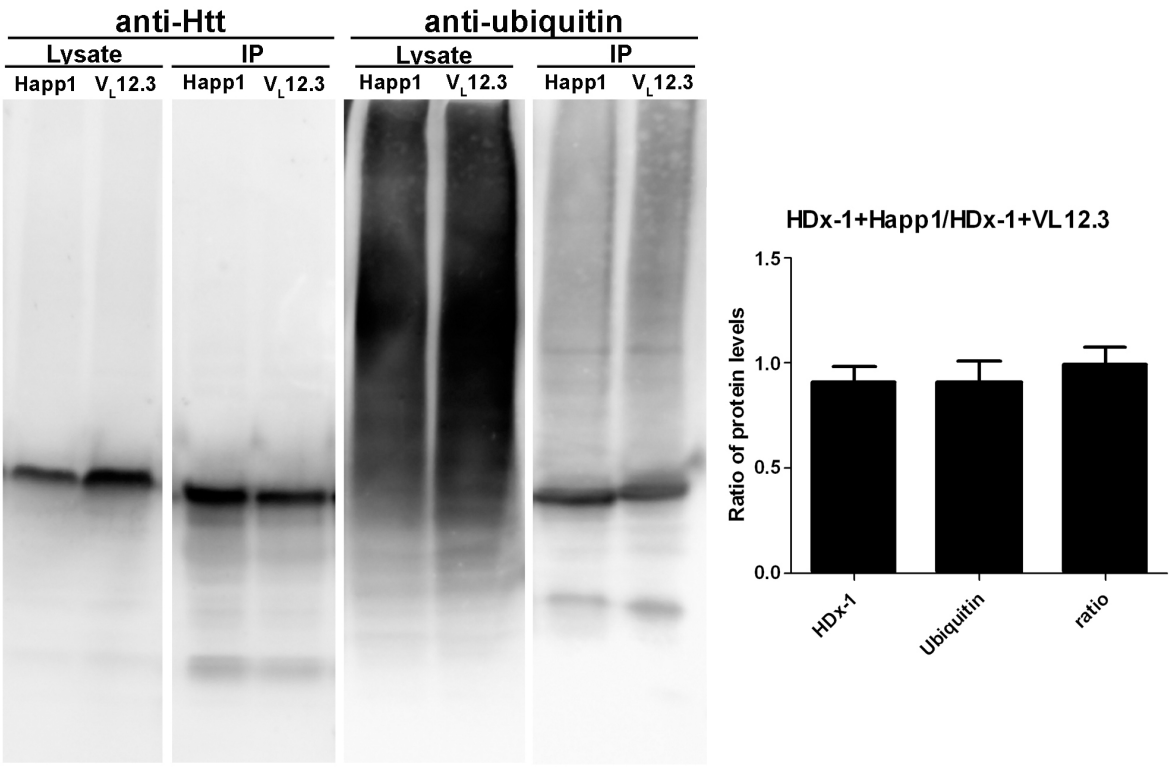

Figure 1. Happ1 does not increase ubiquitination of mHDx-1. mHDx-1 was immunoprecipitated from the lysates of HEK 293 cells cotransfected with mHDx-1 and iAb. Lysates and IPs were Western blotted for Htt and ubiquitin. The ratio of immunoprecipitated Htt (total mHDx-1) to immunoprecipitated ubiquitin (ubiquitinated mHDx-1) was compared. There are no iAb specific effects on this ratio. N = 3

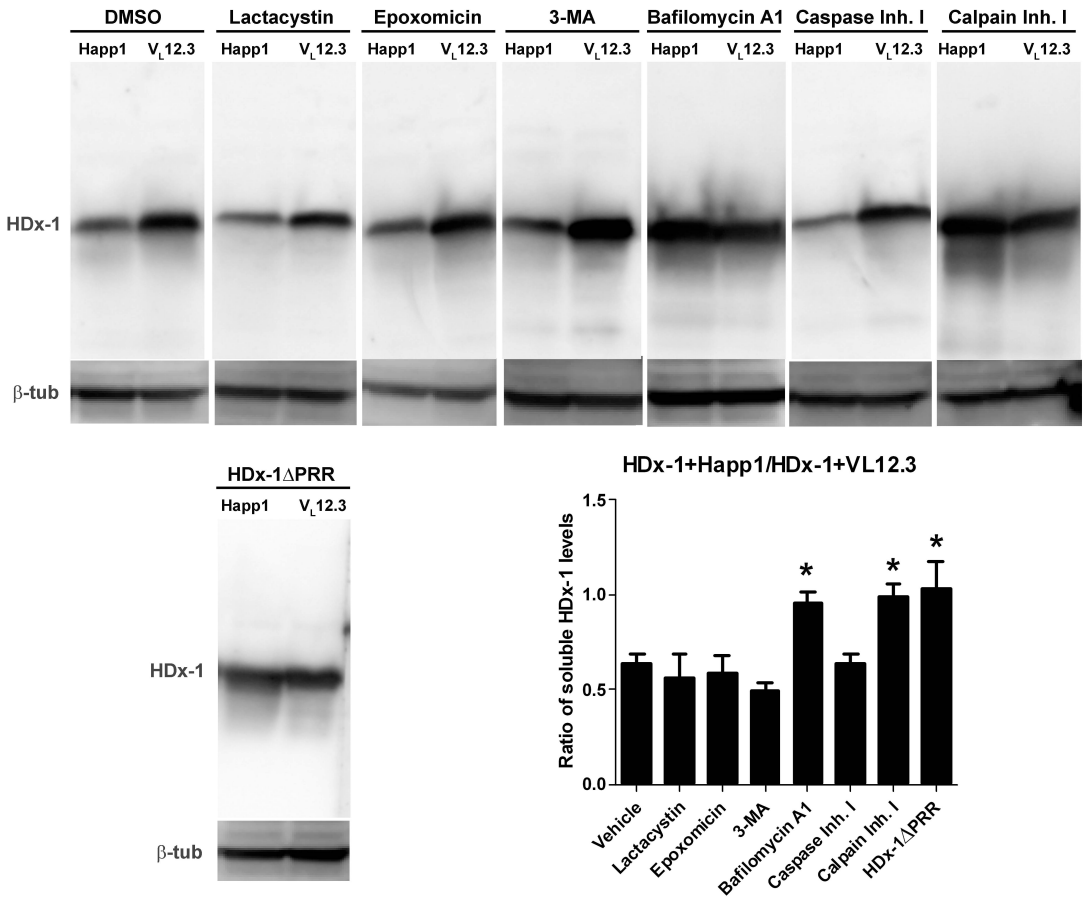

Figure 2. Happ1-mediated reduction of mHDx-1 protein levels is calpain-dependent. HEK 293 cells were cotransfected with mHDx-1 and iAb in the presence of inhibitors of proteolysis or DMSO vehicle. mHDx-1 protein levels in transfected cell lysates was compared by Western blotting and densitometry. There is less mHDx-1 protein in the Happ1 transfected cells as compared to the $V_L12.3$ transfected cells in the presence of vehicle, Lactacystin, epoxomicin, 3-MA or caspase inhibitor 1. Happ1-mediated reduction of mHDx-1 levels is blocked by bafilomycin A1 or calpain inhibitor 1 to the same level as mHDx-1 lacking the Happ1 binding site. *=$p<0.05$, N = 4

Fig 3

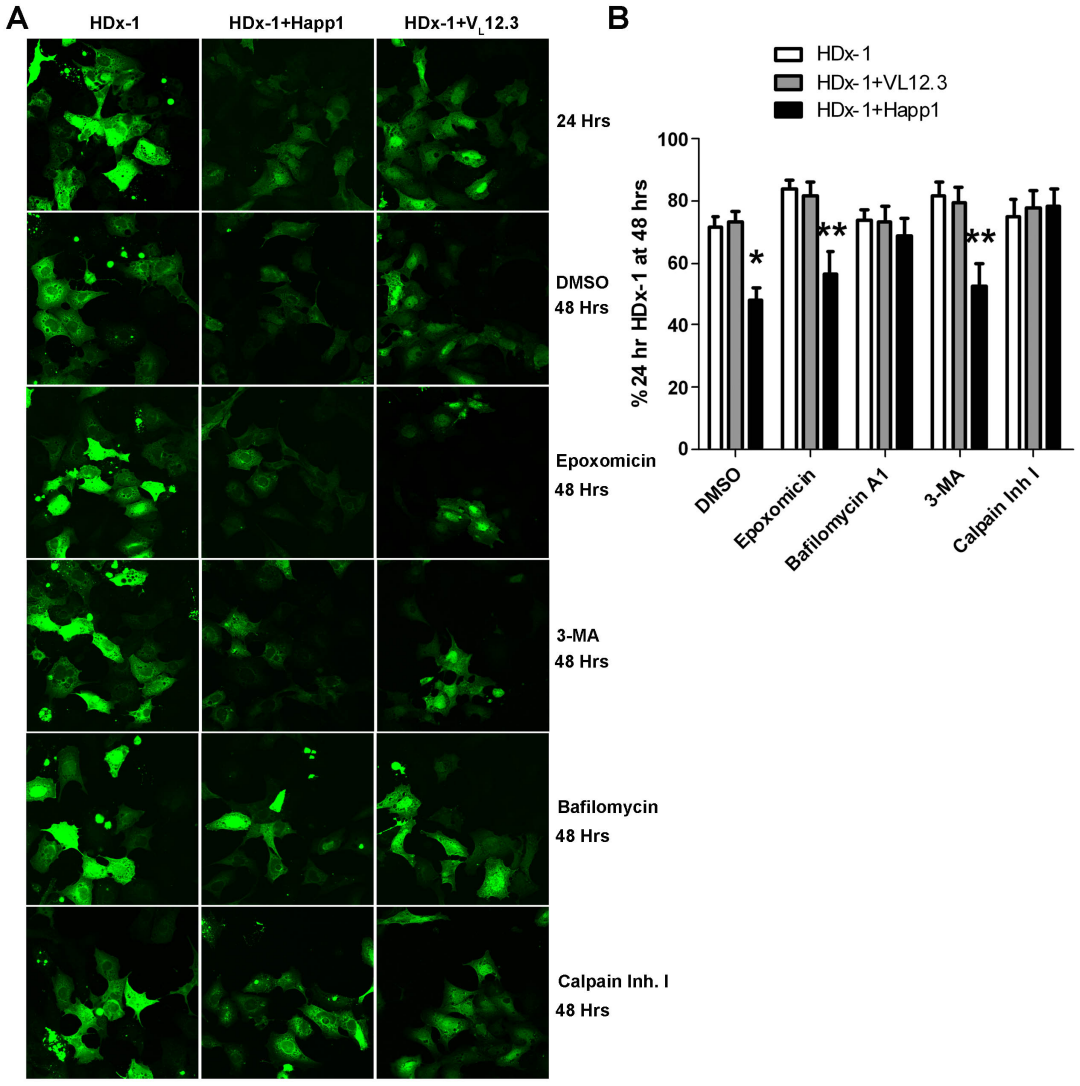

Figure 3. Happ1-enhanced mHDx-1 turnover is calpain-dependent. ST14A cells were cotransfected with mHDx-1-SNAP alone or with iAb in the presence of inhibitors of proteolytic processing or DMSO vehicle. To measure Htt turnover, mHDx-1 protein was labeled 24 hr posttransfection, and the mean cell intensity of label at 24 hr vs. 48 hr was used to determine the percentage of mHDx-1 labeled at 24 hr that still remained at 48 hr. In the presence of epoxomicin or 3MA there is no change in Happ1-enhanced mHDx-1 turnover as compared to in the presence of

DMSO. In the presence of bafilomycin A1 or calpain inhibitor 1, mHDx-1 turnover is not increased by Happ1. *=$p<0.05$, **=$p<0.01$, N=3

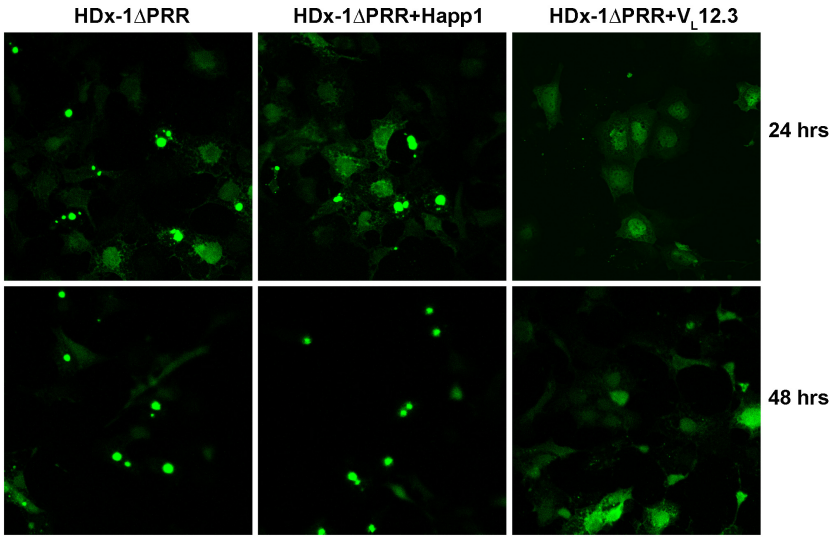

Figure 4. Happ1 does not inhibit aggregation of mHDx-1DPRR. ST14A cells were cotransfected with mHDx-1DPRR-SNAP alone or with iAb. HDx-1-SNAP fusion protein was labeled 24 hr posttransfection, and labeled protein was observed 24 hr later. As expected, Happ1 has no effect on aggregation of mHDx-1 lacking the Happ1 binding site. Conversely, V_L12.3 is still efficient at preventing aggregation of this modified mHDx-1.

site prediction for human HDx-1

Calpain 1

rank	position	site	N fragment	C fragment	specificity
1	12 to 17	ESLK.SF	1.7 kD	8.5 kD	>99.9%
2	5 to 10	EKLM.KA	0.9 kD	9.3 kD	>99%
3	14 to 19	LKSF.QQ	2.0 kD	8.2 kD	>95%

Calpain 2

rank	position	site	N fragment	C fragment	specificity
1	12 to 17	ESLK.SF	1.7 kD	8.5 kD	>99%
2	5 to 10	EKLM.KA	0.9 kD	9.3 kD	>95%
3	51 to 56	PQLP.QP	6.3 kD	3.9 kD	>95%
4	57 to 62	PPQA.QP	6.9 kD	3.3 kD	>95%
5	62 to 67	PLLP.QP	7.5 kD	2.7 kD	>95%
6	61 to 66	QPLL.PQ	7.4 kD	2.8 kD	>95%
7	80 to 85	PAVA.EE	9.2 kD	1.0 kD	>95%

Figure 5. There are predicted calpain cleavage sites at AAs 12-17 and 5-10 of HDx-1 with high specificity for calpains 1 and 2. Human HDx-1 sequence was analyzed using the web tool SitePrediction for predicted calpain 1 and 2 cleavage sites. This analysis determined that AAs 12-17 is predicted to have the greatest specificity for both proteases. There is a secondary predicted cleavage site at AA 5-10 that is also predicted to be highly specific for both calpain 1 and 2.

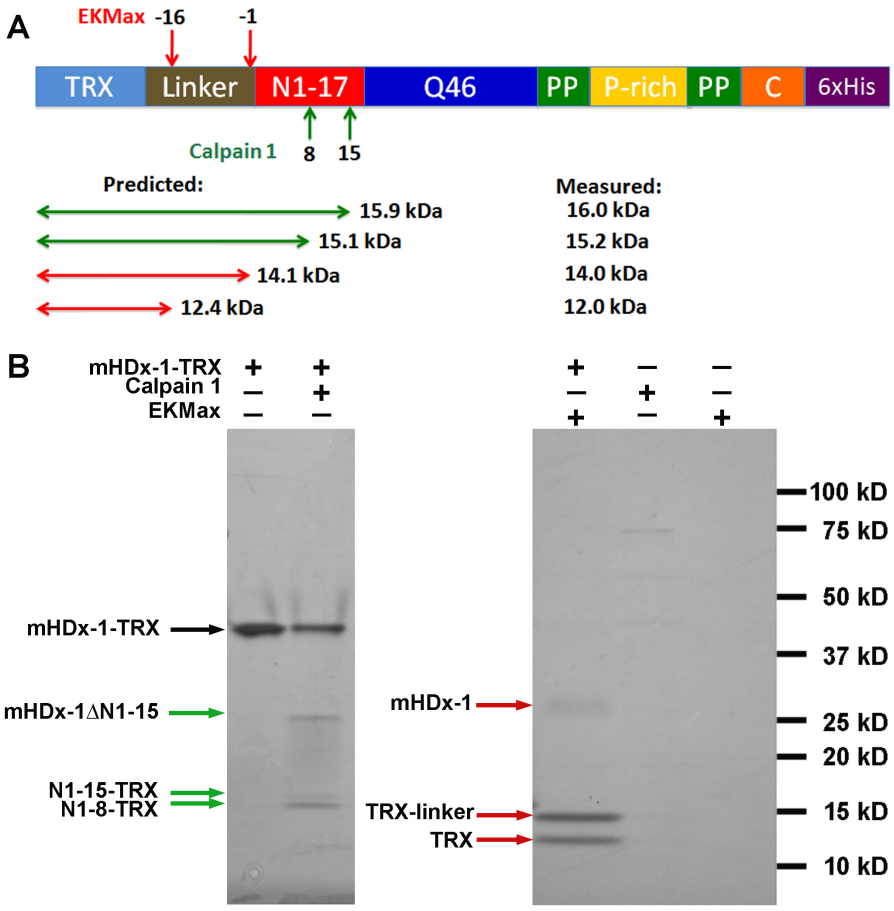

Figure 6. Purified calpain 1 cleaves HDx-1 *in vitro* generating cleavage fragments consistent with the predicted sites at AA8 and AA15. HDx-1 Q46 fused to thioredoxin (mHDx-1-TRX) was incubated with purified calpain 1 *in vitro,* separated by PAGE and stained with coomassie to assess cleavage. (A) mHDx-1-TRX construct showing known EKMax cleavage sites and predicted calpain 1 cleavage sites. (B) Coomassie stained PAGE gel showing mHDx-1-TRX in lane 1, which appears as a single band. Cleavage by calpain 1 in lane 2 yields 3 smaller bands which correspond to the predicted products after cleavage at AA 8 and AA 15. Cleavage by EKMax in lane 3 yields 3 bands which correspond to the known cleavage sites. The N-terminal fragments generated by EKMax cleavage, which

include the entire TRX tag and linker, are smaller than those generated by calpain cleavage indicating that calpain cleavage must occur within HDx-1. Lanes 4 and 5 are calpain 1 alone and EKMax alone respectively.

A

Peptide	Position	Sequence	Binding
1	N1-14	MATLEKLMKAFESL	No
2	N4-17	LEKLMKAFESLKSF	No
3	N7-20	LMKAFESLKSFQQQ	Yes
4	N10-23	AFESLKSFQQQQQQ	Yes
5	N13-26	SLKSFQQQQQQQQQ	Yes
6	N16-29	SFQQQQQQQQQQQQ	No
7	N19-32	QQQQQQQQQQQQQQ	No

B

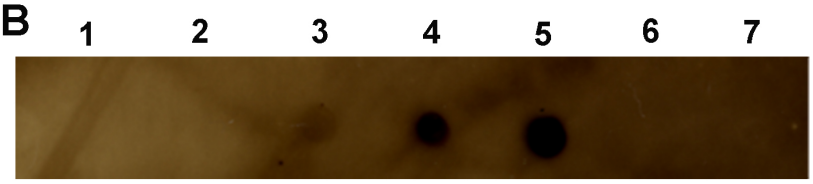

Figure 7. V_L12.3 recognizes AAs 13-20 of HDx-1. Three AA stepped 14-mer peptides were spotted onto nitrocellulose and binding of V_L12.3 was assessed. (A) Peptide table. (B) Dot blot showing binding of peptides 3, 4 and 5 illustrating that V_L12.3 requires AAs 15-18 at the minimum and 13-20 at the maximum for recognition of Htt.

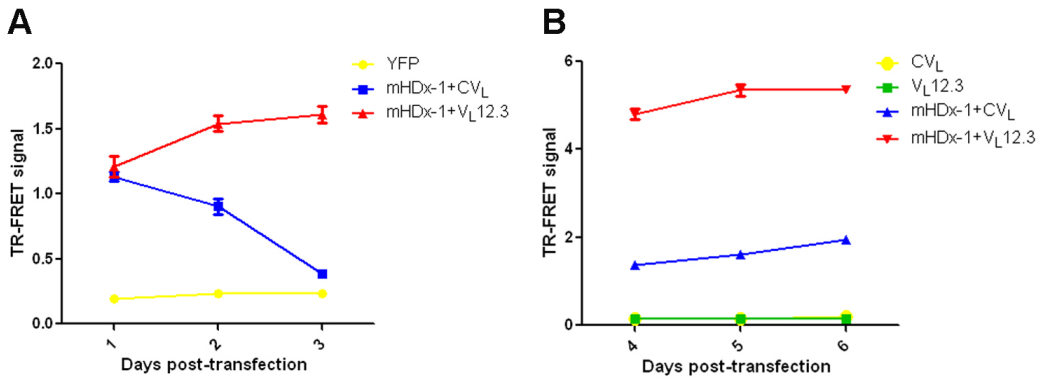

Figure 8. V_L12.3 binding prevents turnover of HDx-1. (A) Organotypic brain slice cultures were cotransfected with mHDx-1 and V_L12.3 or CV_L, a control iAb. Soluble mHDx-1 protein level was assessed in lysates collected 1, 2 or 3 days posttransfection by TR-FRET. The level of mHDx-1 protein declines over time in the presence of CV_L, but not in the presence of V_L12.3 indicating impaired clearance. (B) Primary striatal and cortical neurons co-cultured with astroglia were transfected with iAb or mHDx-1 plus iAb. Soluble mHDx-1 protein level was assessed in lysates collected 4, 5 or 6 days posttransfection by TR-FRET. At these later time points, there is dramatically more mHDx-1 protein in the presence of V_L12.3 as compared to CV_L.